SAN/0499-22
MDC G8214

10 MWe Solar Thermal
Central Receiver Pilot Plant

SOLAR FACILITIES DESIGN INTEGRATION

COLLECTOR FIELD OPTIMIZATION REPORT (RADL ITEM 2-25)

Revised January 1981
October 1979

WORK PERFORMED UNDER CONTRACT
DE-AC03-79SF10499

ENERGY FOUNDATION OF TEXAS
4800 CALHOUN
HOUSTON, TEXAS 77004

U.S. Department of Energy

MCDONNELL DOUGLAS CORPORATION

Energy Foundation of Texas

Solar Energy

DISCLAIMER

SAN/0499-22
MDC G8214

NOTICE

PORTIONS OF THIS REPORT ARE ILLEGIBLE. It has been reproduced from the best available copy to permit the broadest possible availability.

MDC-G--8214-Rev.

DE83 001647

10-MWe Solar-Thermal Central-Receiver Pilot Plant, Solar Facilities Design Integration:

COLLECTOR-FIELD OPTIMIZATION REPORT (RADL ITEM 2-25)

October 1979
Revised January 1981

DISCLAIMER

This report was prepared as an account of work sponsored by the United States Government. Neither the United States nor the United States Department of Energy, nor any of their employees, makes any warranty, express or implied, or assumes any legal liability or responsibility for the accuracy, completeness, or usefulness of any information, apparatus, product, or process disclosed, or represents that its use would not infringe privately owned rights. Reference herein to any specific commercial product, process, or service by trade name, mark, manufacturer, or otherwise, does not necessarily constitute or imply its endorsement, recommendation, or favoring by the United States Government or any agency thereof. The views and opinions of authors expressed herein do not necessarily state or reflect those of the United States Government or any agency thereof.

ENERGY FOUNDATION OF TEXAS
4800 CALHOUN
HOUSTON, TEXAS 77004

PREPARED FOR THE
U.S. DEPARTMENT OF ENERGY
SOLAR ENERGY
UNDER CONTRACT DE-AC03-79SF10499

PREFACE

This document is provided by the McDonnell Douglas Astronautics Company (MDAC) in accordance with Department of Energy Contract No. DE-AC-03-79 SF 10499, Reports and Deliverables List, Item 2-25. The material contained herein documents work performed at the University of Houston Energy Laboratory under the direction of Lorin L. Vant-Hull.

The original document (released October 1979) provided the design basis for the pilot plant collector field based on a DOE-defined 450 square foot heliostat and initial heliostat reflectivity and receiver absorption performance assumptions (0.86 and 0.93 respectively). This revised document provides expanded information regarding the evolution of the collector field design. Unique performance characteristics resulting from the selection of the Martin Marietta 430 square foot heliostat and revisions in the heliostat reflectivity and receiver performance assumptions (0.89 and 0.95 respectively) are included. It also documents the results of special studies which were in progress at the time of the original publication involving:

- Heliostat aim strategies
- Total receiver power and heat flux distribution
- Effects of cloud passage on receiver power

Major technical contributions were provided by Clifford L. Laurence, Frederick W. Lipps, and Michael D. Walzel. Questions concerning this document should be directed to R. G. Riedesel at (714) 896-3357.

CONTENTS

FIGURES

TABLES

Section 1
INTRODUCTION AND SUMMARY

1.1 COLLECTOR FIELD OPTIMIZATION

The general objective of collector field optimization is to produce the most cost-effective central receiver solar-energy collector. To this end, the size of the receiver and its height above the heliostat field, and the field boundaries and distribution of heliostats within those boundaries are varied. For the optimization to be meaningful, the size and performance of each component must be specified, together with cost scaling relationships valid over the appropriate range.

Since 1973, the University of Houston has been working with McDonnell Douglas to develop the appropriate cost and performance models and the computer codes appropriate to carry out this optimization. Additional computer codes have been developed to define the actual heliostat locations in the optimized field and to compute in detail the performance to be expected of the defined field. This entire arsenal of models and codes has been employed to generate the results reported herein.

Since the objective of the pilot plant is to emulate a commercial system, the optimization process is carried out on a commercial size collector field and receiver and then scaled down to meet the pilot plant design point power level. The optimization process is not sensitive to the aiming strategies and flux distribution on the receiver. Consequently an idealization to the final aiming strategy is used for the optimization work. Once the field is designed, minor adjustments to its boundaries can be made, if necessary, to satisfy thermal power and flux constraints introduced by the receiver design. The final heliostat aim strategy required to distribute the heat flux vertically over the surface of the receiver is determined once the final receiver length has been established.

The aiming strategy used to achieve a satisfactory vertical flux distribution is described in Section 5.2. Section 5.1 describes in detail receiver design data pertaining to the power level on each panel for selected days and times of day throughout the year. The remainder of Section 5 describes other special studies carried out under the contract. Among them are the analysis of receiver transients associated with startup and cloud transits.

1.2 DEFINITION OF THE OPTIMAL COMMERCIAL SYSTEM

The Phase 1 pilot plant preliminary design study completed in June of 1977 provides a complete set of cost and performance models for a 100 MWe central receiver power plant. With a solar multiple of 1.3, this system requires a peak design point power of 560 MW_t incident on the receiver. This system employs an external cylindrical receiver and a surround field of essentially square, silvered glass, inverting heliostats. As a result of this revised cost model, more powerful optimization techniques, and an unrestricted optimization, it was determined, using heliostat costs appropriate to an early commercial plant, that a receiver height of 184 m (rather than the previous 264 m) would be the most cost-effective way to generate the required 560 MW_t incident on the receiver.

1.3 SPECIFICATION OF THE 10 MWe SOLAR THERMAL CENTRAL RECEIVER PILOT PLANT

The Barstow pilot plant is to replicate, as completely as possible in a scaled-down version, the characteristics of the optimized commercial system. During the Phase 1 study, it was shown that direct application of the optimization procedures to a 10-MWe scale/pilot plant would produce a north rather than a surround field because of the high pilot plant heliostat costs and the low cost of the relatively short tower. Consequently, the approach must be to optimize the commercial plant and then to design a pilot plant that retains as many of the significant features of the commercial plant as possible. In the Phase 1 study, hydro/thermodynamic scaling laws were applied to the commercial receiver to specify a pilot-plant receiver diameter of 23 ft (7 m) and a length of 41 ft (12.5 m), which has since been increased to 45 ft (13.7 m) to accommodate higher required power levels. Although this receiver is relatively narrower than the commercial receiver, the use in the pilot plant of canted segment heliostats rather than flat heliostats results in a substantially improved beam interception from an equivalent point in the

field. The heliostat field associated with this receiver in the Phase 1 study consisted of 1706 heliostats, 408 ft^2 (38 m^2) in area. This would correspond to 1547 of the 450-ft^2 (41.8 m^2) nominal heliostats defined by Sandia, were all other factors to remain constant; however, including an allowance for dust accumulation and degradation, currently attainable values for heliostat reflectivity are 5.5% lower and for receiver absorptivity 2.1% lower. In addition, the defined value for insolation at the design point is reduced by 5.5%, the design point shifted to time when the field efficiency is reduced by 12%, and a requirement for rated operation with one field controller down reduces the field effectiveness by 1.6%.

The overall effect of these revisions in the requirements since Phase 1 increases the required number of heliostats by nearly 30%, from 1547 to 2000.

The ideal approach to defining the pilot plant would be to start with a design for a fully optimized 100 MWe early commercial plant, apply appropriate requirement corrections, such as those listed above, and then simply compute the receiver height for a similar field by scaling as the square root of the required power level. This procedure results in a requirement for a 200-ft (60 m) receiver centerline elevation, and a heliostat field area of 140 acres (0.56 km^2). In fact, because of the need to file an environmental impact statement, obtain appropriately located soil samples, and freeze certain aspects of the design, the tower height was specified as 260 ft (80 m) from grade to the receiver centerline, it was located somewhat too far to the south, and the area available for heliostat placement was restricted to approximately 100 acres (0.40 km^2).

Fortunately, the taller tower allows closer packing of the heliostats without excess blocking, with the result that the required power can be provided from the designated field. However, it was necessary to severely restrict the boundaries allowed to the commercial field in operating the optimization code. In this sense, the pilot plant is representative of a repowering application, where a non-optimum but cost-effective system has been designed to produce a specified power from a limited land area of specified shape.

After the appropriate procedures had been followed, the final field using the nominal 450-ft^2 (41.8 m^2) heliostat required 1910 heliostats. Thus, applica-

tion of our improved optimization, field design, and layout procedures resulted in a heliostat number 4.5 percent smaller than predicted by the scaling relationships indicated earlier.

1.4 VOLUME OVERVIEW

1.4.1 Section 2. Definition of 100-MWe Commercial Baseline System

Section 2 describes the range of capabilities of the available optimization and performance codes. Some idea of the limitations of the codes is introduced, and references to more lengthy descriptions of the various components of the codes are given. Both the cellwise structure used in the optimization process and the actual radial-stagger array of heliostats assumed in all the current work are defined. The various loss models included in the analysis are described, including atmospheric attenuation, heliostat absorptivity and receiver reflectivity, thermal losses, etc.

The role of the optimization code in the definition of the pilot plant is specified, with a complete description of the optimization process itself relegated to Appendix A. For current purposes, the primary output from the optimizer is a set of curve fit coefficients to the heliostat spacing data that is delivered to the layout program.

The detailed cost model used by the optimizer for the commercial system optimization is presented in the form of equations relating the cost element to each of the factors that determine it.

The design basis for the commercial system is presented together with the rationale for its selection. The many input requirements to define the site, insolation, and field of configuration are also specified. The results from the unrestricted optimization run are presented and described in the form of a series of outputs from the computer run defining the nth commercial plant.

Finally, this section presents the procedures used in moving from this unrestricted nth commercial system to an early commercial system, an early commercial system constrained to a geometry identical to that of the pilot plant, and finally such a system forced to a power level scalable to satisfy the

pilot plant requirements. This process ends, once the plant to be emulated has been defined, with a special run that produces the information required by the layout processor described in Section 4.

1.4.2 Section 3. Development of the Individual Heliostat Performance Code

The optimizer and the standard performance code are both cellwise in structure. That is, a lattice consisting of about 250 cells is generated, and the performance of all heliostats in a cell is represented by a heliostat at the center of that cell. This procedure is adequate for conceptual and preliminary design studies, but for a final design, a more careful look at the performance of each heliostat surrounded by exactly located neighbors is required. In addition, the more accurate representation of the field generated by the layout processor is required to present a true picture of system performance, particularly in the vicinity of discontinuities such as roads, boundaries, and internal slip planes. The individual heliostat (IH) code was used successfully in defining the precise scaling relationship to the pilot plant needed to provide the required power level.

The IH code is ideally suited for accurately generating the power to each receiver panel vs time for the design of receiver controls. However, at the time these results were needed, the full capabilities of the annual program had not yet been incorporated into the IH code, so the panel power output was generated from the cellwise performance code.

Use of the IH code in a completed study of receiver panel power under sunrise startup conditions is described. Because of the low solar elevation, 50 rather than 8 neighbors are investigated for shading or blocking interactions. A cloud cover study currently underway could have been performed using the IH code, but the very coarse structure of the available cloud transmission function data led to a decision to use the cellwise performance model. As cloud passage is essentially instantaneous, compared to changes in shading, blocking, and cosine, the sun is held fixed during the cloud passage. Consequently, the routine is very fast and a variety of "clouds" and directions of approach can be run. Preparations have been made for generating the panel power associated with each of 60 defined segments of the collector field. This will be accomplished by dividing the field into 12 equal (30 deg) sectors and summing the power from appropriate circles of heliostats.

1.4.3 Section 4. Collector Field Layout for the SFDI Pilot Plant

Section 4 consists of two parts. Part 1 describes the procedure whereby performance and heliostat spacing data from the representative commercial-scale system are converted into coefficients of use in the layout processor. The objective is to emulate as closely as possible the performance, i.e., the shading and blocking losses, for each region of the field. Since the heliostat array is radial-stagger, the local heliostat azimuthal separation is defined by its radial location, and hence is a constrained rather than a free variable. The more sophisticated technique described here responds to this constraint and acts to match as closely as possible the local performance associated with the optimization.

Part 2 describes in detail the actual procedure used in the layout processor. This processor must define the radius of subsequent circles subject to the loss and azimuthal constraints. It then strings heliostats on the circle in the radial-stagger configuration, subject to boundary and road constraints. If the azimuthal separation becomes less than optimal, a slip plane is defined at which every fourth heliostat is deleted to relieve the strain. Six adjacent heliostats are also slid by defined amounts along their respective circles to minimize the chaos and associated excess shading and blocking at the slip plane.

Various controls exist to adjust the starting and transition points and to delete specified heliostats from the output coordinate file. In practice, the layout processor is very fast, and exists as a subroutine to the individual heliostat performance code. The inputs to the code are described in detail in Appendix B.

1.4.4 Section 5. Special Studies

In support of the pilot plant design, numerous special studies were required by the SFDI. Each of these is described in Section 5.

The power to each panel of the receiver at 42 instants in time was delivered early in the study in support of controls development. The cellwise model was used.

Several allowable heliostat aim point shifts and the resulting receiver flux distribution were delivered in support of the development of an aim strategy responsive to the conflicting requirements of low spillage, low peak power, no regions of negative net power on the receiver, and a finite number of predefined aim points.

The individual heliostat program was used to deliver a series of panel powers for eight closely spaced times near 10-deg solar elevation (startup) on equinox and 1 month from summer solstice.

The cellwise model was equipped with a subroutine to advance a cloud front (specified by Aerospace from measurements at Barstow) over the field in any direction while holding the sun fixed at any position. Detailed study results for representative clouds are presented.

1.4.5 Appendix

The three appendixes provide, for the more dedicated reader, an adequate description of the optimization theory, the layout procedure, and the individual heliostat code. While the casual reader may not benefit from studying these sections, it may be profitable for him to skim them when he reaches the appropriate point in the main text.

1.4.6 Conclusion

The procedures and codes described in this report have led to the definition of a collector field for the 10 MWe Solar Thermal Central Receiver Pilot Plant. This field is specified in SAN/0499-18, Collector Field Layout Specification (RADL item 2-12). While this field was designed to accommodate the 450-ft^2 (41.8 m^2) heliostat defined by Sandia, it will be implemented using either a Martin 430-ft^2 (40 m^2) or a McDonnell Douglas Astronautics Company (MDAC) 479-ft^2 (44.5 m^2) heliostat.

Using the oversized (relative to 450 ft^2) MDAC heliostat will result in an increase of 1.42% in shading and blocking at the design point, while the undersized Martin heliostat enjoys a decrease of 1.48% in shading and blocking. These effects accrue only because the same foundations are specified for all three heliostats. Were the foundation spacings expanded to maintain

the same ground coverage, the field areas and shading and blocking losses would be essentially identical.

The field defined in this work meets all the imposed requirements and restrictions. It is not representative of a cost-effective 10 MWe commercial system - such a system would probably use a north field configuration. Because of the constraints imposed and the use of currently available absorptivity, reflectivity, etc., a more cost-effective commercial system than the one emulated here could readily be designed. Whether this would produce a cheaper pilot plant design is neither clear nor important at this time. The restrictions are real, an effective pilot plant has been defined that satisfies them, and construction of the plant is under way.

Section 2
DEFINITION OF A COMMERCIAL SYSTEM

2.1 INTRODUCTION

In keeping with the purpose of the pilot plant to be representative of future commercial scale systems, the optical design of the pilot plant is based on scaling from an updated commercial system design. It was deemed necessary to update the commercial system design because considerable improvement and revision of cost and performance models and of computer codes representing performance and optimization theory have been made since completion of the previous optimization studies. These studies led to the commercial system design published in the Phase 1 Final Report of 1977 (1). Some of the cost and performance models used in the optimization studies described in reference (1) were frozen in 1975 and the remainder in 1976, and although they were updated for the final report, the optimization itself was not udpated. Several more-recent studies of advanced systems, hybrid systems, and small systems have revealed new possibilities for improved performance in relation to cost. A pertinent example of this is the required tower height. In 1977, the design of a system with a nominal nameplate capacity of 100 MW electric required a 242-meter tower. More recent analysis techniques combined with revised cost data have shown that the design of a system of this size can be based on a 180-meter tower. It is also necessary for the purpose of proper scaling to pilot plant size to introduce currently attainable values for pertinent performance factors such as heliostat reflectivity, receiver absorptivity, and convection and reradiation losses.

This section will present all the pertinent parameters used to form the new commercial system design and the indicated cost effectiveness of that design. A discussion of the comprehensive computer performance models and system cost models used in the design work is included. It was necessary to apply a set of restrictions to the commercial design to facilitate proper scaling to existing pilot plant physical constraints. The impact of these restrictions is presented.

The next important step in the design process is the scaling and application of the commercial system design parameters to the design of the pilot plant system. A detailed discussion of this will be given, including the application of additional physical constraints required for the pilot plant. The use of output parameters from the computer codes to derive actual heliostat locations will be discussed in detail in separate sections.

The optical properties of the pilot plant design, such as heliostat focusing, heliostat aiming and tracking, heliostat shading and blocking, receiver interception, and receiver flux distribution, are closely representative of future considerations for large-scale system design and control. Notwithstanding the obvious economics of large-scale mass production, because of physical constraints (field size, tower location, receiver size, tower height, etc.) the plant is not fully representative of the cost/performance potential of central receiver systems. Considerable additional economy can be realized from designs with fewer arbitrary constraints.

2.2 SYSTEM PERFORMANCE MODELS

Almost every aspect of central receiver optical performance is carefully and extensively modeled in the University of Houston computer codes. These models have been developed over a period of several years, starting in 1973. During this time the theory and implementation of these models have been documented in a large number of contract technical reports, publications, and conference proceedings. Space does not permit inclusion of all the modeling in this report. A descriptive summary of the models will be given here, together with appropriate references. An exception to this is the optimization theory. Because of the importance of this theory in determining the layout of heliostats in a field design, a complete description (although brief) is given in Appendix A. This will also serve to supplement the discussion of commercial system optimization to be given later in this report.

2.2.1 Solar Models

The diurnal motion of the sun is described sufficiently to permit solar azimuth and elevation to be established to within 0.1 degree as a function of solar time. The analysis is given by Pitman and Vant-Hull (2) and in Technical Addendum 8 of reference (3).

While our programs can accept solar data, or compute instantaneous direct-beam solar intensities based on current meteorologic data, their primary requirement is for data representative of long-term (30 year) averages so the resulting system design will not be influenced by a specific, perhaps anomalous, year. Consequently, site-specific, long-term, monthly mean values of atmospheric contaminants such as water vapor, dust (turbidity), and clouds are used in the model. For this defined atmosphere, the programs compute the attenuation of the seasonally adjusted extraterrestrial solar intensity along the instantaneous slant path from the top of the atmosphere to the elevation of the site. Performance is reported under cloud-free conditions, while for optimization purposes the monthly integrated insolation is modified by the mean monthly percent of possible sunlight (a cloud-cover correction) for the specific site. The insolation models are discussed in Technical Addendum 9 of reference (3).

The profile of the limb-darkened solar image is accurately represented by appropriate numerical equations. This representation is given in detail in Technical Addendum 18 of reference (3). The use of the solar image will be discussed further under the topic of image generation.

2.2.2 Collector Field Models

There are two fundamental schemes for field representation; the cell model with representative heliostats and the individual heliostat model. The cell model is used most extensively for design analysis where, for economy of computation, it is necessary to sample the anticipated extent of the collector field. The individual heliostat model represents the exact locations of heliostats in the field and determines the contribution to performance of each heliostat. For practical computer core storage limitations, several thousand individual heliostats can be represented. The individual heliostat model provides the most definitive look into system performance. Almost all the performance models discussed here are available in computer codes for both cellwise and individual heliostat representations. Exceptions are, of course, the optimizer, which can function in only a cellwise manner, and the output of the image forming code (node file), which is also cellwise. A node file represents the fraction of energy available on each node of a receiver

from each cell in the field. To date it has not seemed practical or even necessary to create node files on an individual heliostat basis. Currently, there is an interpolation procedure available that enables the individual heliostat code to interpolate from a cellwise node file to generate receiver performance data on an individual heliostat basis. Used in conjunction with the individual heliostat shading and blocking routines, this represents the highest level of sophistication available for system performance analysis.

2.2.3 Heliostat Models

The variety of heliostat types that can be accommodated by the computer codes is closely connected to the level of generality in the image-generation codes and in the shading and blocking codes. The image-forming codes determine the types and shapes of reflective surfaces that can be analyzed and the shape of the heliostat boundary. The shading and blocking code also determines the shape of heliostat boundary that can be processed. Generally, any heliostat with a boundary formed by a regular n-sided polygon or by a rectangle can be accommodated. The reflective surface can be curved or it can be segmented with flat segments that are canted (tilted) with respect to the heliostat primary plane for image focusing. The current practical limit to the number of segments is 12. The image code execution time is proportional to the number of segments.

2.2.4 Image Generators

Image generation refers to the process of finding the flux distribution on a receiver due to one heliostat or any number of heliostats located in a collector field. In the process of doing this, one also determines the fraction of energy the receiver actually intercepts to that redirected to the receiver vicinity. The heliostat flux density problem has been treated in some detail in several published papers and many technical reports by Lipps, Walzel, and Vant-Hull. The technical reports are references (3-5) and published papers are references (6-8).

Image generation is available in two forms: (1) the analytic model, and (2) the Hermite polynomial approximation. For most analytical situations, the latter is used, because it affords a much greater economy of computer

time, and the accuracy of the analytic method is seldom required. The analytic method is based on an exact solution to the flux density integral. With this method, the flux density from a heliostat is determined from a numerical integration over the solid angle of incoming rays. This is applicable to flat heliostats with polygonal boundaries (8). Several alternative formulations have also been developed (6). The Hermite function expansion provides a close approximation to the analytic integration operating at one-tenth the computer time (7). With this speed, it is possible to treat the multisegmented heliostat by running the code for one segment and superimposing the result according to displacement in the image plane resulting from non-ideal canting and off-axis aberrations.

The most common output required from the image-generation code is a node file. A receiver can be divided into a number of nodes by subdivision in both the horizontal and vertical directions. Core storage limits the number of nodes to about 1000. Typically, for a cylindrical receiver, 456 nodes will be used, 24 in the horizontal direction (around the cylinder) and 19 in the vertical direction. The node file is run for a specified ratio of cell size to tower height (the optical phenomina depend only on the angles, not the actual field and tower dimensions) and for a selected day of the year and time of day. The node file represents the fraction of the energy reaching the plane of the receiver that would be intercepted by each node from each cell in the field. The number of cells and location of the tower in the cell structure must be specified. Typically there are 14 rows of cells north to south and 15 rows east to west, with the tower in the ninth row from the north and in the central column from east to west. Thus, a node file might consist of 96,000 values. When the file is summed over nodes, the fraction of energy intercepted by the receiver to that delivered into the receiver region is formed. These are called FINT's and are represented in the theory by η. These purely geometrical quantities can also be modified by the atmospheric attenuation between the heliostat and the receiver to form modified FINT's. Their role is vital in the optimizer theory discussed in Appendix A.

The node file is formed for a specified set of heliostat aiming conditions and is used to produce maps of the flux distribution on the receiver. A variety of aim points can be chosen and the images can be shifted on the receiver in proportion to the image size. This permits aiming to achieve more-uniform flux distributions without appreciable increases in interception losses.

2.2.5 Shading and Blocking Model

An exact analytical formulation has been made for the shading of the active area of a heliostat by its neighbors and for the blocking by its neighbors of the energy redirected toward the receiver (3,4,9). In all cases, cosine of angle of incidence on the heliostats is implicitly included in the following discussions of shading and blocking and of cell efficiency. The examination of insolation-weighted annual average shading and blocking data for a large number of heliostat packing configurations led to the identification of radial-stagger as the most efficient method for positioning neighboring heliostats. A generalized program for the study of shading and blocking called the LOSS program was developed using the shading and blocking code. The results of this study are reported by Lipps on page 249 of reference (10). The radial-stagger configuration is illustrated in Figure 2-1. The heliostats are placed on alternate intersections of concentric circles centered at the tower and radial lines intersecting the tower. The radial spacing, R, is the distance between heliostats along a radial line, and the azimuthal spacing, Z, is the distance between heliostats along a circle. Unless otherwise specified, the current shading and blocking code determines the fraction of energy lost from a heliostat due to shading and blocking by neighbors whose spacings are R and Z and whose relative locations are given by radial-stagger.

An important example of the use of shading and blocking is in the formation of a shading and blocking data base for the optimizer. The optimizer will be selecting optimum values for R and Z for the cells in a field. To do so it must know how the cell efficiency varies as a function of R and Z. An insolation-weighted annual average of cell efficiency is used. The cell efficiency must include shading and blocking, but this cannot be expressed as an analytic function. Therefore, a numerical data base of cell efficiency factors is formed based on a set of four variations for both R and Z from the nominal values of R and Z for each cell. The usual variations are ±5% and ±15%. Thus,

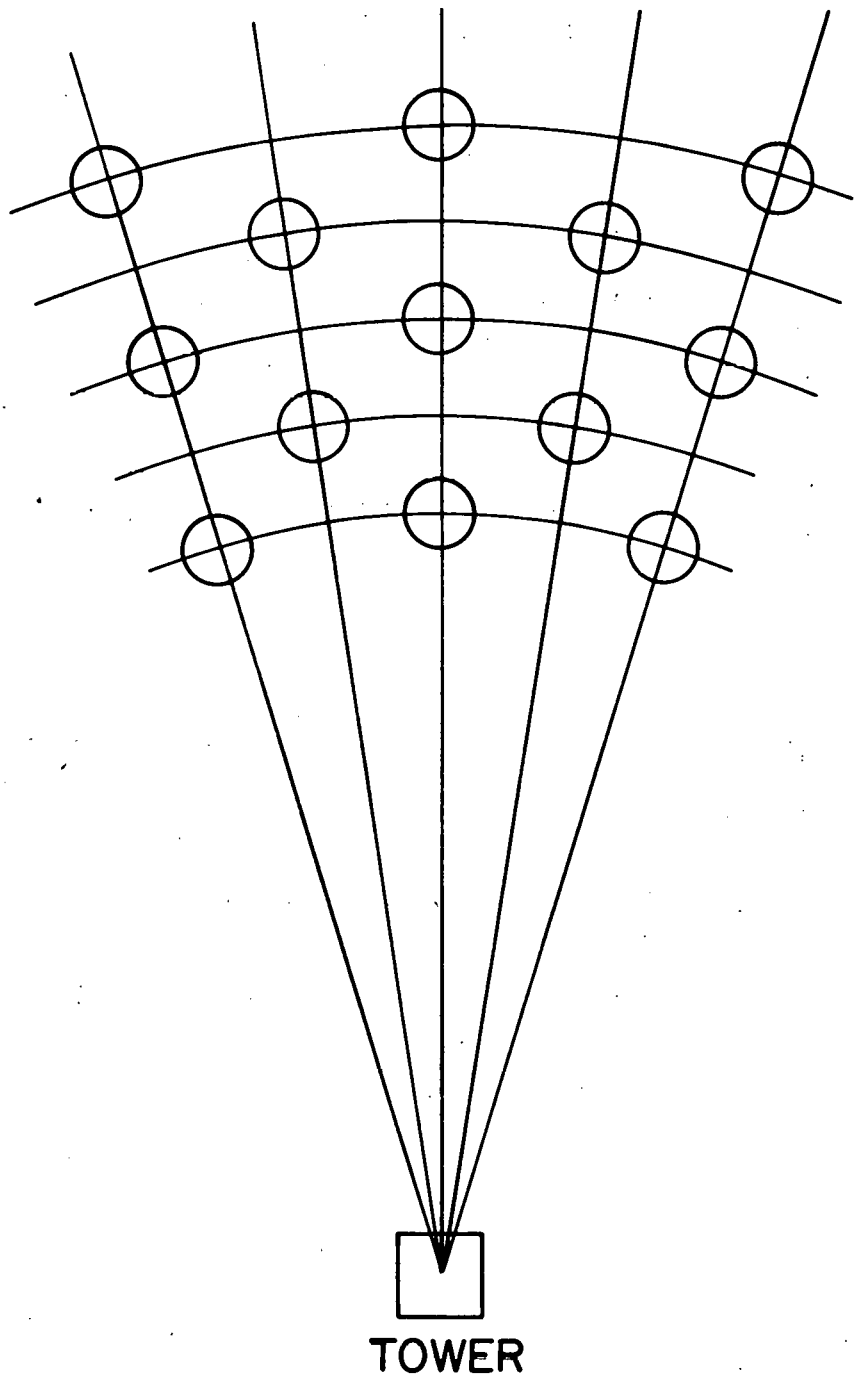

Figure 2-1. Radial-Stagger Heliostat Packing Configuration

the optimizer will have numerical values for cell efficiency over a reasonable range of possible values of R and Z. In Appendix A, the insolation-weighted cell efficiency function, including both cosine and shading and blocking effects, is denoted by λ.

2.2.6 Atmospheric Attenuation

Atmospheric absorption is a loss factor depending on the slant range from heliostat to receiver. In all analyses, atmospheric losses are included. Estimates of the losses are made from computations using a detailed computer simulation of atmospheric absorption developed by the Air Force Cambridge Research Laboratories (11). For large systems, the atmospheric attenuation amounts to about 1% plus 5% per kilometer of slant range. In the computations, atmospheric attenuation is combined with interception fractions and the shading and blocking (and cosine) data to form a net efficiency for each cell to get energy onto the receiver. Thus, atmospheric attenuation is usually reported in conjunction with interception fractions.

2.2.7 Energy Loss Models

Values for the following efficiency factors are entered as input to the computer programs:

A. Effective heliostat reflectivity (dust, aging, etc., included)

B. Effective direct-normal receiver absorptivity (the effects of angle of incidence are included in the computer code).

C. Mean receiver reradiation per m^2

D. Mean receiver convection losses per m^2

2.2.8 Optimization Process

The optimization process is the fundamental procedure for determining the most cost-effective layout of specified heliostats in a collector field for a given cost model, tower height, and receiver size. The optimization process is contained in the RCELL computer code. Additional processors called CELLAY and LAYOUT are required to convert the output of the RCELL program to actual heliostat locations. The use of CELLAY and LAYOUT are discussed in the section on pilot plant layout. The theory of the optimization process is presented in detail in Appendix A.

The actual input data used to design the commercial system and the output data produced by the optimizer will be discussed in the section on commercial system optimization.

The optimization computer code requires as input data a node file, a shading and blocking data base, the basic geometry of the system, the various loss factors for the system, and the cost factors required by the cost model. The cost model is presented in the next section. The optimization also requires as input an estimated figure of merit, which is the ratio of total system cost to annual energy produced. From this, the optimizer will form a set of optimized heliostat spacings (R and Z) for each cell and will perform a two-dimensional curve fit, using as independent variables the receiver elevation angle and cell azimuth. Experience has shown that the optimized heliostat spacings can be accurately represented in the form

$$R(\theta,\phi),Z(\theta,\phi) = \frac{C_1}{\theta} + C_2 + C_3\theta + \left(\frac{C_4}{\theta} + C_5 + C_6\theta\right)\cos\phi$$

where θ is the receiver elevation, ϕ is the cell azimuth and C_1 - C_6 are the curve fit coefficients. This reduces the large set of heliostat spacings to a few curve fit coefficients and provides an interpolation to smooth the transition from cell to cell. The curve fit coefficients are used by the layout code to form the actual heliostat locations. (Note: here R and Z are in meters, but in all other papers and in Appendix A they are given in heliostat widths, D_H, for scaling convenience. Therefore, wherever they appear, a factor D_H also appears).

2.3 SYSTEM COST MODELS

For the purposes of the optimized design process to be discussed in the next section, the total system cost, C_S, including operations and maintenance, is represented by

$$C_S = C_F + C_T + C_R + C_D + C_P + C_L + C_H + C_1 + C_2 + C_3 \qquad (1)$$

where the subscripts refer to the costs of the following subsystems:

F - Fixed costs (computer, buildings, beam characterization, etc.)

T - Tower R - Receiver D - Riser/downcomer

P - Feedpump L - Land H - Heliostat

1 - Primary feeders (trenching, cabling, installation, operations, maintenance)

2 - Radial headers (trenching, cabling, etc.)

3 - Azimuthal branches (trenching, cabling, etc.)

The fixed costs (C_F) are a lump estimate of all costs that would not vary significantly as a function of plant design, but would be estimated on the basis of costs expected for plants in a general size range.

The tower cost (C_T) including accessories can be input as a fixed number, or, if some variation of tower height is to be investigated, it can be estimated from a numerical fit to cost estimates of several different commercial system towers given by,

$$C_T = C_t \left(\frac{H_T - 22}{200\ \text{m}}\right)^{1.875} \quad \text{M\$} \tag{2}$$

where H_T is the focal height in meters (vertical distance from the plane of the heliostats to the receiver centerline) and M\$ is 10^6 \$.

The receiver cost, C_R, has been estimated from designs chosen at various power levels. The receiver cost has been determined to be essentially independent of receiver size (for small ranges) but is scaled according to the design point equinox noon power level as determined in the optimizer code. The numerical scaling equation is

$$C_R = C_r \left(\frac{P_q}{506.5\ \text{MW}}\right)^{0.62} \quad \text{M\$} \tag{3}$$

where p_q is in megawatts.

The cost of the riser/downcomer, C_D, is scaled according to tower height and system power level by

$$C_D = \left[C_u \frac{(H_T-9)}{255\ m} + C_d \frac{(H_T+19)}{283\ m} \right] \left[1 + \frac{(H_T+24)}{800\ m} \right] \left[\frac{P_q}{506.5\ MW} \right]^{0.62} M\$ \qquad (4)$$

The term in the second bracket accounts for increases in assembly and installation time with height, and is mainly due to transit time effects (both for material and for workers).

The feed pump cost is also scaled according to tower height and system power level. The numerical equation fitting the cost data is given by

$$C_p = C_P \left[\left(\frac{P_q}{506.5\ MW} \right) \left(\frac{H_T+66}{330\ m} \right) \right]^{0.62} M\$ \qquad (5)$$

The cost of land, C_L; cost of heliostats, C_H; and cost of wiring (both data and power), C_{1-3}; are built into the differential equations of the optimizer theory and are considered in the tradeoff between cost factors and performance capability. As shown in Appendix A, the solution for optimized conditions includes the cost factors, which depend on the area of land required (field boundary), the area of glass required (number of heliostats, cleaning materials, washing, maintenance), and the spacing from tower to heliostats and between heliostats (wiring, trenching, cabling, operations and maintenance).

The cost of land, C_L, is given by

$$C_L = C_\ell A_L \sum_c \phi_c \qquad (6)$$

where

C_ℓ = cost of land in \$/m

A_L = area of a cell

ϕ_c = fraction of the cell within the field boundary

The quantity ϕ_c is determined by the optimizer and can have values of 0,1/4,1/2,3/4, and 1. For $\phi_c = 0$, the cell is outside the field, $\phi_c = 1$, the cell is inside the field, and for $\phi_c = 1/4, 1/2$, or 3/4, the cell is on the boundary.

The cost for heliostats is determined from

$$C_H = C_h A_L \sum_c \phi_c f_c \tag{7}$$

where

C_h = cost of heliostats in \$/m (including fabrication, shipping, installation, gimbals, drives, internal wiring, etc., and the present value of that portion of operations and maintenance costs depending on the number of heliostats, such as primary drive repairs and washing solvents)

f_c = ground coverage fraction in each cell (ratio of the total glass area in a cell to area of the cell)

The cost of wiring from a central location to the primary stations (transformers, controllers) is called primary feeder cost and is given by

$$C_1 = C_{w1} N_L \sum_c \phi_c f_c r_c \tag{8}$$

where

C_{w1} = cost of primary feeders for data and power in \$/m/heliostat (including cabling, trenching, and installation, and the present value of that portion of operations and maintenance costs depending on the time spent in traveling to a specific heliostat circle)

N_L = A_L/A_H = maximum number of heliostats per cell
(A_H = area of a heliostat)

r_c = radial distance from the tower to cell c in meters

The cost of wiring from the transformers radially inward and outward to the strings of heliostats is called radial header cost and is formed from

$$C_2 = C_{w2} N_L \sum_c \phi_c f_c R_c \qquad (9)$$

where

C_{w2} = cost of radial headers for data and power in \$/m/heliostat (including cabling, trenching, and installation).

R_c = radial heliostat spacing in meters

The cost of wiring from a radial branch along a row (or circle) of heliostats is called azimuthal branching cost and is given in the cost model by

$$C_3 = C_{w3} N_L \sum_c \phi_c f_c Z_c \qquad (10)$$

where

C_{w3} = cost of azimuthal branches for both data and power in \$/m/heliostat (including cabling, trenching, and installation, and the present value of that portion of operations and maintenance costs depending on the time spent in traveling azimuthally along a specific heliostat circle, particularly in washing the heliostats)

Z_c = azimuthal heliostat spacing in meters.

The optimizer uses the performance models and cost factors such as C_ρ, C_h, C_{1-3} together with an input figure of merit, F_i (see Appendix A, F_i is used to form the cell matching parameter $\hat{\mu}$) to determine a set of new cell spacings, R_c and Z_c, which will minimize the output system figure of merit. The performance data and cost model (equation 1), are used with the new set of spacings to determine the optimized (output) system figure of merit, F_o.

2.4 COMMERCIAL SYSTEM OPTIMIZED DESIGN

2.4.1 Introduction

The collector system design is carried out in two phases. The goal of the first phase is to establish a best design based on the presently established commercial system surround field configuration, projected overall performance parameters (absorptivity, reflectivity, etc.), projected early commercial plant cost goals, and present, unrestricted, capability of the University of Houston Central Receiver design optimization computer codes. The goal of the second phase is to design a commercial system that can be scaled in a straightforward manner into a pilot plant design that meets presently existing site restrictions, and design and performance requirements. The scalable commercial design is "optimized" within the scope of the existing restrictions. The results of the first-phase, unrestricted, collector system design are used in conjunction with presently attainable performance parameters, first plant cost estimates, site-restricted trim boundary, receiver total flux requirements, etc., to establish a scalable collector system design. By referring to the best system design, we can assess the impact on cost/performance capability of the applied restrictions. Within the design characteristics of the pilot plant (tower height, receiver size, field boundary, and congruence to the early commercial design), the final layout of heliostats will deliver the maximum possible daily and annual energy from the least number of heliostats of a given size.

The scale of the commercial system design is based on a nameplate rated system output of 100 megawatts electric (MWe). The Phase I Central Receiver Solar Thermal Power System Studies (1) indicated that a system of this size could be based on a cylindrical receiver 25.5 m high with a diameter of 17.0 m mounted on a tower at a centerline elevation of 264 m above grade, or 260 m above the heliostat axis (the focal height). Subsequent unrestricted studies based on final Phase I cost models (12) demonstrated that, all else remaining the same, focal height scales to the 1.36 power of equinox noon thermal power level. Without restriction, a 260-m tower produced 735 MW thermal, and 560 MW thermal are required from the present best commercial design. Thus, the required tower height is approximately

$$260 \text{ m} \left(\frac{560 \text{ MW}}{735 \text{ MW}}\right)^{1.36} = 179.7 \text{ m}$$

Consequently, the basis for this reexamination of the commercial system is a

tower focal height (H_T) = 180 m

and a

receiver height = 25.5 m

receiver diameter = 17.0 m.

2.4.2 Best Commercial System Collector Design

The input parameters used for the commercial collector system design are drawn from results of previous studies, currently existing design concepts (heliostats), early commercial plant estimated cost factors, and long-term weather and insolation modeling. The most important physical characteristics, performance parameters, and cost factors are listed in Table 2-1.

Tower height and receiver size are based on previous studies. Heliostat and receiver structure are based on current design concepts provided by the Solar Facility Design Integrator (SFDI). This existing design is most compatible with commercial system requirements. For the formation of interception fractions, the number of segments, segment surface shape, and canting focal length are significant input parameters. Computer runs show that, for the present design, the glass area can vary by as much as ±10% without significantly affecting the interception fractions. All heliostats have identical segment canting to a focal length that is approximately 75% of the maximum required slant range. It has been shown that canting by flat segments provides adequate focusing, and that very little additional loss is incurred if all heliostats are canted at the same distance (13). This simplification serves to reduce heliostat manufacturing costs. The interception fractions peak when this focusing distance is about 75% of the maximum slant range. Other critical parameters for the collector field design process are the overall height and width of the reflective area, and the clearance radius. Due to shading and blocking effects, the optimal spacing of the heliostats in the field will scale in proportion to the size of the reflective area. Thus, while the optimizer produces a field defined in terms of the effective mirror diameter, the layout processor generates heliostat coordinates appropriate to a particular heliostat size (D_H).

Table 2-1. Best Commercial Collector System Design Basis
(Page 1 of 2)

Physical Characteristics		
Focal Height		180 m
Receiver Size	Height	25.5 m
	Diameter	17.0 m
Receiver Lateral Partitioning		24 panels total (4 preheater, 20 boiler)
Panel Area (each)		56.7 m^2
Heliostat*	Glass area	49.05 m^2 (528 ft^2)
Overall glass height*		7.379 m
Overall glass width*		7.417 m
Number of segments*		6
Segment Surface*		Flat
Segment Width*		3.3528 m
Segment Height*		2.4384 m
Design Width (D_H)*		7.3977 m
Minimum Clearance Radius*		5.3033 m
Canting Focal Length		1080 m
Mount axes type		az-el
Image Degradation (1σ) (tracking, surface waviness, mechanical deflection)		2.83 mr (RMS)
Performance Parameters		
Heliostat Reflectivity*		0.90
Receiver Absorptivity		0.95
Allowance for Inactive Heliostats (outages, repairs)		0.992

*Based on advanced low-cost heliostat design information

Table 2-1. Best Commercial Collector System Design Basis
(Page 2 of 2)

Allowance for translation from the cell structure to actual heliostat layout (additional shading and blocking)			0.971
Receiver Radiative and Convective Losses			
Per Preheater Panel			580 KW (10 kW/m^2)
Per Boiler Panel			1160 KW (20 kW/m^2)
Cost Inputs			
C_F	= 5.22	fixed	M$
C_ℓ	= 1.49	land	$\$/m^2$
C_{w1}	= 0.0412	wire	$/m/heliostat
C_{w2}	= 0.4237	wire	$/m/heliostat
C_{w3}	= 14.25	wire	$/m/heliostat
C_h	= 100.0	heliostat	$\$/m^2$
C_t	= 4.95	tower	M$
C_r	= 14.87	receiver	M$
C_u	= 0.553	riser	M$
C_d	= 1.155	downcomer	M$
C_p	= 1.655	feed pump	M$

The resulting heliostat spacings are only truly optimized for that particular heliostat size. Additional sensitivity studies are required to determine the performance or cost sacrifice of using an alternative heliostat in a field designed for another heliostat. The minimum-clearance radius determines the highest heliostat packing density. It is determined from the circle formed by the farthest corner of the reflective area as the heliostat pivots in azimuth while the mirror surface is parallel to the ground. An additional

20 cm is added to the radius to ensure physical clearance between heliostats. For cells very near the tower, the optimum spacings may be less than those required by the clearance limit, and the optimizer defaults to the minimum spacing.

The heliostat reflectivity is slightly optimistic for presently existing low-cost heliostats but is a realistic 10th plant goal. The allowance for translation from cell structure to actual heliostat layout is based on previous design studies and is the ratio of shading and blocking losses at the design point, as calculated within the cellwise optimizer, to the shading and blocking losses determined by the individual heliostat performance computer codes. Radiative and convective receiver losses were estimated by the receiver designer based on average operating temperatures and wind velocities.

The cost factors have been estimated by the SFDI. All costs are based on 1978 dollars. The fixed costs, C_F, include beam calibration equipment, design and support engineering, the added costs of the master controller, and 50% of the solar engineering and design costs.

The cost of land is based on projected values for desert land, with access roads, and water and power lines in place, and includes an allowance of \$1045/acre ($\$26¢/m^2$) for yardwork and contingency on the heliostat field.

The cost for wiring, C_W, Type 1 is for primary radial wiring from the tower to each of the main field distribution points and includes 4160-volt cable at \$6.69/m, data link (optical fiber) at \$0.31/m, trenching at \$5.50/m, and installation at \$0.85/m. Type 2 costs are for the radial headers going to each heliostat array controller (typically taken as 14 per field transformer, each feeding a string of 24 heliostats). The costs include low-voltage armored cabling at \$2.56/m, optical fiber data link at \$0.31/m, plowing in of the cable at \$2.00/m, and installation costs of \$0.85/m. Type 3 wiring costs are multiplied by the azimuthal distance between heliostats and include the final serial string branch wiring as well as the present value of the operations and maintenance (PV of O&M) costs associated with time spent in traveling along the circles while washing heliostats and performing other scheduled

maintenance functions. The wiring costs per meter are identical to the Type 2 costs, resulting in a charge of \$5.72/m. The O&M costs per heliostat are \$6.60 for the first year and \$5.70 for subsequent years, resulting in a PV of O&M of \$131 per heliostat. For the mean azimuthal separation between heliostats, this converts to \$8.53/m. Thus, the total Type 3 cost is \$14.25/m.

The optimization process is based on a heliostat cost \$ (C_h) of \$100/m^2. This includes PV of O&M of \$11.84/m based on the costs per heliostat of unscheduled maintenance (\$40.70 for the first year, \$17.10 for subsequent years) and cleaning and maintenance materials (\$0.157/m^2 for the first year, \$0.147/m^2 for subsequent years). The resulting PV of O&M is \$415 per heliostat (\$8.48/m^2) plus \$3.36/m^2, or \$11.84/m^2. The remainder, \$88.16, corresponds to approximately 10th plant costs for installed heliostats.

The most critical factors used in forming the annualized insolation model, cell structure, and nodal structure are given in Tables 2-2 and 2-3. In developing an insolation model for design purposes, the emphasis is on long-term data (30 years) insofar as that is available. The year has been divided into twelve intervals and each day into nineteen intervals. For all variables depending on only solar position there are only seven unique days, and the morning and afternoon hours are symmetrical, i.e., it is assumed that the plant will be symmetrical with respect to a north-south line through the receiver center. When the weather model is added in all, twelve days become unique and are included in the averaging process. At present, the weather modeling for design purposes is not time dependent within a day, i.e., morning and afternoon performances are symmetrical. Previous studies have concluded that nearly all useful energy is collected during the time period the sun is above 10.0 degrees in elevation. Earlier or later times are marked by very low direct normal insolation levels and very high shading losses in the heliostat field.

The atmospheric turbidity factors shown in Table 2-3 are based on an interpolation from Flowers (14) "summer" and "winter" values, with the interpolation

Table 2.2 Best Commercial Collector System Optimizer Computational Basis

Insolation model	
Latitude	35 deg north
Sample days	21st of each month
Sample hours in each day	19 points in time concentrated at low sun elevations
Definition of the start and end of each day	10 deg of solar elevation
Hours/year the sun is above 10 deg at lat 35 deg	3697 hours
Monthly atmospheric factors	See Table 2-3
Total yearly direct normal energy; energy based on clear days as reduced by clouds	3.092 MWh/m^2 2.643 MWh/m^2
Julian day of the vernal equinox for 3/21/1980 (day zero)	2444320
Site elevation	550 m
Radius of the Earth	6370 km
Equivalent thickness of atmosphere	8.430 km
Cell Structure	
Cell size (Order 5)	$\sqrt{5}/2 \cdot H_T = 201.25$ m
Number of rows (north to south)	14
Number of columns (east to west)	15
Tower location (Row 1 is northernmost) (Column 1 is westernmost)	 Row 9 Column 8
Node Structure on Receiver	
Number of nodes	456
Vertical	19
Horizontal	24 (one for each panel)

Table 2-3. Insolation Model Data for Latitude 35° N

Month	Day from vernal equinox	Daily duration (hours)	Percent clear sky	Precipitable water (cm)	Atmospheric turbidity factor (/atm)	Direct normal clear day insolation at noon (W/m^2)	Total direct normal energy per clear day (KWH/m^2)
Jan	307	8.14	0.75	1.524	0.05	917	6.75
Feb	338	9.19	0.75	1.575	0.05	948	7.87
Mar	0	10.35	0.80	1.524	0.05	969	9.04
Apr	31	11.42	0.85	1.651	0.05	970	10.00
May	61	12.22	0.90	1.956	0.07	943	10.25
June	93	12.55	0.90	1.778	0.07	941	10.50
July	124	12.22	0.90	2.235	0.10	907	9.68
Aug	155	11.42	0.92	2.667	0.10	901	8.97
Sept	186	10.35	0.92	2.032	0.10	895	8.08
Oct	216	9.19	0.92	1.905	0.07	907	7.41
Nov	246	8.14	0.85	1.473	0.05	911	6.71
Dec	276	7.69	0.75	1.524	0.05	897	6.25

biased by observed cloud cover and precipitable water values (cloudy humid days tend to have higher turbidity).

Values in the model for precipitable water shown in Table 2-3 are derived from monthly contour maps prepared by the US Department of Commerce (15) showing long-term average precipitable water in the United States.

The fractions of clear sky (one minus the fraction of sky in cloud cover) given in Table 2-3 are taken from sheet A-7 of the National Climatic Atlas of the US (Barstow).

The cell and node structures used in the computations are shown in Table 2-2. The number of cells is chosen to given adequate computational resolution for acceptable computer execution times. The cell order 5 was chosen to provide sufficiently large cells to ensure that the optimized boundary did not overflow the cell structure in the unrestricted design. The use of 24 circumferential receiver nodes is compatible both with computer run times and formats and with a design using 24 panels, while 19 vertical nodes provide more than adequate receiver flux density resolution without undue stress on computer execution time, core storage availability, and data storage availability.

From the heliostat design, tower height, receiver size, and cell structure, the image formation computer code forms the interception fractions for each cell. These are given in Table 2-4. The optimizer code determines the fraction of loss due to atmospheric absorption for each cell. These are given in Table 2-5. The product of these two quantities determines the fraction of energy leaving each cell that is delivered to the receiver. This is represented by the symbol η_C in Appendix A. On the right of each table is a contour plot of the data values given on the left. The symbol, T, denotes the location of the tower. The data are represented by the symbols 1 to 9 and U (for unity). The contour interval is the interval in the data represented by an increment of one in the contour symbol. A symbol appears only when the data "passes through" the corresponding value. Thus, the data never get sufficiently above 1.00 for U's to appear in the plot. Thus, for Table 2-4, 9 represents 0.95, 8 represents 0.90, 7 represents 0.85, etc.

Table 2-4. Interception Fractions For the Best Commercial Collector Design

INTERCEPTION FACTORS FROM RECEIVER PROGRAM * * * * * UNIVERSITY OF HOUSTON AND DOE

8	9	10	11	12	13	14	15	
0.736	0.732	0.715	0.689	0.655	0.615	0.571	0.526	0.
0.825	0.819	0.800	0.771	0.731	0.684	0.632	0.579	0.
0.904	0.898	0.880	0.849	0.807	0.754	0.694	0.632	0.
0.961	0.957	0.943	0.915	0.874	0.818	0.754	0.684	0.
0.990	0.988	0.980	0.962	0.927	0.874	0.806	0.731	0.
0.999	0.998	0.995	0.986	0.962	0.915	0.849	0.771	0.
1.000	1.000	0.999	0.995	0.980	0.943	0.879	0.800	0.
0.997	0.999	1.000	0.998	0.988	0.957	0.898	0.818	0.
0.	1.001	1.000	0.999	0.990	0.961	0.903	0.823	0.
0.999	1.000	1.000	0.998	0.988	0.956	0.896	0.817	0.
1.000	1.000	0.999	0.995	0.979	0.941	0.877	0.798	0.
0.998	0.997	0.994	0.984	0.959	0.912	0.846	0.768	0.
0.987	0.984	0.976	0.958	0.922	0.869	0.802	0.728	0.
0.954	0.950	0.936	0.909	0.868	0.813	0.749	0.681	0.

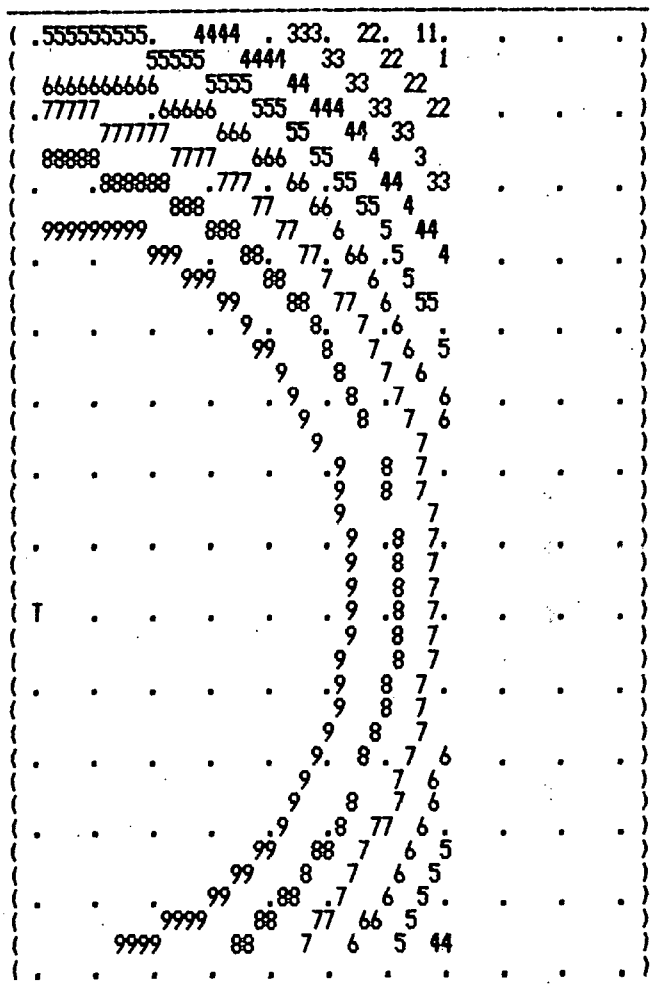

CONTUR INTERVAL = 0.050

0. 0. 0. 0. 0. 0. 0. 0. 0.

NOTE: IN GENERAL AVERAGES ARE WEIGHTED BY THE AMOUNT OF GLASS IN EACH CELL.

Table 2-5. Fraction of Energy Lost Due to Atmospheric Absorption

VISUAL RANGE MULTIPLIER FOR INTERCEPTION FRACTIONS

ROW NO.									
1	0.909	0.908	0.907	0.904	0.900	0.895	0.889	0.883	0.908 (ROW AVERAGES)
2	0.919	0.918	0.916	0.913	0.908	0.903	0.897	0.890	0.915
3	0.929	0.928	0.926	0.922	0.917	0.911	0.904	0.897	0.923
4	0.939	0.938	0.935	0.931	0.925	0.918	0.911	0.903	0.930
5	0.949	0.948	0.944	0.939	0.932	0.925	0.917	0.908	0.938
6	0.958	0.957	0.953	0.946	0.939	0.931	0.922	0.913	0.945
7	0.968	0.966	0.960	0.953	0.944	0.935	0.926	0.916	0.953
8	0.976	0.973	0.966	0.957	0.948	0.938	0.928	0.918	0.957
9	0.981	0.977	0.968	0.959	0.949	0.939	0.929	0.919	0.956
10	0.977	0.973	0.966	0.957	0.948	0.938	0.928	0.918	0.958
11	0.968	0.966	0.960	0.953	0.944	0.935	0.926	0.916	0.955
12	0.959	0.957	0.953	0.946	0.939	0.931	0.922	0.913	0.949
13	0.949	0.948	0.944	0.939	0.932	0.925	0.917	0.908	0.943
14	0.939	0.938	0.935	0.931	0.925	0.918	0.911	0.903	0.937
	0.956	0.957	0.954	0.946	0.939	0.932	0.924	0.917	0.947 (NET AVERAGE)

(COLUMN AVERAGES)

(TRIM AND GLASS WEIGHTED AVERAGES)

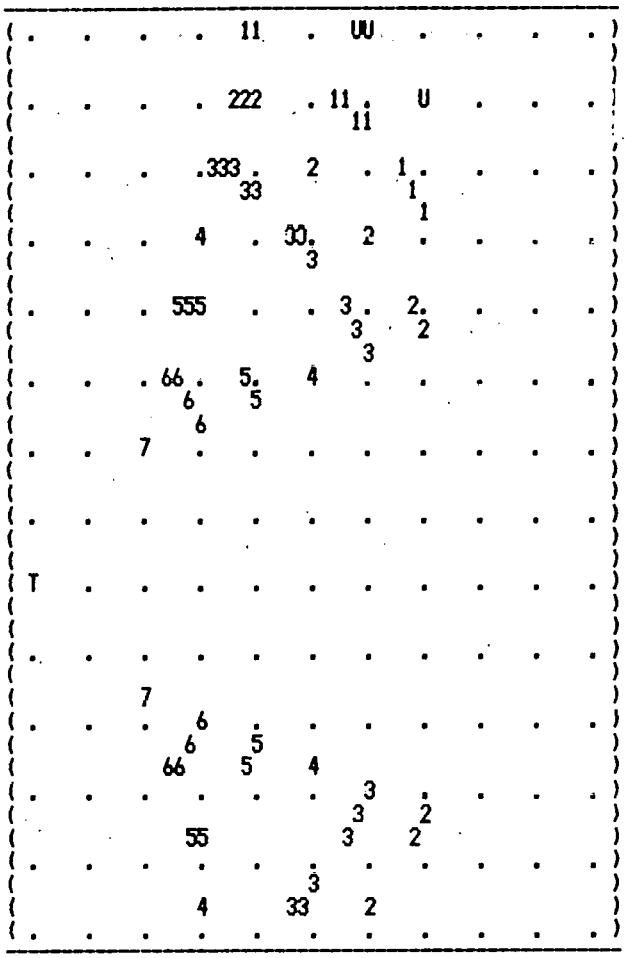

CONTUR INTERVAL = 0.010

The results of the unrestricted collector system design computer run are given in Tables 2-6 to 2-12. These tables represent some of the more important output data from an optimizer run. Table 2-6 shows that the optimization process generated 23,182 heliostats. The matrix of integers at the top of Table 2-6 on the left is the number of quarters of each cell in use, i.e., a four indicates the cell is full and a zero indicates a cell is not used (trimmed out). North is at the top of the page, east to the right, and only the eastern half of the cell structure is shown, starting on the left with the column containing the tower. The tower is in the ninth row from the top. This format for outputting cell structure is always used by the optimizer. The matrix on the right indicates when mechanical limits constrained the solution, thus the cells nearest the tower are at maximum packing density. The second through eighth columns in the Number of Heliostats Per Cell matrix are the actual numbers times two, reflecting also their symmetric counterpart. All power or energy figures are based on the insolation model unless scaling to a particular insolation is indicated. The power and energy values are for thermal energy absorbed at the receiver. The cost figures for the tower are, from right to left, cost of the feed pump, cost of the riser/downcomer, cost of the receiver, cost of the tower, and total of these. The three values given for total heliostat cost and total system cost are based on, from right to left, heliostat costs of $\$120/m^2$, $\$100/m^2$, and $\$80/m^2$. The printed output figure of merit is also based on these three heliostat cost values, but only one of the three represents an optimized system, since the optimization is based on the second cost option ($\$100/m^2$). We compare the second value for the figure of merit ($106.23/aMWh*) to the input figure of merit $107/aMWh* to look for convergence. Table 2-7 gives the optimized radial spacing, R, for each cell (represented by $X\text{-}R/D_H$) in units of D_H, which for this case is 7.3977 meters. The optimized azimuthal spacings, $Y=Z/D_H$, are given in Table 2-8. Note that cell spacings outside the trim receive nonoptimized default values. These are used in the contour plots, so regions outside the trim should be ignored. In the contour plot for Table 2-7, note that the symbols cycle, i.e., the inner circles of U's, represent 5.000 and the interval is 0.500, so the outer circle of U's represents 10.000.

*aMWh - annual thermal megawatt hours collected

Table 2-6. Best Commercial System Design Summary

```
NGON =   4  ; MAX. NUMBER OF HELIOS./CELL=   825.6   ; HGLASS/DMIR**2 =  0.8963   ; TOTAL GLASS = 0.11371E 07
TRIM CONTROL    LIMITS      23182. HELIOS    AHELI=  54.7263    ASEG=  54.7263    ; TOTAL LAND  = 0.62066E 07

   43210000    00000000
   44443000    00000000
   44444300    00000000
   44444430    00000000
   44444441    00000000
   44444442    00000000
   44444443    00000000
   23444443    33000000
   02444442    03000000
   23444441    33000000
   44444430    00000000
   44444410    00000000
   44443100    00000000
   33320000    00000000

* * * * * * * * * * * * * * NUMBER OF HELIOSTATS PER CELL* * * * * * * * * * * * ; HT =  180.0 METERS

    79.7   118.4    76.8    36.2     0.      0.      0.      0.
    95.3   188.7   181.1   171.0   118.3     0.      0.      0.
   114.1   223.6   214.4   200.2   182.8   123.0     0.      0.
   136.7   269.1   254.5   233.9   210.9   185.9   121.1     0.
   168.6   329.5   303.8   273.9   240.2   209.5   179.1    38.1
   217.4   417.3   371.3   318.1   271.9   229.4   194.4    82.0
   303.1   556.1   456.5   366.5   300.5   249.3   208.1   130.0
   158.2   475.1   554.5   411.4   323.3   262.2   216.9   134.1
     0.    319.7   606.0   429.8   332.2   266.6   219.1    89.8
   160.7   497.9   559.2   412.3   322.5   260.4   212.5    43.4
   314.3   570.9   455.4   360.5   292.4   241.1   149.6     0.
   214.3   414.0   361.6   306.3   256.4   214.7    44.6     0.
   158.5   312.9   287.8   253.3   164.1    46.2     0.      0.
    91.0   180.2   171.1   102.4     0.      0.      0.      0.

PERFORMANCE SUMMARY AND COST BREAKDOWN FOR OPTIMIZED COLLECTOR FIELD - TRIM LINE AT  1.000

    EQNOON POWER   =  625.314   591.538 IN MW - (SCALED TO 950 W/M2)
    ANNUAL ENERGY  = 1477.402 IN GWH
    FIXED COSTS    =    5.2200 IN $M
    TOWER COST     =   22.7070     3.1817    16.3720     1.6346     1.5188 IN $M FOR 950. EQUINOON POWER
    LAND COST      =    9.2479 IN $M
    WIRING COST    =    6.0595 IN $M
    HELIOSTAT COST =   90.9706   113.7132   136.4559 IN $M
    TOTAL COST     =  134.2050   156.9476   179.6903 IN $M
    FIGURE OF MERIT=   90.839   106.232   121.626 IN $/MWH , FOR AN INPUT OF   107.000 USING HELIOSTAT COST OPTION 2
```

Table 2-7. Best Commercial System Radial Spacing
(Units of D_H)

X = FIRST SPACING PARAMETER

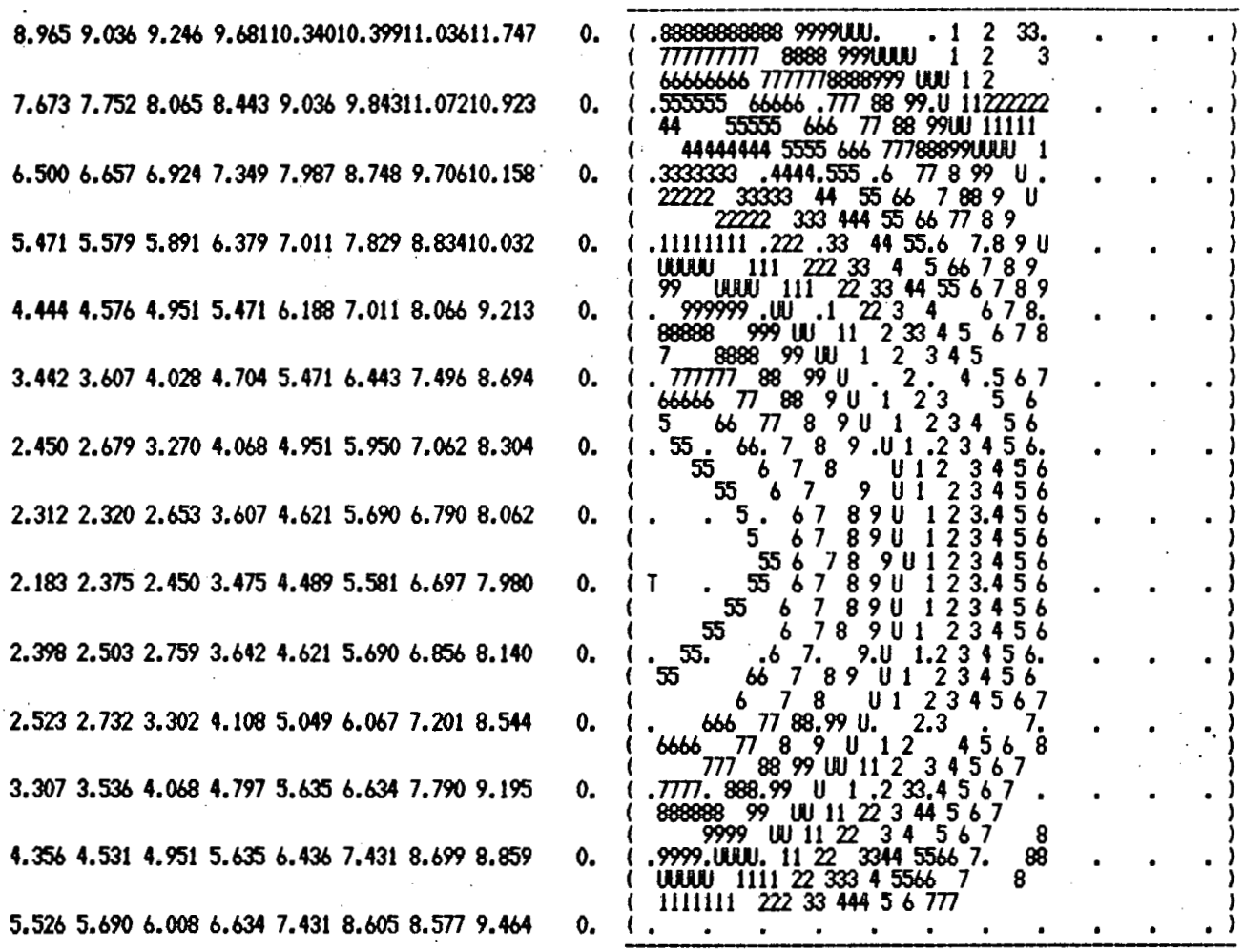

CONTUR INTERVAL = 0.500

0. 0. 0. 0. 0. 0. 0. 0. 0.

Table 2-8. Best Commercial System Azimuth Spacing (Units of D_H)

Y = SECOND SPACING PARAMETER

2.072	2.075	2.085	2.115	2.165	2.084	2.088	2.092	2.081
2.023	2.023	2.027	2.050	2.077	2.120	2.249	2.087	2.039
1.996	1.989	1.994	2.012	2.028	2.063	2.128	2.082	2.010
1.980	1.972	1.974	1.984	2.002	2.034	2.075	2.159	1.997
1.975	1.963	1.968	1.975	1.991	2.015	2.049	2.109	1.989
1.978	1.967	1.979	1.978	1.990	2.003	2.031	2.075	1.989
1.993	1.987	1.983	1.986	1.989	1.996	2.014	2.056	1.994
2.023	2.014	2.012	1.995	1.981	1.984	2.010	2.053	2.006
4.424	1.949	1.994	1.982	1.985	1.990	2.018	2.065	1.989
1.921	1.781	1.919	1.971	1.986	1.998	2.031	2.093	1.930
1.867	1.898	1.969	1.999	2.005	2.024	2.061	2.138	1.959
2.089	2.022	2.012	2.015	2.048	2.078	2.130	2.253	2.040
2.143	2.088	2.077	2.074	2.103	2.156	2.259	2.072	2.094
2.206	2.165	2.159	2.179	2.214	2.320	2.069	2.077	2.173
2.001	1.971	1.995	2.003	2.007	2.017	2.035	2.067	2.000

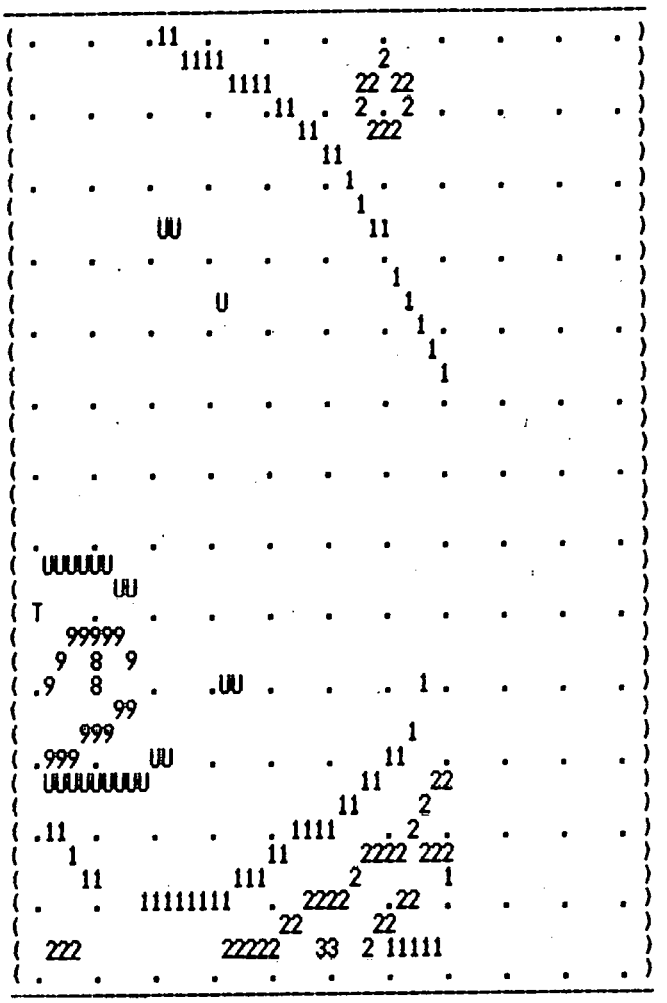

CONTUR INTERVAL = 0.100

Table 2-9. Best Commercial System Trim Ratio (ρ_T)

TRIM RATIO FOR OPTIMUM SPACINGS

1.053	1.042	1.009	0.963	0.901	0.827	0.751	0.674	1.028
1.201	1.187	1.151	1.097	1.024	0.938	0.834	0.750	1.134
1.340	1.327	1.287	1.225	1.142	1.043	0.936	0.827	1.236
1.460	1.443	1.402	1.335	1.244	1.137	1.022	0.900	1.313
1.550	1.526	1.483	1.413	1.323	1.215	1.093	0.963	1.381
1.604	1.577	1.529	1.460	1.373	1.267	1.143	1.008	1.431
1.605	1.605	1.542	1.469	1.386	1.286	1.165	1.031	1.453
1.590	1.554	1.496	1.429	1.358	1.274	1.164	1.034	1.409
0.000	1.476	1.420	1.374	1.316	1.241	1.138	1.015	1.339
1.399	1.351	1.331	1.306	1.263	1.193	1.097	0.980	1.286
1.283	1.262	1.245	1.229	1.195	1.132	1.040	0.926	1.221
1.192	1.188	1.177	1.154	1.117	1.055	0.966	0.855	1.149
1.118	1.115	1.106	1.080	1.033	0.966	0.875	0.790	1.089
1.038	1.033	1.019	0.987	0.935	0.859	0.794	0.714	1.021

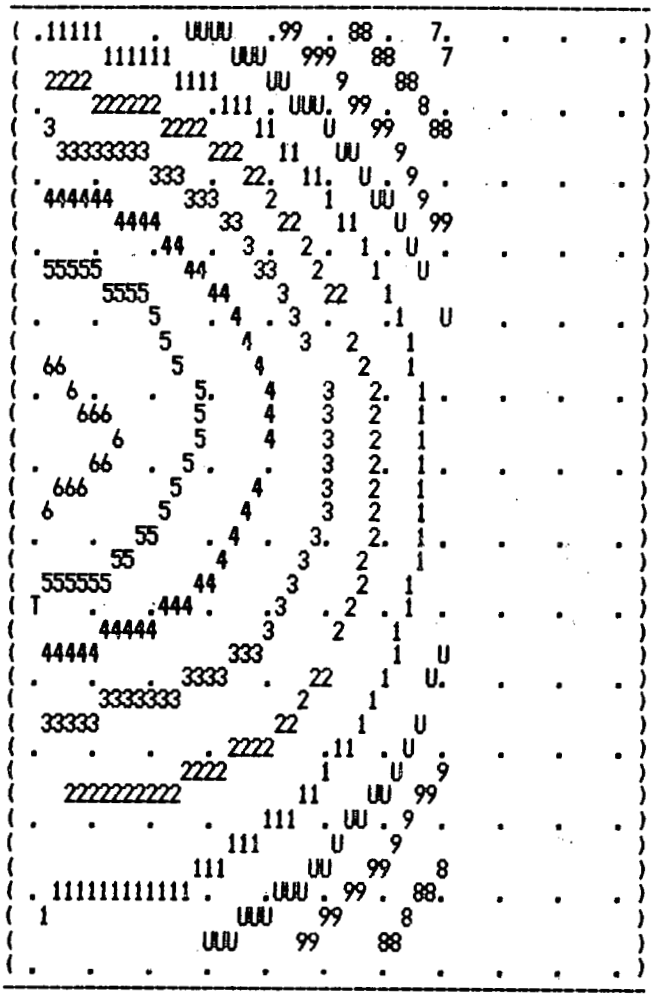

CONTUR INTERVAL = 0.100

1.381 1.378 1.352 1.305 1.256 1.191 1.111 1.016 1.300

Table 2-10. Best Commercial System Ground Coverage Fractions

FRACTION OF GROUND COVERED

0.097	0.096	0.093	0.088	0.080	0.083	0.078	0.073	0.
0.115	0.114	0.110	0.104	0.096	0.086	0.072	0.079	0.
0.138	0.135	0.130	0.121	0.111	0.099	0.087	0.085	0.
0.166	0.163	0.154	0.142	0.128	0.113	0.098	0.083	0.
0.204	0.200	0.184	0.166	0.145	0.127	0.108	0.092	0.
0.263	0.253	0.225	0.193	0.165	0.139	0.118	0.099	0.
0.367	0.337	0.276	0.222	0.182	0.151	0.126	0.105	0.
0.383	0.384	0.336	0.249	0.196	0.159	0.131	0.108	0.
0.186	0.387	0.367	0.260	0.201	0.161	0.133	0.109	0.
0.389	0.402	0.339	0.250	0.195	0.158	0.129	0.105	0.
0.381	0.346	0.276	0.218	0.177	0.146	0.121	0.098	0.
0.260	0.251	0.219	0.185	0.155	0.130	0.108	0.087	0.
0.192	0.189	0.174	0.153	0.132	0.112	0.091	0.098	0.
0.147	0.145	0.138	0.124	0.109	0.090	0.101	0.091	0.

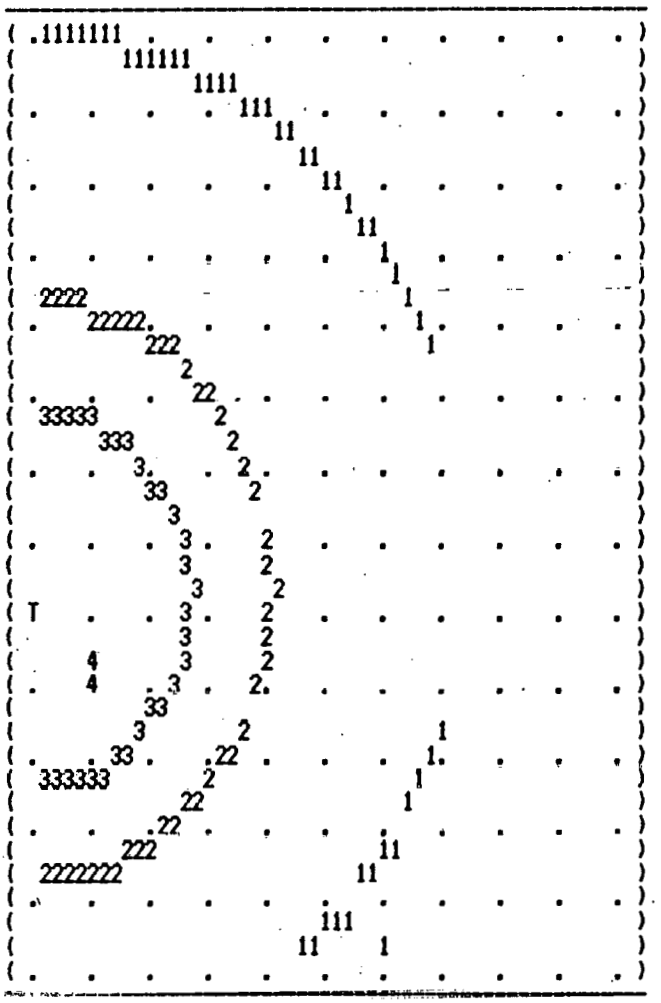

CONTUR INTERVAL = 0.100

0. 0. 0. 0. 0. 0. 0. 0. 0.183

Table 2-11. Theta Times Radial Spacing ($/D_H$) Curve Fit Coefficients

WEIGHTED LEAST SQUARES FIT OF ORDER 2 AND 1 : EXPONENTS OF LEADING TERM ARE 0 0

THE NUMBER OF CONSTANTS IS 6 (6) THE NUMBER OF WEIGHTED OBSERVATIONS IS 72.9

I	C(I)	COVARIANCE MATRIX
1	6.5352936508860 01	1.096D-03
2	-1.4323417946160 00	-1.142D-04 1.288D-05
3	5.3884383534380-02	2.381D-06-2.819D-07 6.571D-09
4	2.4395165749930 00	6.385D-04-5.737D-05 1.091D-06 2.123D-03
5	-2.1445012616280-01	-5.685D-05 5.111D-06-9.699D-08-2.207D-04 2.494D-05
6	5.9107872194240-03	1.075D-06-9.647D-08 1.820D-09 4.601D-06-5.471D-07 1.280D-08

THE AVERAGE ABSOLUTE ERROR IS 8.4622E-01
THE ROOT MEAN SQUARE ERROR IS 1.2356E 00
THE RECPIROCAL RM WEIGHT IS 5.6070E-02
THE CHECK SUM FOR ERRORS IS 5.6801E-07

THETA X RADIAL SPACING COORDINATES IN HELIOSTAT WIDTHS

57.16 57.18 57.21 57.83 59.03 56.30 56.39 56.49
57.10 57.14 57.25 57.44 57.67 57.95 58.24 58.55

55.84 55.86 56.46 56.53 57.18 58.41 61.33 56.38
56.59 56.64 56.79 57.01 57.30 57.63 57.98 58.34

55.08 55.65 55.70 55.78 56.45 57.13 58.39 56.27
56.04 56.10 56.28 56.55 56.91 57.31 57.72 58.14

55.45 55.47 55.52 55.60 55.72 56.42 57.70 59.53
55.50 55.56 55.76 56.09 56.51 56.98 57.47 57.95

55.97 55.96 55.96 55.46 55.57 55.73 57.02 58.31
55.18 55.22 55.36 55.67 56.14 56.68 57.24 57.79

57.07 56.90 56.08 55.97 55.47 56.17 56.91 58.22
55.91 55.67 55.36 55.43 55.85 56.44 57.07 57.68

58.93 58.33 57.33 56.65 55.98 56.09 56.84 58.16
61.38 59.20 56.45 55.52 55.70 56.29 56.97 57.63

96.45 74.86 57.79 56.94 56.55 56.61 56.79 58.12
95.57 74.05 59.47 56.00 55.72 56.26 56.97 57.66

196.51 99.30 59.03 57.70 56.57 56.60 56.78 58.10
372.91 99.66 62.12 56.42 55.86 56.37 57.08 57.78

100.51 81.00 60.18 57.54 56.57 56.62 57.36 58.68
103.81 76.62 60.01 56.34 56.06 56.61 57.32 58.00

60.89 59.64 57.99 57.26 57.13 57.23 57.97 59.85
62.88 60.28 57.17 56.19 56.39 56.99 57.66 58.30

54.96 55.90 56.72 57.14 57.18 57.88 59.17 61.60
56.94 56.68 56.36 56.45 56.89 57.48 58.10 58.67

54.96 55.50 56.04 57.19 57.85 59.11 61.52 56.09
56.53 56.57 56.73 57.06 57.53 58.06 58.59 59.10

56.09 56.65 56.70 57.89 59.12 62.05 56.05 56.19
57.24 57.31 57.51 57.83 58.23 58.67 59.12 59.55

Table 2-12. Azimuthal Spacing ($/D_H$) Curve Fit Coefficients

WEIGHTED LEAST SQUARES FIT OF ORDER 2 AND 1 : EXPONENTS OF LEADING TERM ARE 0 0

THE NUMBER OF CONSTANTS IS 6 (6) THE NUMBER OF WEIGHTED OBSERVATIONS IS 72.9

I	C(I)	COVARIANCE MATRIX
1	2.177787106913D 00	1.096D-03
2	-1.639005458912D-02	-1.142D-04 1.288D-05
3	2.650641038850D-04	2.381D-06-2.819D-07 6.571D-09
4	1.572695767281D-01	6.385D-04-5.737D-05 1.091D-06 2.123D-03
5	-1.132721232894D-02	-5.685D-05 5.111D-06-9.699D-08-2.207D-04 2.494D-05
6	1.1181415194520-04	1.075D-06-9.647D-08 1.820D-09 4.601D-06-5.471D-07 1.280D-08

THE AVERAGE ABSOLUTE ERROR IS 2.6268E-02
THE ROOT MEAN SQUARE ERROR IS 3.6815E-02
THE RECPIROCAL RM WEIGHT IS 5.6070E-02
THE CHECK SUM FOR ERRORS IS -9.9629E-10

AZIMUTHAL SPACING COORDINATES IN HELIOSTAT WIDTHS	* * * * * * *COSINE OF AZIMUTH * * * * * * *
2.07 2.07 2.09 2.11 2.16 2.08 2.09 2.09 1.99 2.00 2.00 2.00 2.01 2.01 2.02 2.03	-1.000-0.992-0.970-0.936-0.894-0.848-0.800-0.753
2.02 2.02 2.03 2.05 2.08 2.12 2.25 2.09 1.99 1.99 2.00 2.00 2.01 2.01 2.02 2.03	-1.000-0.990-0.962-0.919-0.868-0.814-0.759-0.707
2.00 1.99 1.99 2.01 2.03 2.06 2.13 2.08 1.99 1.99 1.99 2.00 2.01 2.01 2.02 2.03	-1.000-0.986-0.949-0.894-0.832-0.768-0.707-0.651
1.98 1.97 1.97 1.98 2.00 2.03 2.08 2.16 1.98 1.99 1.99 2.00 2.01 2.02 2.03 2.04	-1.000-0.981-0.928-0.857-0.781-0.707-0.640-0.581
1.97 1.96 1.97 1.98 1.99 2.02 2.05 2.11 1.98 1.98 1.99 2.00 2.01 2.02 2.03 2.04	-1.000-0.970-0.894-0.800-0.707-0.625-0.555-0.496
1.98 1.97 1.98 1.98 1.99 2.00 2.03 2.07 1.98 1.98 1.98 1.99 2.01 2.02 2.03 2.05	-1.000-0.949-0.832-0.707-0.600-0.514-0.447-0.394
1.99 1.99 1.98 1.99 1.99 2.00 2.01 2.06 1.99 1.98 1.98 1.99 2.01 2.02 2.04 2.05	-1.000-0.894-0.707-0.555-0.447-0.371-0.316-0.275
2.02 2.01 2.01 2.00 1.98 1.98 2.01 2.05 2.08 1.99 1.96 1.98 2.01 2.03 2.05 2.06	-1.000-0.707-0.447-0.316-0.243-0.196-0.164-0.141
4.42 1.95 1.99 1.98 1.99 1.99 2.02 2.06 2.85 1.96 1.94 1.98 2.01 2.04 2.06 2.07	0. 0.000 0.000 0.000 0.000 0.000 0.000 0.000
1.92 1.78 1.92 1.97 1.99 2.00 2.03 2.09 1.84 1.86 1.93 1.99 2.03 2.05 2.07 2.08	1.000 0.707 0.447 0.316 0.243 0.196 0.164 0.141
1.87 1.90 1.97 2.00 2.00 2.02 2.06 2.14 1.89 1.91 1.97 2.01 2.05 2.07 2.09 2.10	1.000 0.894 0.707 0.555 0.447 0.371 0.316 0.275
2.09 2.02 2.01 2.01 2.05 2.08 2.13 2.25 1.98 1.99 2.02 2.05 2.07 2.09 2.10 2.11	1.000 0.949 0.832 0.707 0.600 0.514 0.447 0.394
2.14 2.09 2.08 2.07 2.10 2.16 2.26 2.07 2.05 2.05 2.07 2.08 2.10 2.11 2.12 2.13	1.000 0.970 0.894 0.800 0.707 0.625 0.555 0.496
2.21 2.17 2.16 2.18 2.21 2.32 2.07 2.08 2.09 2.10 2.10 2.11 2.12 2.13 2.14 2.14	1.000 0.981 0.928 0.857 0.781 0.707 0.640 0.581

The trim ratio, ρ_T, from equation (52) of Appendix A is given for each cell in Table 2-9. This is a measure of the net annual energy productivity of each cell. The field is the most cost effective when cells are eliminated whose trim ratio is less than 1.0. The effect of field size on cost and performance for a given tower and receiver can be evaluated by varying the value of trim ratio for which cells are kept in the field. Notice on the contour plot of trim ratio the shape of the trim boundaries are elliptical and as the trim ratio increases (the field is trimmed down) the field becomes more northerly; a trim of 1.5 would produce an efficient but expensive North field.

The ratio of glass area in a cell to surface area in a cell or fraction of ground covered is given in Table 2-10. The trim weighted (cells outside the optimum boundary are not included) average is 18.3%. It should be noted that this number is affected by heliostat cost and land cost (as well as other cost factors, of course). In this case, the costs used were $\$100/m^2$ and $\$1.49/m^2$. If these costs were higher the optimizer would have increased the ground coverage and constricted the trim line.

Tables 2-11 and 2-12 show examples of the output from the optimizer of two-dimensional curve fit coefficients, C(I), for the heliostat spacings. All spacings given here are in heliostat widths, D_H. In Table 2-11 the quantity curve fit is $\theta R/D_H$, thus, the form of the curve fit is

$$\theta R(\theta,\phi)/D_H = C_1 + C_2\theta + C_3\theta^2 + (C_4 + C_5\theta + C_6\theta^2) \cos \phi$$

Also shown in the table are the optimizer values and curve fit values for the azimuthal spacing coordinates in heliostat widths, $\theta R/D_H$, the first above the second for direct comparison. In Table 2-12 the curve fit is for $Z(\theta,\phi)/D_H$ and therefore has the same form given in Section 2.2.8.

2.5 RESTRICTED COMMERCIAL SYSTEM COLLECTOR DESIGN (FOR SCALING TO PILOT PLANT)

2.5.1 Scaling Requirements

The purpose of the scaled commercial collector system design is to generate a set of heliostat spacing curve fit coefficients which the layout processor can use to produce a heliostat field which will meet the pilot plant requirements. The fundamental constraints are the thermal power level which must be met to achieve design requirements, the existing collector field boundary, and the existing tower height design. If the pilot plant were scaled down from the best commercial design these constraints would not necessarily be met. To assure that they are met the following steps have been taken to produce a scalable design.

The optimizer code was altered to accept an input field trim matrix rather than generating an optimized field trim. The input trim matrix was determined by superimposing the cell structure over the pilot plant field boundary and observing which cells, and what portion of cells on the boundary, fall within the boundary. The input trim matrix will be shown in one of the tables in the next section.

The thermal power requirements used for scaling is 34.4 MW of thermal power absorbed into steam at the receiver on winter solstice (day 276), 2:00 PM, for an insolation level of 917 W/m^2. The insolation level is from 1976 Barstow data. The optimizer outputs the thermal power level of the plant at equinox noon, for 950 W/m^2. Therefore, it is necessary to scale up from the 34.4 MW value to arrive at a value for commercial plant power level required from an optimizer run. When the heliostat spacing curve fit coefficients are used from this run to lay out the pilot plant, then the desired power level should be achieved. Recall that the curve fit coefficients are functions of tower elevation, and cell azimuth, and that the cell sizes are generated in proportion to tower height. The coefficients also produce spacing values in heliostat diameters. Thus, we simply employ the coefficients generated in the scalable commercial run, with the pilot plant focal height and heliostat size, and the resulting layout process will be properly scaled. The scale up of power level has been done using the following factors,

$$\underset{1}{\left(\frac{180m}{75.438m}\right)^2}\ \underset{2}{\left(\frac{1932}{1900}\right)}\ \underset{3}{\left(\frac{1932+134}{1932}\right)}\ \underset{4}{\left(\frac{1}{0.9537}\right)}\ \underset{5}{\left(\frac{950\ w/m^2}{917\ w/m^2}\right)}\ \underset{6}{\left(\frac{0.8220}{0.7110}\right)}\ \underset{7}{\left(\frac{0.90}{0.86}\right)}\ \underset{8}{\left(\frac{0.95}{0.93}\right)}$$

$$= 8.2429$$

The first term scales for the focal heights. The power of systems of defined geometry scales as the square of focal height and it is assumed that this one will scale similarly. The second term accounts for possible outage by one field controller (a design requirement). The third term scales up one additional circle of heliostats due to the fact the pilot plant is to be designed for the Sandia baseline design heliostat with an area of 41.8067 m^2 (450 ft^2), but must still produce rated power with the smaller (40.0 m^2) Martin heliostat. The fourth term is an allowance for roads that must be included in the layout process. Out of 82 cells about 3.8 are needed for roads. The fifth term scales up to the optimizer output insolation level of 950 W/m^2. The sixth term represents the cosine and shading and blocking factors occurring in a commercial field at equinox noon (numerator) and at winter solstice, 2:00 PM. (denominator). Terms seven and eight account for the fact that the heliostat reflectivities and the receiver absorptivity of the pilot plant are less than those used in the commercial system design.(1)

It is necessary to apply this scale factor to the incident power to the receiver. The expected radiative and convective losses for the pilot plant receiver are 4.8 MW and for the commercial receiver 25.5 MW. Thus, the incident power requirement on the pilot plant receiver is 39.2 MW. Multiplying by the scaling factors

$$39.2\ MW \times 8.2429 = 323.122\ MW$$

and after subtracting receiver losses the result is an equinox noon absorbed power level of 297 MW thermal.

The scalable commercial design optimization is further improved by the use of first plant type cost values. The wiring costs ($C_{W1,2,3)}$ have been multiplied

(1) The final collector field design was based on revised assumptions related to heliostat reflectivity (0.89) and receiver absorptivity (0,95) - See Section 5.1 for field performance data.

by a factor of 1.5 over those used in the best commercial design. The cost of heliostats must also be increased. This will also be necessary to get an optimizer run which produces the required power level. As heliostat costs go up the optimizer will decrease the local ground coverage, thus decreasing the number of heliostats within the fixed boundary of the field. A heliostat cost of 200 $/m^2 ($C_h$) resulted in a power level meeting the above given requirement. This cost is representative of expected first plant costs, and includes an allowance of \$11.82/m^2 for present value of operations and maintenance. If typical pilot plant heliostat costs of 300 $/m^2 were used the power level would be inadequate.

In response to the fixed boundary it was found that cells of size order 3 would be adequate to cover the field and would result in greater computational resolution than the cells of order 5. Thus, the cell size for the scalable commercial plant is $\sqrt{3}/2*180m=155.88$ m and for the pilot plant is $\sqrt{3}/2*75.438m = 65.33m$.

Table 2-13 contains a cost of all the changes made to the input specifications listed in Tables 2-1 and 2-2 for the scalable commercial system design run of the optimizer. All other specifications have remained the same.

Table 2-13. Input Specification Changes

Minimum Heliostat Clearance Radius	5.682 m	
C_{w1} =	0.0618	\$/m/heliostat
C_{w2} =	0.6356	\$/m/heliostat
C_{w3} =	21.375	\$/m/heliostat
C_h =	200.0	\$/m^2
Cell size =	155.88 m (order 3)	
Restricted trim	See Table 2-16	

The interception fractions for the scalable commercial system are given in Table 2-14. These values are higher than those shown in Table 2-4. The cells are smaller and the slant ranges, therefore, less. It is obvious from the contour plots of Tables 2-4 and 2-14 that the interception fractions are a function of slant range. The values in Table 2-14 are relatively high, indicating that the receiver is larger than necessary for the given boundary. The effect of losses due to atmospheric absorption is shown in Table 2-15. Again, these values are higher than the corresponding ones in Table 2-5 because of the decreased slant range.

2.5.2 Scalable Commercial System Collector Design

A summary of system design and performance is given in Table 2-16. The restricted field trim matrix is shown in the upper left representing quarters of cells occupied. When scaled down to the pilot plant this represents the existing physical boundary. The equinox noon power scaled to 950 W/m^2 is 307.6 MW, a value very close to the 297 MW required by the power level scaling. This optimization is based on a heliostat cost of $\$200/m^2$. The final converged figure of merit for this design is \$187.2/aMWh.

It is interesting to compare some of the results in Table 2-16 to the results for an unrestricted system like that presented in Section 2.4 but with heliostat and wiring costs used in the scalable design (first plant costs). This gives some idea of how far the scalable design is from a fully optimized system. The comparison is given in Table 2-17. The fully optimized system uses 62% more heliostats with the same receiver and tower, it produces 63% more energy annually, it costs 60% more, and delivers energy at 3.2% less cost per aMWh.

The fraction of ground covered for the scalable design is given in Table 2-18. This figure is greatly increased over the unrestricted designs due to the arbitrary deletion of distant, sparsely occupied cells. Fully optimized systems tend to cover only about 19% of the ground with glass.

Table 2-14. Scalable Commercial System Interception Fractions

INTERCEPTION FACTORS FROM RECEIVER PROGRAM * * * * * UNIVERSITY OF HOUSTON AND DOE

0.944	0.943	0.937	0.927	0.913	0.893	0.870	0.840	0.
0.970	0.969	0.964	0.956	0.943	0.926	0.902	0.873	0.
0.987	0.986	0.983	0.976	0.966	0.951	0.929	0.902	0.
0.996	0.996	0.994	0.990	0.982	0.969	0.951	0.926	0.
0.999	0.999	0.998	0.996	0.991	0.982	0.966	0.943	0.
1.000	1.000	1.000	0.999	0.996	0.990	0.977	0.956	0.
0.999	1.000	1.000	1.000	0.998	0.994	0.983	0.964	0.
0.994	0.997	1.000	1.000	0.999	0.996	0.987	0.970	0.
0.	1.002	1.000	1.000	0.999	0.996	0.988	0.970	0.
0.999	1.000	1.000	1.000	0.999	0.996	0.987	0.969	0.
0.999	1.000	1.000	1.000	0.998	0.994	0.983	0.964	0.
1.000	1.000	0.999	0.998	0.996	0.989	0.976	0.955	0.
0.998	0.998	0.997	0.995	0.990	0.981	0.965	0.942	0.
0.994	0.993	0.992	0.987	0.980	0.967	0.949	0.924	0.

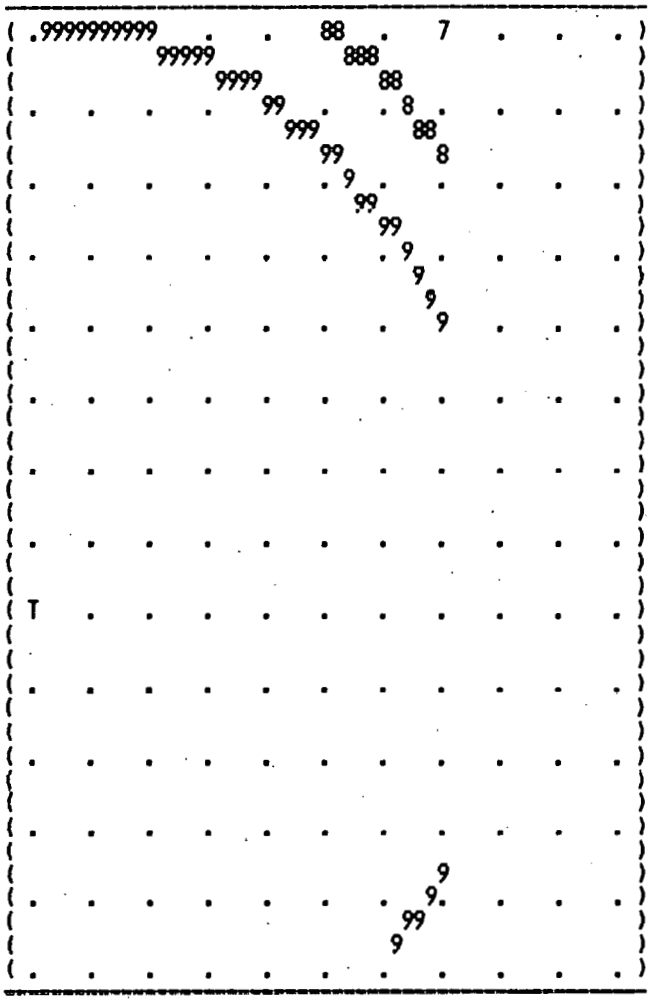

CONTUR INTERVAL = 0.050

0. 0. 0. 0. 0. 0. 0. 0. 0.

Table 2-15. Scalable Commercial System Fraction of Energy Lost Due to Atmospheric Absorption

VISUAL RANGE MULTIPLIER FOR INTERCEPTION FRACTIONS

0.927 0.926 0.925 0.923 0.920 0.916 0.912 0.907	0.	. . . .
0.935 0.934 0.933 0.930 0.926 0.922 0.918 0.912	0.	. . . .
0.942 0.942 0.940 0.937 0.933 0.928 0.923 0.918	0.941	. . . .
0.950 0.949 0.947 0.944 0.939 0.934 0.928 0.922	0.947	. . . .
0.958 0.957 0.954 0.950 0.945 0.939 0.933 0.927	0.952	. . . 66 . . . .
0.965 0.964 0.960 0.956 0.950 0.944 0.937 0.930	0.957	. . 7 . 6 . . . . . .
0.972 0.970 0.966 0.960 0.954 0.947 0.940 0.933	0.962	. . . 7 . . . .
0.978 0.976 0.970 0.964 0.957 0.949 0.942 0.934	0.965	. . . .
0.981 0.978 0.972 0.965 0.958 0.950 0.942 0.935	0.965	T . . . .
0.978 0.976 0.970 0.964 0.957 0.949 0.942 0.934	0.967	. . . .
0.972 0.970 0.966 0.961 0.954 0.947 0.940 0.933	0.966	. . . 7 . . . .
0.965 0.964 0.961 0.956 0.950 0.944 0.937 0.930	0.963	. . 7 . 6 . . . . . .
0.958 0.957 0.954 0.950 0.945 0.939 0.933 0.927	0.	. . . 66 . 5 5 . . . .
0.950 0.949 0.947 0.944 0.939 0.934 0.928 0.922	0.	. . . . 55 . . . . . .

CONTUR INTERVAL = 0.010

0.966 0.966 0.964 0.959 0.954 0.947 0.941 0. 0.961

Table 2-16. Scalable Commercial System Design Summary

```
NGON =   4  ; MAX. NUMBER OF HELIOS./CELL=   495.4   ; HGLASS/DMIR**2 =  0.8963   ; TOTAL GLASS = 0.55157E 06
TRIM CONTROL    LIMITS      11244. HELIOS    AHELI=  54.7263    ASEG=  54.7263    ; TOTAL LAND  = 0.20473E 07

   00000000    00000000
   00000000    00000000
   33200000    00000000
   44440000    00000000
   44444200    00000000
   44444400    00000000
   44444410    33000000
   23444410    33300000
   02444410    33300000
   23444200    33000000
   44442000    30000000
   44210000    00000000
   00000000    00000000
   00000000    00000000

* * * * * * * * * * * * * NUMBER OF HELIOSTATS PER CELL* * * * * * * * * * * ; HT =  180.0 METERS

    0.     0.     0.     0.     0.     0.     0.     0.
    0.     0.     0.     0.     0.     0.     0.     0.
   65.2  128.9   82.7    0.     0.     0.     0.     0.
  103.5  203.6  193.0  178.5    0.     0.     0.     0.
  126.4  246.8  228.6  206.4  183.1   81.0    0.     0.
  158.9  305.5  275.8  238.8  205.2  176.8    0.     0.
  189.1  379.4  330.7  271.3  224.4  189.0   40.5    0.
   96.2  298.1  377.9  301.4  240.5  198.7   41.7    0.
    0.   198.8  377.3  311.7  246.5  200.3   42.0    0.
   98.9  284.5  378.6  296.3  237.5   97.7    0.     0.
  198.5  394.1  321.0  260.1  108.6    0.     0.     0.
  151.6  289.1  128.5   55.4    0.     0.     0.     0.
    0.     0.     0.     0.     0.     0.     0.     0.
    0.     0.     0.     0.     0.     0.     0.     0.

PERFORMANCE SUMMARY AND COST BREAKDOWN FOR OPTIMIZED COLLECTOR FIELD - TRIM LINE AT  1.000

   EQNOON POWER   =  325.840   307.606 IN MW - (SCALED TO 950 W/M2)
   ANNUAL ENERGY  =  742.015 IN GWH
   FIXED COSTS    =    5.2200 IN $M
   TOWER COST     =   16.1991     3.1817    10.9151     1.0898     1.0125 IN $M FOR 950. EQUINOON POWER
   LAND COST      =    3.0504 IN $M
   WIRING COST    =    4.1169 IN $M
   HELIOSTAT COST =   96.5243   110.3135   124.1027 IN $M
   TOTAL COST     =  125.1108   138.9000   152.6892 IN $M
   FIGURE OF MERIT=  168.609   187.193   205.776 IN $/MWH , FOR AN INPUT OF   190.000 USING HELIOSTAT COST OPTION 2
```

Table 2-17. Comparison to an Unrestricted System Design With The Same Costs as The Scalable System

	Scalable Design	Unrestricted Design
Number of heliostats	11,244	18,219
Fraction of ground covered	27%	19%
Equinox noon power scaled to 950 W/m^2	307.6 MW	489.6 MW
Annual energy	742 GWh	1,210 GWh
Total system cost	139 M$	219 M$
Figure of merit	187 $/MWh	181 $/MWh

Tables 2-19 and 2-20 give the heliostat spacing curve fit coefficients for the scalable commercial system. These coefficients could be used to lay out the pilot plant. However, there is one additional step performed by the CELLAY program which generates several sets of curve fit coefficients. These provide for a set of variations in heliostat spacings which will produce nearly the same net cell efficiency. This additional degree of freedom is required by the LAYOUT program where rapidly varying azimuthal spacing, when moving toward the tower, can be compensated for by variations in the radial spacing. These concepts will be explained in more detail in Section 4.

Table 2-18. Scalable Commercial System Fraction of Ground Coverage

FRACTION OF GROUND COVERED

0.131	0.130	0.127	0.123	0.117	0.109	0.102	0.094	0.
0.151	0.149	0.145	0.138	0.130	0.122	0.112	0.103	0.
0.175	0.173	0.167	0.157	0.146	0.134	0.123	0.111	0.
0.209	0.205	0.195	0.180	0.164	0.148	0.134	0.119	0.
0.255	0.249	0.231	0.208	0.185	0.164	0.145	0.128	0.
0.321	0.308	0.278	0.241	0.207	0.178	0.154	0.135	0.
0.382	0.383	0.334	0.274	0.227	0.191	0.163	0.142	0.
0.388	0.401	0.381	0.304	0.243	0.201	0.168	0.145	0.
0.381	0.401	0.381	0.315	0.249	0.202	0.170	0.145	0.
0.399	0.383	0.382	0.299	0.240	0.197	0.166	0.143	0.
0.401	0.398	0.324	0.263	0.219	0.185	0.159	0.136	0.
0.306	0.292	0.259	0.224	0.192	0.167	0.146	0.128	0.
0.228	0.225	0.209	0.188	0.167	0.148	0.130	0.115	0.
0.179	0.178	0.171	0.158	0.145	0.129	0.117	0.102	0.

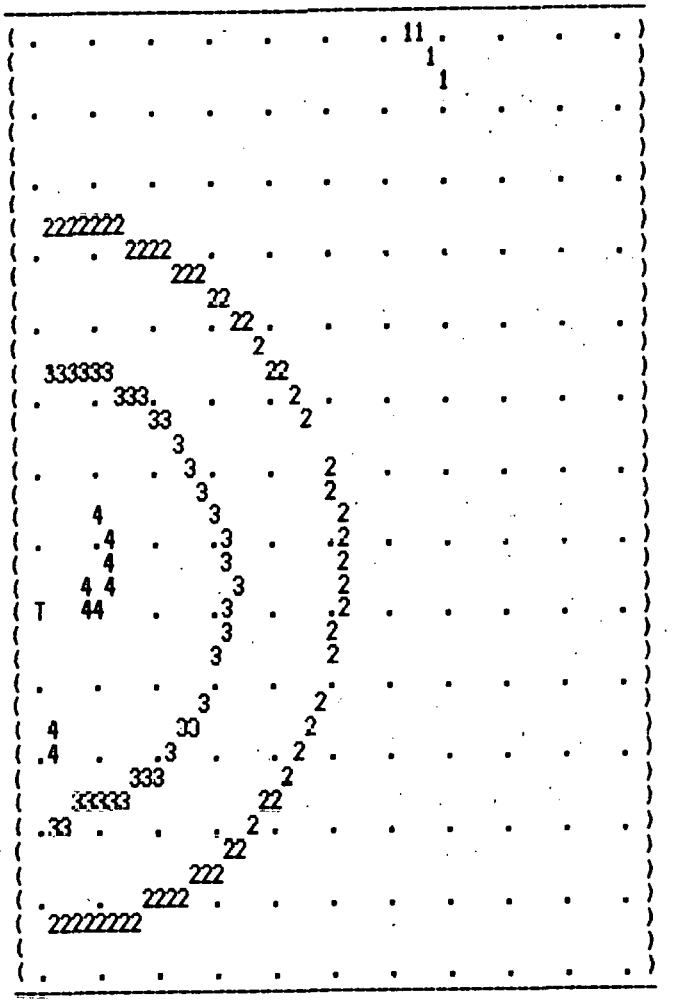

CONTUR INTERVAL = 0.100

0. 0. 0. 0. 0. 0. 0. 0. 0.269

Table 2-19. Scalable Commercial System Radial Spacing ($/D_H$) Curve Fit Coefficients

WEIGHTED LEAST SQUARES FIT OF ORDER 2 AND 1 : EXPONENTS OF LEADING TERM ARE 0 0

THE NUMBER OF CONSTANTS IS 6 (6) THE NUMBER OF WEIGHTED OBSERVATIONS IS 44.5

I	C(I)	COVARIANCE MATRIX
1	6.8839915405615D 01	5.806D-03
2	-1.6435182686280 00	-4.280D-04 3.314D-05
3	5.5979513256760-02	6.898D-06-5.546D-07 9.703D-09
4	9.9441755653130-01	4.796D-03-3.149D-04 4.656D-06 1.151D-02
5	4.6864444210500-02	-3.105D-04 2.047D-05-3.033D-07-8.420D-04 6.495D-05
6	-1.5790818493050-03	4.546D-06-3.004D-07 4.450D-09 1.352D-05-1.086D-06 1.902D-08

THE AVERAGE ABSOLUTE ERROR IS 1.1594E 00
THE ROOT MEAN SQUARE ERROR IS 2.0610E 00
THE RECPIROCAL RM WEIGHT IS 6.2924E-02
THE CHECK SUM FOR ERRORS IS -9.7923E-07

THETA X RADIAL SPACING COORDINATES IN HELIOSTAT WIDTHS

55.64 55.64 55.64 55.65 55.66 56.26 56.28 56.89
57.85 57.90 58.07 58.33 58.66 59.04 59.46 59.88

55.65 55.65 55.64 55.64 55.64 55.65 56.25 56.28
57.06 57.13 57.34 57.66 58.06 58.52 59.01 59.51

55.73 55.72 55.70 55.67 55.65 55.64 55.65 56.25
56.26 56.35 56.59 56.97 57.45 58.00 58.57 59.15

55.98 55.94 55.86 55.77 55.70 55.66 55.65 56.24
55.60 55.68 55.92 56.32 56.87 57.50 58.16 58.82

56.61 56.50 56.24 55.99 55.81 55.70 55.66 56.23
55.55 55.53 55.58 55.87 56.39 57.07 57.81 58.53

58.27 57.88 57.08 56.41 56.00 55.78 56.26 56.24
57.75 57.15 56.19 55.84 56.13 56.78 57.55 58.33

68.23 62.92 58.80 57.70 56.85 56.47 56.30 56.25
68.84 64.67 59.04 56.57 56.18 56.65 57.41 58.22

116.89 97.83 61.94 57.93 57.13 56.57 56.92 56.84
123.12 90.05 65.19 57.98 56.50 56.72 57.43 58.23

201.84122.69 67.51 58.96 57.26 57.20 56.94 56.85
374.36123.12 69.92 59.05 56.89 56.93 57.58 58.36

122.38 90.64 62.99 59.18 57.75 57.17 56.93 56.85
123.11 90.98 66.23 58.81 57.15 57.24 57.86 58.59

74.97 68.83 60.16 58.37 57.49 57.08 56.91 57.42
70.99 66.75 60.86 58.05 57.38 57.64 58.24 58.93

58.44 59.84 58.99 58.26 57.81 57.57 57.46 57.42
60.35 59.64 58.42 57.74 57.73 58.13 58.71 59.33

57.32 57.20 58.10 58.41 58.20 58.07 58.02 58.58
58.23 58.13 57.98 58.00 58.26 58.70 59.23 59.79

57.25 57.79 57.11 57.59 58.08 58.61 58.59 59.75
58.27 58.29 58.38 58.58 58.91 59.32 59.79 60.28

Table 2-20. Scalable Commercial System Azimuthal Spacing ($/D_H$) Curve Fit Coefficients

WEIGHTED LEAST SQUARES FIT OF ORDER 2 AND 1 : EXPONENTS OF LEADING TERM ARE 0 0

THE NUMBER OF CONSTANTS IS 6 (6) THE NUMBER OF WEIGHTED OBSERVATIONS IS 44.5

I	C(I)	COVARIANCE MATRIX
1	2.048093262828D 00	5.806D-03
2	1.636453567769D-03	-4.280D-04 3.314D-05
3	-1.268893271405D-04	6.898D-06-5.546D-07 9.703D-09
4	2.575522459046D-01	4.796D-03-3.149D-04 4.656D-06 1.151D-02
5	-1.865844664373D-02	-3.105D-04 2.047D-05-3.033D-07-8.420D-04 6.495D-05
6	2.844577571763D-04	4.546D-06-3.004D-07 4.450D-09 1.352D-05-1.086D-06 1.902D-08

THE AVERAGE ABSOLUTE ERROR IS 3.8954E-02
THE ROOT MEAN SQUARE ERROR IS 6.5447E-02
THE RECPIROCAL RM WEIGHT IS 6.2924E-02
THE CHECK SUM FOR ERRORS IS -3.8722E-08

AZIMUTHAL SPACING COORDINATES IN HELIOSTAT WIDTHS								* * * * * * *COSINE OF AZIMUTH * * * * * * *
2.01	2.01	2.01	2.02	2.03	2.04	2.05	2.08	-1.000-0.992-0.970-0.936-0.894-0.848-0.800-0.753
1.93	1.93	1.93	1.93	1.93	1.93	1.94	1.94	
2.00	2.00	2.00	2.01	2.02	2.02	2.04	2.06	-1.000-0.990-0.962-0.919-0.868-0.814-0.759-0.707
1.94	1.94	1.94	1.94	1.94	1.95	1.95	1.95	
2.00	1.99	1.99	2.00	2.01	2.02	2.03	2.05	-1.000-0.986-0.949-0.894-0.832-0.768-0.707-0.651
1.96	1.96	1.96	1.96	1.96	1.96	1.96	1.96	
1.99	1.99	1.99	2.00	2.00	2.01	2.02	2.04	-1.000-0.981-0.928-0.857-0.781-0.707-0.640-0.581
1.98	1.98	1.98	1.98	1.98	1.98	1.98	1.98	
2.00	1.99	2.00	2.00	2.00	2.01	2.02	2.03	-1.000-0.970-0.894-0.800-0.707-0.625-0.555-0.496
2.01	2.01	2.00	2.00	1.99	1.99	1.99	1.99	
2.02	2.01	2.00	2.01	2.01	2.02	2.02	2.03	-1.000-0.949-0.832-0.707-0.600-0.514-0.447-0.394
2.04	2.03	2.02	2.02	2.01	2.01	2.01	2.01	
2.06	2.03	2.03	2.01	2.01	2.01	2.02	2.03	-1.000-0.894-0.707-0.555-0.447-0.371-0.316-0.275
2.03	2.03	2.03	2.03	2.02	2.02	2.02	2.02	
1.93	1.79	2.07	2.04	2.02	2.02	2.01	2.02	-1.000-0.707-0.447-0.316-0.243-0.196-0.164-0.141
1.80	1.94	2.02	2.03	2.03	2.04	2.04	2.04	
2.10	1.79	2.09	2.03	2.03	2.02	2.02	2.04	0. 0.000 0.000 0.000 0.000 0.000 0.000 0.000
1.17	1.82	1.98	2.03	2.04	2.05	2.05	2.05	
1.81	2.03	2.04	2.03	2.03	2.03	2.04	2.05	1.000 0.707 0.447 0.316 0.243 0.196 0.164 0.141
1.85	1.89	1.98	2.03	2.05	2.06	2.07	2.07	
1.79	1.79	2.05	2.08	2.06	2.06	2.06	2.07	1.000 0.894 0.707 0.555 0.447 0.371 0.316 0.275
1.94	1.96	2.01	2.05	2.07	2.08	2.08	2.08	
2.11	2.06	2.08	2.10	2.10	2.09	2.09	2.11	1.000 0.949 0.832 0.707 0.600 0.514 0.447 0.394
2.02	2.03	2.05	2.07	2.09	2.09	2.10	2.10	
2.21	2.18	2.14	2.12	2.12	2.13	2.16	2.16	1.000 0.970 0.894 0.800 0.707 0.625 0.555 0.496
2.07	2.08	2.09	2.10	2.11	2.11	2.11	2.11	
2.28	2.23	2.22	2.20	2.18	2.19	2.21	2.25	1.000 0.981 0.928 0.857 0.781 0.707 0.640 0.581
2.11	2.11	2.12	2.12	2.13	2.13	2.13	2.13	

REFERENCES

1. Hallet, R. W. and Gervais, R. L., McDonnell Douglas Astronautics Co., "Central Receiver Solar Thermal Power System, Phase 1: CDRL Item 2, Pilot Plant Preliminary Design Report," U.S. Dept. of Energy, SAN/1108-8/1 (1977).

2. Pitman, C. L. and Vant-Hull, L. L., "Errors in Locating the Sun and Their Effect on Solar Intensity Predictions", Proc. of 1978 Annual Meeting of American Section of ISES, Vol. 2.2, p. 706, Denver, Colorado (August 1978).

3. Vant-Hull, L. L. and Easton, C. R., "Solar Thermal Power Systems Based on Optical Transmission," Final Report, NSF/RANN/SE/GI-39456/FR/75/3, October 21, 1975, NTIS Accession No. PB 253 167/AS.

4. Vant-Hull, L. L. and Easton, C. R., "Solar Thermal Power Systems Based on Optical Transmission," Progress Report No. 1, NSF/RANN/SE/FI-39456/PR/73/4, prepared by the University of Houston and McDonnell Douglas Astronautics Co., Feb. 15, 1974, NTIS Accession No. PB237 005.

5. Vant-Hull, L. L. and Easton, C. R., "Solar Thermal Power Systems Based on Optical Transmission," Progress Report No. 2, NSF/RANN/SE/GI-39456/PR/74/2, Dec. 21, 1974, NTIS Accession No. PB 244 436/AS.

6. Lipps, F. W. "Four Different Views of the Heliostat Flux Density Integral," Solar Energy, 18, p. 555 (1976).

7. Walzel, M. D., Lipps, F. W., and Vant-Hull, L. L., "A Solar Flux Density Calculation For A Solar Tower Concentrator Using A Two-Dimensional Hermite Function Expansion," Solar Energy, 19, p. 239 (1977).

8. Lipps, F. W. and Walzel, M. D., "An Analytic Evaluation of the Flux Density Due to Sunlight Reflected from a Flat Mirror having a Polygonal Boundary," Solar Energy, 21, p. 113 (1978).

9. Lipps, F. W. and Vant-Hull, L. L., "Shading and Blocking Geometry for a Solar Tower Concentrator with Rectangular Mirrors," ASME Proceedings, 74-WA/501-11, p. 2. (1974).

10. "Proceedings of the ERDA Solar Workshop on Methods for Optical Analysis of Central Receiver Systems," University of Houston, Sandia Labs, ERDA, Houston, Texas, Oct. 1977, NTIS Accession No. CONF 770850.

11. Selby, J. E. A. and McClalche, R. A., AFCRL-72-0745 (1972).

12. Lipps, F. W. and Vant-Hull, L. L., "Parametric Study of Optimized Central Receiver Systems," Proceedings of the 1978 Annual Meeting, American Section, ISES, Vol. 2.1, p. 793.

13. Laurence, C. L., "Pilot Plant Optical Performance Evaluation," Aerospace Corp. Technical Report, ATR-77 (7689-03)-1, Sept. 1977.

14. Flowers, E. C., McCormick, R. A., and Kurtis, K., "Atmospheric Turbidity over the United States, 1961-1966," Journal of Applied Meteorology, 8, No. 6, p. 955-962, Dec. 1969.

15. Shands, A. L., "Mean Precipitable Water in the United States," U.S. Dept. of Commerce Technical Paper. No. 10, 1949.

Section 3

DEVELOPMENT OF INDIVIDUAL HELIOSTAT PERFORMANCE CODE TO MEET SFDI REQUIREMENTS

3.1 EARLY HISTORY OF THE INDIVIDUAL HELIOSTAT CODE

Beginning in 1973, the first central receiver computer simulation codes were cellwise performance models intended for the conceptual design of large commercial systems. Collector field optimization and parametric systems analysis began in 1975. Since then, RCELL has become a versatile, efficient, cellwise optimization code with comprehensive outputs, including coefficients for a subsequent layout procedure. It is important to realize that, because of the multitude of heliostat interactions, a mathematically rigorous optimum layout is impossible to achieve by computer technology; hence, a cellwise optimization that ignores some of the actual constraints is a necessary preliminary to layout.

The LAYOUT program was developed during the system definition phase of the central receiver project. Heliostat coordinates were delivered to Sandia for a preliminary pilot plant and a first commercial baseline plant. After these deliveries, an increase of interest in small systems occurred, and funding to the Energy Foundation of Texas (EFT), lead to the development of the Individual Heliostat Performance Model (k.e., IH-System), which starts with LAYOUT and feeds the actual heliostat locations into the performance model.

The individual heliostat program is equipped with variable dimensions for the heliostat field variables, so that the core size of the program is under input control. A variety of output styles are provided to handle the large amount of output data. Special options are available to reduce the CPU time required to study restricted regions of the collector field. See Appendix C for description of SUBFLD.

3.2 THE IH OUTPUT STYLES

There are four major output styles which are available for each of the field variables such as receiver interception (FINT), shading and blocking fraction (FMIRR), afternoon insolation weighted averages of FMIRR (FSAB), and many others. The four outputs are as follows:

A. Individual Heliostat Output as in Figure 3-1 for the shading and blocking fraction.

B. Circle-Sector output with circle and sector averages provides a much needed review of layout efficiency. See Figure 3-2.

C. North/South cellwise averages over the individual responses. This output is needed to see the overall tends in response. See Figure 3-3.

D. Contour output based on the cellwise averages locates contour of varous percentiles of performance in the collector field. See Figure 3-4.

3.3 THE FIRST FOUR OBJECTIVES UNDER SFDI FUNDING

The University of Houston work under the SFDI contract was initiated on March 1, 1979, and at that point in time our first four objectives were:

A. To provide heliostat layouts to SFDI specifications,

B. To write a heliostat coordinates file for card delivery,

C. To provide shading and blocking output to verify the layout procedure, and

D. To output total redirected power for the design time.

A Job Control Language (JCL) set-up for both time-sharing and batch execution was required. Most work can be done in time-sharing mode, but the final annual performance study will be too lengthy for a time-sharing job.

3.3.1 SFDI UNIT REQUIREMENTS

The SFDI requires all quantities having the dimension of length to be input in feet, instead of meters as originally specified by NSF. Consequently, we installed a conversion from feet to meters in the input module, and the reverse conversion from meters to feet for the output to the heliostat coordinate file. All internal variables are still metric.

SECTOR 8

2 0918 0908 0908 0908 0918 0911 0904 0902 0897 0896 0905 0895
3 0938 0803 0980 0920 0940 0792 0968 0909 0941 0784 0960 0902 0945 0780 0952
4 0867 0909 0959 0916 0868 0898 0948 0920 0871 0890 0940 0925 0877 0884 0933
5 0904 ** 0953 0864 0908 ** 0939 0853 0909 ** 0929 0846 0913 ** 0922
* 6 0935 0901 0868 0931 0892 0869 0928 0835 0873 0926 0880
7 0927 0926 0925 0924 0924 0924 0924 0924 0925 0926 0925
8 0926 0925 0925 0925 0925 0923 0921 0919 0918 0917 0916
9 0937 0932 0927 0923 0919 0916 0914 0911 0910 0909 0908
10 0792 0932 0884 0925 0779 0921 0873 0922 0773 0917 0869
11 0873 0900 0926 0912 0873 0839 0919 0914 0875 0881 0918
12 ** 0916 0804 0873 ** 0899 0791 0870 ** 0887 0786
*13 0942 0893 0856 0943 0880 0860 0947 0871
14 0954 0955 0956 0950 0947 0938 0934 0933 0936
15 0962 0909 0934 0790 0945 0888 0934 0778
16 0911 0950 0919 0878 0894 0937 0922 0881 0884
17 0954 0874 0858 ** 0927 0852 0877 **
*18 0900 0844 0913 0901 0863 0959
19 0922 0914 0900 0911 0923 0938 0958
20 0900 0769 0911 0868 0916 0789
21 0889 0838 0902 0905 0890 0864 0888
22 0836 ** 0886 0970 0850 **
*23 0910 0892 0915 0945 0981
24 0897 0987 0900 0919
25 0936 0892 0908 0816 0931
26 0920 0921 0909 0921
27 0929 0969 0915 ** 0922
*28 0918 0898 0895 0915
29 0904 0896 0874
30 1000 1000 1000 1000

SECTOR 9

2 0895 0907 0909
3 0900 0951 0781 0947 0902 0958 1000 1000 1000
4 0932 0884 0880 0929 0939 0890 0876 0926 0948 0899 0874 0924 0959
5 0844 0920 ** 0917 0849 0929 ** 0914 0859 0942 ** 0914 0873 0958 **
* 6 0878 0927 0877 0887 0933 0876 0897 0939 0877 0909 1000
7 0924 0925 0927 0929 0930 0931 0932 0933 0934 0935 0943
8 0916 0918 0920 0922 0925 0929 0933 0934 0935 0936
9 0908 0908 0909 0910 0912 0914 0916 0920 0923 0927 0988
10 0918 0773 0920 0872 0920 0779 0927 0882 0930 0791
11 0919 0880 0877 0916 0919 0887 0875 0913 0925 0897 1000
12 0884 ** 0874 0791 0896 ** 0878 0805 0914 **
*13 0868 0949 0863 0879 0949 0863 0894 0950
14 0935 0932 0933 0938 0947 0952 0957 1000
15 0942 0885 0937 0780 0936 0900 0953 0802
16 0926 0931 0889 0880 0921 0945 0902 1000
17 0909 0862 0917 ** 0856 0857 0940 **
*18 0894 0909 0932 0842 0894 0978
19 0944 0927 0915 0903 0905
20 0947 0884 0920 0767 0892 0988
21 0914 0914 0895 0848 0882
22 0873 0988 0882 ** 0839 1000
*23 0983 0946 0915 0892
24 0947 0919 0898 0886 1000
25 0900 0911 0824 1000
26 0937 0915 0923 0899
27 0973 0924 ** 1000
*28 0900 0883
29 0876 0880 0970
30 1000 1000

Figure 3-1. Shading and Blocking Fraction FMIRR for Individual Heliostats at 3 P.M. on Vernal Equinox.

Sectors 8 and 9 are Just North of East. FMIRR is Printed in the Form of a batting Average (i.e., 1000 = 1.0). The ** symbols Mark the Place of a deleted Heliostat, and each Twelfth of the Field is Shown Conformally Mapped into a Rectangle: Tower is at the Bottom.)

FRACTION OF MIRROR REFLECTING ON THE 0 DAY AT 3.00 HOURS , UNIVERSITY OF HOUSTON

TRUE VALUES= 10 ** 0 X PRINTED VALUES OUTPUT#= 2

2	0.	0.	0.	0.978	0.974	0.960	0.913	0.906	0.904	0.	0.	0.	0.940
3	0.	0.	0.	0.949	0.959	0.945	0.936	0.901	0.938	0.	0.	0.	0.937
4	0.	0.	0.	0.971	0.950	0.935	0.932	0.908	0.913	0.	0.	0.	0.935
5	0.	0.	0.	0.965	0.968	0.934	0.922	0.904	0.902	0.	0.	0.	0.932
6	0.	0.	1.000	0.977	0.957	0.931	0.914	0.899	0.909	0.926	0.	0.	0.932
7	0.	0.	0.998	0.976	0.969	0.957	0.936	0.925	0.932	0.944	0.	0.	0.952
8	0.	0.	0.999	0.961	0.962	0.950	0.935	0.922	0.927	0.943	0.	0.	0.947
9	0.	0.	1.000	0.957	0.957	0.949	0.944	0.919	0.922	0.945	0.	0.	0.948
10	0.	0.	1.000	0.965	0.936	0.930	0.919	0.872	0.871	0.911	0.	0.	0.925
11	0.	1.000	1.000	0.937	0.945	0.923	0.923	0.899	0.910	0.927	0.952	0.	0.941
12	0.	1.000	1.000	0.960	0.930	0.912	0.893	0.854	0.864	0.908	0.899	0.	0.919
13	0.	1.000	1.000	0.972	0.938	0.928	0.911	0.899	0.902	0.938	0.934	0.	0.942
14	0.998	1.000	1.000	0.975	0.954	0.953	0.952	0.945	0.950	0.957	0.957	0.963	0.965
15	0.981	1.000	1.000	0.972	0.946	0.936	0.921	0.893	0.892	0.926	0.938	0.951	0.946
16	0.990	1.000	1.000	0.991	0.956	0.933	0.929	0.909	0.925	0.932	0.936	0.962	0.955
17	0.988	1.000	1.000	0.974	0.945	0.939	0.923	0.891	0.891	0.924	0.937	0.961	0.948
18	0.989	1.000	1.000	0.982	0.943	0.940	0.924	0.897	0.907	0.933	0.946	0.957	0.951
19	0.996	1.000	1.000	0.994	0.959	0.956	0.932	0.924	0.919	0.936	0.962	0.966	0.962
20	0.993	1.000	1.000	0.991	0.962	0.946	0.920	0.859	0.900	0.902	0.952	0.958	0.947
21	0.994	1.000	1.000	0.993	0.973	0.938	0.929	0.883	0.891	0.929	0.949	0.970	0.954
22	0.987	0.999	1.000	0.987	0.988	0.961	0.941	0.886	0.917	0.918	0.975	0.985	0.961
23	1.000	1.000	1.000	1.000	0.993	0.978	0.931	0.929	0.934	0.913	0.975	0.994	0.971
24	1.000	1.000	1.000	1.000	0.999	0.977	0.904	0.901	0.930	0.914	0.975	0.999	0.966
25	1.000	1.000	1.000	1.000	1.000	0.976	0.928	0.897	0.909	0.936	0.977	1.000	0.969
26	1.000	0.999	0.999	1.000	0.998	0.953	0.951	0.918	0.919	0.963	0.960	1.000	0.971
27	1.000	0.996	1.000	1.000	0.996	0.988	0.972	0.934	0.966	0.990	0.975	1.000	0.983
28	1.000	0.999	1.000	1.000	1.000	0.992	0.949	0.907	0.892	0.953	0.990	1.000	0.974
29	1.000	0.996	0.996	1.000	1.000	0.962	0.931	0.892	0.909	0.951	0.968	1.000	0.966
30	1.000	0.995	1.000	1.000	0.984	0.917	1.000	1.000	1.000	0.999	0.916	0.974	0.981
131	0.993	0.999	1.000	0.977	0.962	0.943	0.929	0.905	0.913	0.933	0.952	0.973	0.950

MAX(A) = 1.0000E 00 MIN(A) = 8.8766E-01 AVR(A) = 9.4962E-01

Figure 3-2. Circle-Sector Output of FMIRR Corresponding 3 P.M. on Day of Vernal Equinox.

Right Hand-Column Contains Circle Averages. Left Hand Column Contains Circle Numbers. Last Row Contains Sector Averages.

AIJ = (10 ** 0) X PRINTED VALUES

0.	0.	0.	0.	0.	0.	0.	0.	0.	0.	0.	0.	0.	0.	0.
0.	0.	0.	0.	0.958	0.955	0.949	0.961	0.938	0.924	0.912	0.	0.	0.	0.943
0.	0.	0.972	0.960	0.928	0.939	0.943	0.939	0.924	0.922	0.917	0.913	0.915	0.	0.932
0.	0.974	0.966	0.959	0.956	0.945	0.942	0.949	0.928	0.928	0.919	0.907	0.894	0.898	0.	0.936
0.	0.966	0.964	0.958	0.936	0.927	0.940	0.938	0.915	0.912	0.891	0.916	0.911	0.894	0.	0.928
0.969	0.957	0.970	0.956	0.939	0.943	0.950	0.951	0.912	0.909	0.898	0.893	0.915	0.902	0.906	0.930
0.943	0.965	0.962	0.956	0.959	0.972	0.979	0.977	0.912	0.895	0.900	0.888	0.908	0.903	0.920	0.938
0.981	0.965	0.963	0.977	0.989	0.997	0.989	0.958	0.933	0.919	0.894	0.906	0.909	0.913	0.921	0.948
1.000	0.993	0.996	0.996	0.999	1.000	0.998	0.	0.965	0.933	0.915	0.947	0.934	0.944	0.	0.967
0.	1.000	1.000	1.000	1.000	1.000	0.999	1.000	0.967	0.954	0.940	0.933	0.923	0.944	0.	0.972
0.	0.	1.000	1.000	1.000	1.000	0.999	1.000	0.984	0.957	0.941	0.921	0.934	0.	0.	0.977
0.	0.	0.	1.000	1.000	0.998	0.992	0.984	0.960	0.945	0.936	0.964	0.	0.	0.	0.974
0.	0.	0.	0.	0.	0.986	0.979	0.984	0.960	0.945	0.	0.	0.	0.	0.	0.971
0.970	0.970	0.976	0.975	0.974	0.975	0.973	0.965	0.940	0.929	0.915	0.913	0.914	0.911	0.940	0.959

Figure 3-3. North-South Cell Structure.

Cell Averages of FMIRR Correspond to the Circle-Sector Output Which is Just Above. The Right Hand and Bottom Outputs Contain Row and Column Averages for the Cells. Note That the Boundary Cells May be Only Partially Occupied.

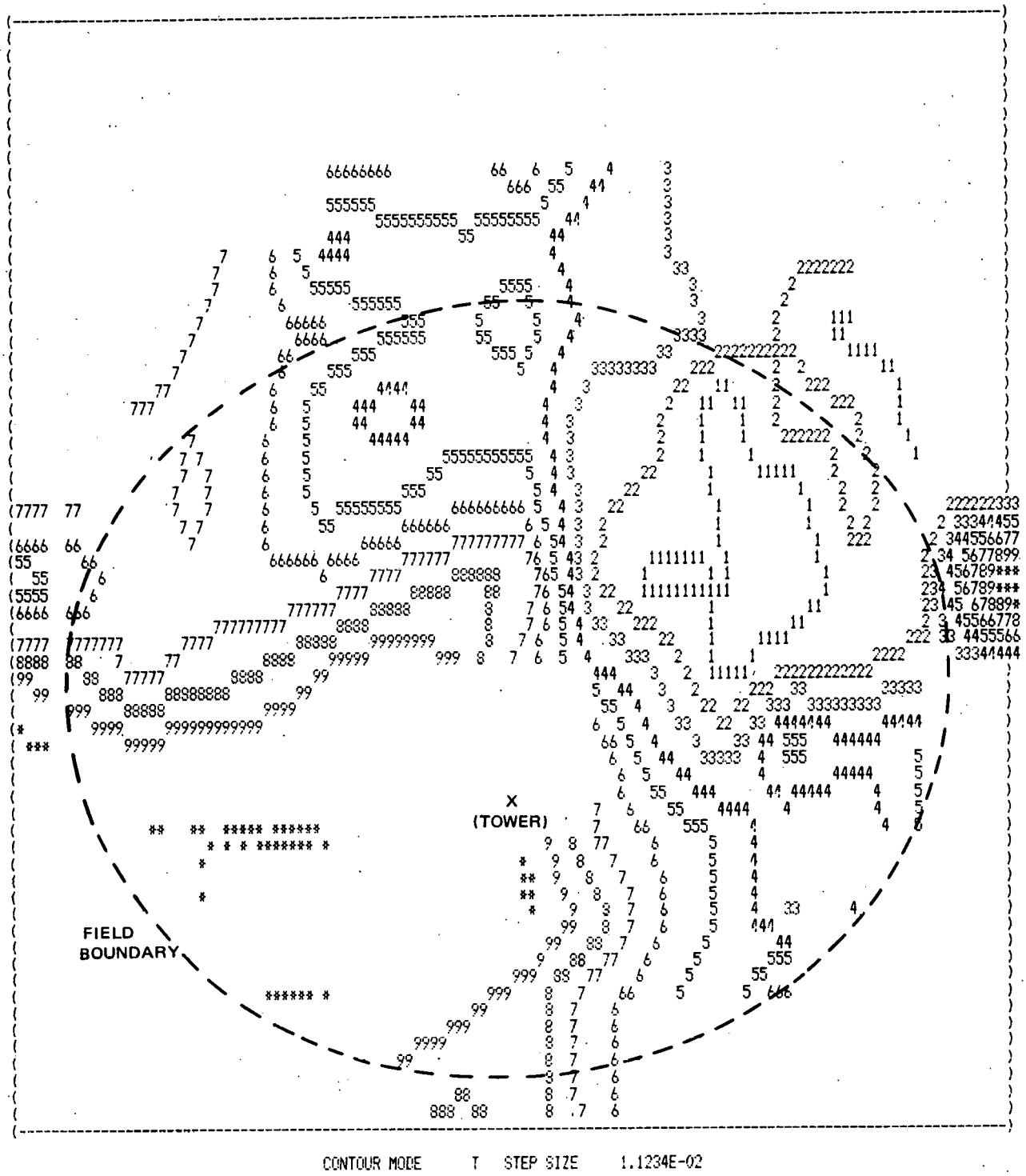

Figure 3-4. Contour Output for FMIRR Based on Cell Averages Shown in Figure 3-3.

In This Diagram the * Represents Unity FMIRR, the 9's Border the Region Where FMIRR is <0.9888, the 8's Border the Region Where FMIRR is >0.9775 etc. The Event on the Right Results From the Fortuitous High of 0.990 on the Right of Figure 3-3, Which is Associated With the 1000's in Circle 3, Sector 9, Figure 3-1.

3.3.2 SFDI Field Boundary

An optimized collector field defines the optimum field boundary. Hence, several methods of transferring the trim (i.e., field boundary) from RCELL to LAYOUT were provided. However, none of them anticipated the SFDI specifications which provide the inner and outer field limits, the tower location, and the location of the exclusions for roads. Consequently, the SFDI field boundary modifications and inputs were required.

3.3.3 SFDI Inclined Field

At present, the RCELL optimization works with a North-South inclined field, but does not permit an East-West component of incline because symmetry is assumed for the morning and afternoon insolation. However, all performance models should be able to accept an arbitrarily inclined flat field. After some discussion about splitting the field into two flats, it was decided to go with a very slight North-South incline. Hence, an IH code modification for inclined fields was provided.

3.3.4 SFDI Heliostat Coordinate File

The SFDI heliostat coordinates file writes one card per heliostat containing a six-character heliostat designator, the (X,Y,Z) coordinates in feet, the azimuth angle in radians and one to three aim points if desired. For further details see Section 4.

Outputs for shading and blocking data and total redirected power were available as soon as the above modifications were completed.

3.4 THE RECEIVER PANEL POWER SUMMARY FOR ROCKETDYNE

The SFDI receiver design subcontractor (Rocketdyne) developed an early need for the annual summary of receiver panel power, in order to study receiver design and control issues. This output was accomplished by the cellwise performance model with an extra output for card delivery to Mr. Fukui of Rocketdyne. The Cellwise model can simulate a year of performance much more efficiently than the Individual Heliostat (IH) model. Furthermore, at this point the IH model had no access to receiver information of any kind, except for a default set of receiver interception fractions which are not properly related to the SFDI receiver design.

The Panel Power Summary outputs are presented in Section 5.1.

3.5 COMPLETION OF THE INDIVIDUAL HELIOSTAT SIMULATION SYSTEM

Heliostat images and receiver interception fractions vary smoothly as a function of heliostat location. Hence it is not necessary to generate a heliostat image for every heliostat in the IH system. The necessary data is already available from the so-called node file which contains a receiver flux density matrix for each representative heliostat in the cellwise performance model. Consequently, it is desirable to keep the receiver model and the image generating subroutines in the cellwise performance code, and to create interpolating subroutines which can utilize the existing node files and generate the individual heliostat response in the IH code system.

With realistic receiver interception data available in the IH system it is relatively easy to transfer the receiver output subroutines and the annual summary subroutines from the cellwise performance system to the IH system. This transfer process completes the IH simulation system in the sense that it now contains all outputs which were previously available in the cellwise system, except those relating to the image generation capabilities of receiver model.

The following subroutines are involved.

XY/FINTP1 → { IH/FINTP1, IH/HINT }

{ XY/FINP2, XY/FINP3 } → IH/FINTP3

XY/PANPOW → IH/PANPOW

XY/PANEFF → IH/PANEFF

FINTP1 reads the node file. HINT provides interpolation to the individual heliostats. FINTP2 provides shading and blocking information to the PANPOW and FINTP3. FINTP3 provides receiver flux density output. PANPOW and PANEFF provide annual summary output for panel powers and system efficiency. Further details concerning the IH subroutines are available in Appendix C.

3.6 DEVELOPMENT OF THE LAYOUT PROCESSOR

Prior to the SFDI contract, the layout processor had been used for both pilot and commercial scale layouts. However, the CELLAY provision for balancing losses within a zone was not available until this year. During the SFDI contract period, three major improvements were made in the layout processor.

A. The step in radius was improved by incorporating the CELLAY coefficients.

B. The step in radius was improved by incorporating the so called "half step" procedure which eliminates the small gaps which used to occur at zone boundaries.

C. Improved shifts near the deleted heliostat were introduced into the CIRCI subroutine which strings heliostats along a layout circle.

These features are explained more fully in Appendix D and also in Section 4.

3.7 REMOVING SELECTED HELIOSTATS

The heliostat coordinate file has exact east-west symmetry, although several western heliostats are marked with stars because they violate the asymmetric western field limit. These coordinates represent all of the locations which are allowed within the field limits. An actual system will not necessarily have heliostats at every site. Conditions in the field may void some of the sites, the field may be reduced to avoid excess power, or the shape of the field may be modified to suit the receiver design. For all of these reasons, we need a means of selectively removing heliostats from the performance model. This is done by defining an ISKIP function which contains data for the removed circles and the selected heliostats.

This option was used to study the possibility of reducing the receiver asymmetry ratio by transferring various numbers of the northern heliostats to the southern field. It was found that the receiver asymmetry ratio could not be eliminated because of the diurnal cosine effects and furthermore, efforts to reduce it caused a significant loss of heliostat performance. Part of the trouble comes from the imposition of field boundaries obtained from the preliminary pilot plant design and its scaling from the commercial system. The given boundaries are in accordance with the determination (in the preliminary design study) that a fully optimized 10 MWe plant would tend toward a north only field. Of course, in a fully optimized system, the boundary heliostats

are all marginal so that deletion, addition, or transferral of a few boundary heliostats has little or no effect on the cost of energy collected.

The receiver asymmetry ratios are shown in Figure 5-12 for the SFDI field as delivered to Rocketdyne.

3.8 THE STARTUP STUDY VIA THE IH SYSTEM

The sunrise startup study outputs shading and blocking performance and receiver panel powers for a sample of early morning times.

These outputs are available from the IH system with inputs set to accept a large set of neighbors in order to generate all possible losses which can occur at low sun angles. The panel powers are obtained from the standard PANPOW subroutine, but minor modifications were needed to force the flow of control into the annual part of the program for the morning startup times. See Section 5.4 for details of study.

3.9 THE CLOUD STUDY VIA THE CELLWISE SYSTEM

The Aerospace Corporation provided the cloud model. Unfortunately, the model is based on relatively sparse data, and the rapid spacial dependence of the cloud effect was just recently realized. Consequently, it is appropriate to carry out the study in cellwise performance system.

The cloud motion is much faster than the diurnal motion of the sun. Consequently, it is appropriate to create a new subroutine which can be called from inside the loop over hours and below the loop over the heliostats. This subroutine interpolates the cloud transmission matrix to provide a transmission factor for each cell, and then calls a modified version of PANPOW for panel power outputs. See Section 5.5 for details of the on-going study.

3.10 THE DEFOCUS STUDY VIA CIRCLE-SECTOR PANEL POWERS IN THE IH SYSTEM

Receiver control studies use the panel power outputs which are given for a suitable set of times. Normally the panel powers represent the entire heliostat field. However, for heliostat defocus studies and possibly cloud studies, it is necessary to have more detailed information. Modifications to FINTP1, FINTP3, and HINT provides a circle-sector panel power output for each sample time in the run stream. See Section 5.6 for details or proposed study.

Section 4
COLLECTOR FIELD LAYOUT

4.1 CELLAY: OBTAINING COEFFICIENTS FOR THE LAYOUT PROCESSOR

4.1.1 Introduction

Once the RCELL optimization approach is applied to a typical commercial size system, coefficients are needed to characterize the collector field and the optimum heliostat spacings for the pilot plant. The layout is radial stagger, and an optimum radial spacing is generated for each cell in the collector field as well as the associated azimuthal spacing. Once these parameters are obtained, the ground coverage and total annual energy reflected for each cell is output. The ground coverage, or heliostat density, results in the number of heliostats located in each cell. This will be used to weight various curve fits to the heliostat spacing data. The energy matrix, which has losses due to shading and blocking and cosine of incidence for the optimum spacings, is also an important output of RCELL to the CELLAY program. These two matrices comprise the data required by CELLAY to compute coefficients needed by LAYOUT to generate the collector field. In addition, CELLAY uses the shading and blocking data base utilized by RCELL which gives the losses resulting from 16 different heliostat neighborhoods, i.e., four azimuthal and four radial spacings are sampled. With this data four sets of three coefficients are generated for radial spacings.

The four sets correspond to four different azimuthal spacings. For each of the four azimuthal spacings for each cell, a radial spacing is chosen such that the loss due to shading and blocking and cosine of incidence is identical to the optimum. Thus for the actual layout, when the azimuthal spacing is a constraint, a radial spacing can be chosen such that the annual energy per square meter of reflector is the same as the optimum, even though the spacings are not optimum. Fortunately, the azimuthal spacing is pretty much the same everywhere. This means the radial and azimuthal spacing are not vastly different from the optimum even though the azimuth is changing somewhat.

The idea of four sets of coefficients for the radial spacing is an improvement on the prior layout approach which used only one set of coefficients and one polynomial. Previously, the fact that the azimuthal separation along the arc was becoming smaller within a zone was ignored as far as the choice for radial spacing was concerned. A zone is a region where all heliostats have the same angular separation as measured from the tower. As one moves towards the tower from the periphery of a zone, the number of heliostats within a fixed angle of azimuth must be reduced to prevent abnormal azimuthal crowding. When this is done, a slip plane is instituted and the regular array of radial stagger is broken, and a new zone begins. The adjustment of radial spacings in accord with the existing azimuthal spacings requires more information than previously, and CELLAY provides this by specifying the radial separation required in each cell to give the same shading and blocking loss observed in the optimized RCELL run for four specified azimuthal spacings. The four spacings are 0.85 Z_0, 0.95 Z_0, 1.05 Z_0, and 1.15 Z_0 where Z_0 is 2.1 times DMIR. DMIR is the width of the heliostat. All optimum values of Z for the collector field fall within this range of azimuth.

LAYOUT uses the information provided by CELLAY by determining the local azimuthal spacing, which is a given (constrained), and then interpolating the four polynomials to find the suitable radial spacing for the particular position in the field, which is determined by receiver elevation angle. Therefore, the resulting azimuthal and radial spacing shows the same annual cosine of incidence and shading and blocking loss as the optimum RCELL run at the same collector field position (receiver elevation).

4.1.2 Procedure and Method

The objective of the CELLAY program is to supply the layout program with more than just three constants for the determination of $R(\theta)$ as was previously done. R is the radial spacing and θ is the receiver elevation.

In addition to R being a function of θ, it should also be a function of Z, the azimuthal spacing, which is available at the time the determination of R is to be made. Thus, we desire $R(\theta,Z)$ where R is dependent on the azimuthal spacing

Z to the extent that we wish to maintain the fraction of shading and blocking loss at a particular circle radius (or alternatively receiver elevation) as recommended by RCELL output. The angular azimuthal spacings are given and are constant within a zone, so that the azimuthal spacing is never ideal, i.e., what RCELL would recommend for a particular position in the collector field. Therefore, we choose a radial separation that maintains the fraction of loss for a particular receiver elevation angle in the field.

The first step in implementing the plan to enhance the choice of radial spacings by adding the parameter Z is to make modifications to RCELL. The first modification is to impose standard azimuthal spacings everywhere in the field. This requires each cell to have an input of Z_0 = 2.1 times DMIR for the azimuthal separation in units of heliostat widths. When RCELL takes variations about the input Z_0 in the course of the optimization, shading and blocking data will be generated for azimuthal spacings of 0.185 Z_0, 0.95 Z_0, 1.05 Z_0, 1.15 Z_0. The previous method took these same variations about Z_0, but Z_0 was different for each cell based upon an earlier curve fit to previous azimuthal spacing data. However, since Z changes only slightly throughout the field, a universal input of 2.1 can be used since the optimum azimuthal spacing was generally found to be between the range of variations taken, i.e., 2.1 (1 ± 0.15).

The final modification to RCELL is to output the optimum energy of each cell, λ_{opt}, on an annual basis to a disc file for future reference. In addition, the number of heliostats per cell is output to the same file.

The next step in obtaining the four sets of coefficients is to implement the program CELLAY. This program reads each cell's shading and blocking data file, the same used by RCELL. A 4 x 4 array has the annual energy, λ_c, for four azimuthal spacings and four radial spacings. This means 16 sample points are taken in the (R, Z) plane. Next, for each cell, the optimum energy, λ_{opt}, and optimum spacings are obtained. Next, for each azimuthal spacing Z_1 = 0.85 Z_0, Z_2 = 0.95 Z_0, Z_3 = 1.05 Z_0, Z_4 = 1.15 Z_0, a radial spacing is obtained such that for each coordinate pair the cell generates the same annual energy as at the optimum spacings (R_{opt}, Z_{opt}). This involves the use of a cubic polynomial

root finder. For Z_1, there are four values of R: $R_i = R_o\ (0.75 + 0.1 * i)$, $i = 1, 4$ where R_o is the input radial spacing for the cell in question. If the optimum energy is located in the range $[R_1, R_4]$ for the azimuth Z_1, a value for R is obtained by using the equation

$$\lambda_c(R) - \lambda_{opt} = 0$$

where

$$\lambda_c(R) = a_o + a_1R + a_2R^2 + a_3R^3$$

is a cubic polynomial in R which interpolates values of λ_c. This process is completed for all four of the Z_i so that each cell has four different (R,Z_i) spacings which have the same annual energy. This results in four different sets of radial spacings for the cellwise collector field. In the first, all azimuthal spacings in the cells are $Z_1 = 0.85 * Z$, and the other three have uniform azimuthal spacings Z_2, Z_3 and Z_4. Next a curve fit of R vs. elevation angle θ is obtained for each of the four sets of radial spacings. A three constant fit is done on each of these, resulting in the desired coefficients.

The coefficients are then input to the LAYOUT processor. For a particular tower elevation angle in the field (i.e., the radius of the position of the current circle) four values of the next radial step, R, are computed for the four azimuths, (Z_i $i = 1, 4$). A cubic polynomial is then used to interpolate a value of R given the current azimuth which lies between Z_1 and Z_4. Thus a value of R is obtained (given the constrained azimuthal spacing Z which is not far from the optimum recommended by RCELL) and when combined with Z, results in optimum shading and blocking loss for that point in the collector field. This is to be distinguished from the previous method which combined the sub-optimal values of Z with the optimal values of R, which resulted in sub-optimal values of shading and blocking. The net effect of the new method is that when the azimuthal separation is less than the optimum, the radial spacing is a little greater than optimum. And when the azimuthal spacing is greater than the optimum recommended by RCELL for a point in the field, the radial spacing will be a little less than the optimum.

4.1.3 Results

The resulting coefficients from CELLAY are determined entirely by the RCELL run which precedes it. The optimum spacings are, of course, affected in a very complex way which is described in an earlier section on the theory of RCELL. All of the cost, loss and simulation models go into computing the final optimum spacings. CELLAY merely takes the output and converts this information into 12 coefficients which LAYOUT can utilize.

The coefficients are input into a polynomial of the form:

$$R = C_1/\theta + C_2 + C_3\theta$$

for each azimuth Z_i, i = 1, 4. The variable θ is in degrees rather than radians. The 12 coefficients are given in Appendix B which describes the /IH/ code's inputs.

4.2 LAYOUT: OBTAINING HELIOSTAT COORDINATES

4.2.1 Introduction

A subroutine called LAYOUT and its associated subroutines are the primary souce for generating heliostat location coordinates. This routine accepts data from RCELL by way of CELLAY to do its job. In addition, data concerning the site, tower and heliostat characteristics are required. Site specifications include imposed boundaries for the collector field, roads, and slope of the land. Tower height (receiver center line elevation above the plane of heliostat centers) is needed to determine field position, and heliostat width and turning radius determine mechanical limits for densest packing. The output of coordinates are given in (X,Y,Z) coordinates where Z is the vertical distance from the level plane which is perpendicular to the tower. Polar coordinates are output as well.

The heliostats are laid out based upon the radial-stagger neighborhood configuration. In the region near a particular heliostat, the configuration is only slightly compressed azimuthally as the distance to the tower decreases.

On the large scale, however, all heliostats are required to be on circles concentric about the tower. If the ground is sloped, the true circles are in the ground plane and not the level plane. In the level plane they will be elliptical, and centered on a point projected from the receiver downward and perpendicular to the ground plane.

The radial-stagger layout gives rise to zones within the collector field. These are annular regions where all heliostats have the same angular azimuthal separation. However, in the region of a zone nearest the tower, the azimuthal compression requires the start of a new zone and the number of heliostats per circle must be reduced, thereby increasing the angular azimuthal spacing. This is typically done with some integer ratio which describes the number of heliostats within a fixed azimuthal range (a sector) in the previous zone to the number in the new zone nearer the tower. For the pilot plant this was 4/3, which reduces the number of heliostats per circle by 25% each time a new zone is required.

Currently only the radial-stagger configuration is generated by LAYOUT as this is the field recommended by previous RCELL runs. Commercial sized fields as well as other configurations (e.g., hexagonal close packed near the tower) are possible modifications, but are not currently available. Another limitation is the fact that the circle radii are identical in the northern and southern fields. Since the collector field will usually be broken by an east-west radial road, the possibility of obtaining different coefficients and therefore different radii for the southern field exists, but is not currently an available option in the code.

The code, as it exists, does layout heliostat coordinates in such a way as to represent in good fashion the commercial field previously optimized. The layout procedure is very fast and therefore many trial runs can be made at minimal expense. Meanwhile, important control parameters are varied to appropriately utilize the information supplied by RCELL so that a properly representative collector field may be produced.

4.2.2 Imposed Boundaries

The boundaries of the collector field were frozen early in the design. The general shape of the field is revealed in Figure 4-1. Important FORTRAN variables are shown and their values are given in Appendix B. As explained in the appendix, the boundaries are important in that they define the region in which heliostat pedestals may be placed. Thus the collector field land area is constrained. This would present a new problem to an optimization run which usually chooses to optimize land area. However, for coordinate generation LAYOUT is designed to use several options for the trim, or boundaries. Data from the RCELL optimization can be used to define the trim or external data can be accepted.

The coefficients defining spaces were obtained from an RCELL run which had its trim imposed on it, so that when the commercial plant data was scaled to a pilot plant sized field, there would be enough heliostats to supply the required power for a 10 MWe plant. The coordinate generator is therefore structured to accept boundaries when layouts are produced, regardless of the source of these boundaries.

4.2.3 Slip Planes and Deletes

A slip plane is the region between two zones of the collector field, i.e., the radial distance from the tower where the heliostat count within a certain fixed sector changes from 4 to 3 in the case of the pilot plant. Therefore, the azimuthal angular separation changes by 4/3 between zones. These slip planes are determined by the code when excessive azimuthal crowding begins to occur within a zone. A discussion of the specification of crowding occurs in Section 4.2.4.

The deletes are shown by the X's in Figure 4-2. They are directly behind the heliostats in the next zone. The blocking would be excessive, therefore they are removed. However, this merely results in that particular circle having the same number of heliostats within a fixed sector as the first circle in the new zone. Therefore the deleted heliostats actually move the slip plane back one circle, although we prefer to acknowledge the removal of such a poor performing heliostat.

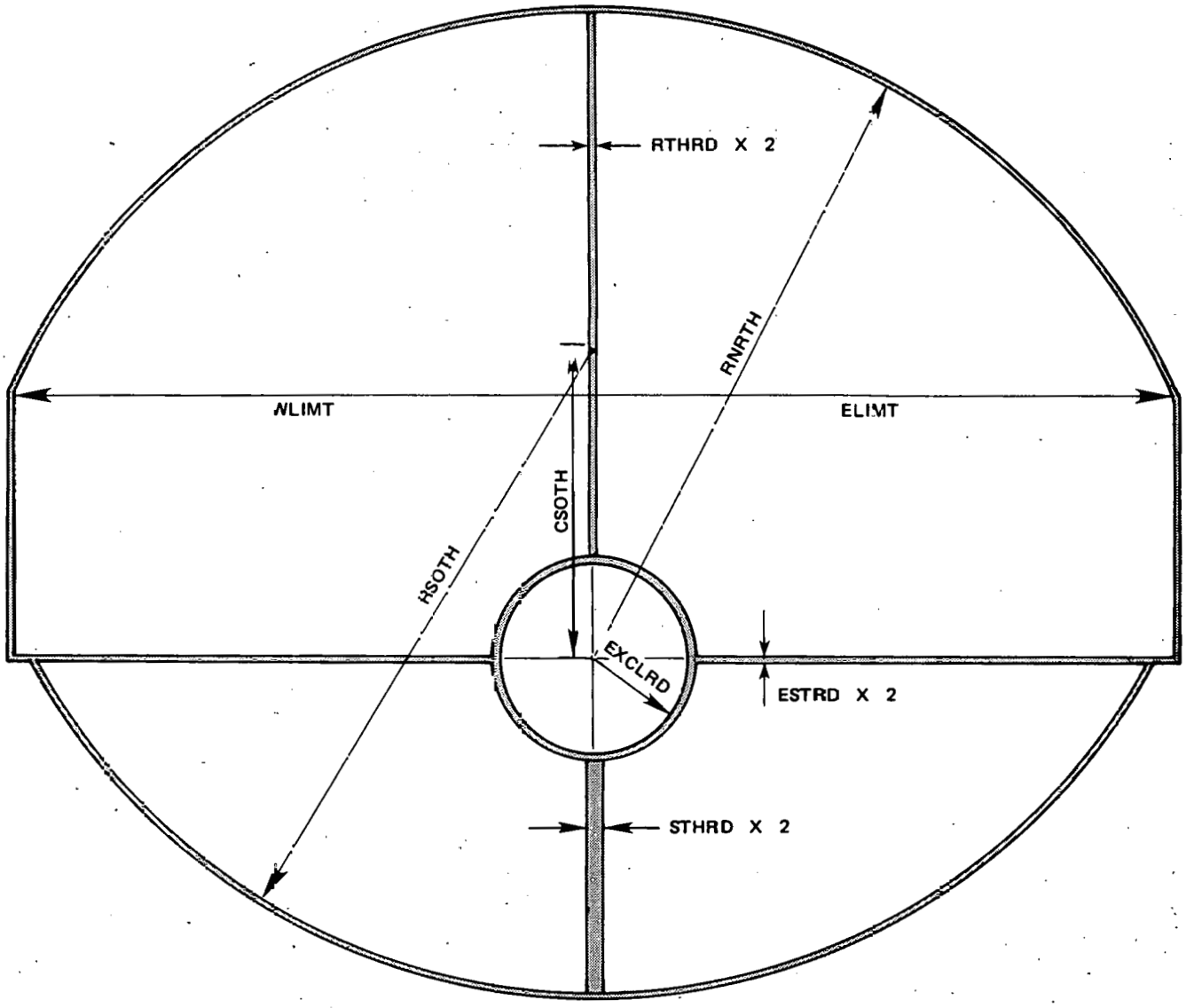

Figure 4-1. Imposed Collector Field Boundaries and Important FORTRAN Variables for the Layout Processor

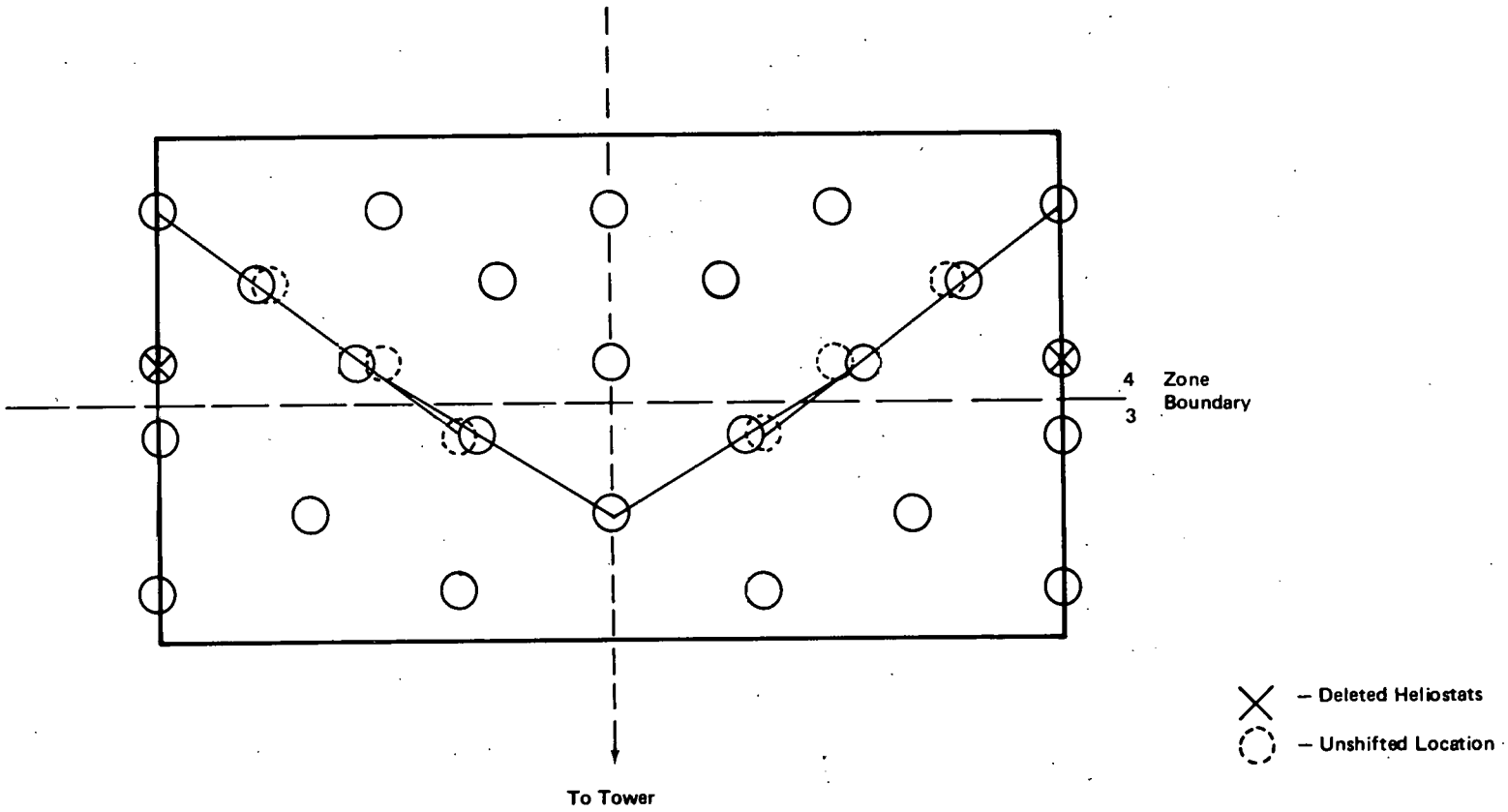

Figure 4-2. Deleted Heliostats and Azimuthal Slides at the Zone Boundary

The solid and dotted circles in Figure 4-2, adjacent to one another in the azimuthal direction, show the direction and distance that a heliostat is moved along the circle to alleviate excessive blocking. Note that four heliostats are moved toward the deleted position as this intuitively fills in the gap and lets the amount of shading and blocking decrease by giving each moved heliostat more room as well as their neighbors. In the first row of the new zone, two heliostats are moved toward one another to alleviate the blocking they cause on heliostats behind them. Here the azimuthal separation is greater than optimum, so there is no harm in sliding them together. The magnitude of the slides is determined by the straight lines drawn diagonally in Figure 4.2. The straight lines insure that the heliostats connected by them have equal angular azimuthal separation, thus insuring the blocking loss is distributed between the heliostats as evenly as possible. This was determined by looking at individual heliostat performance output via the /IH/ system of code and, by inspection, denoting the poor performing heliostats and correcting them via the approach just described. Such a remedy helps smooth out the shading and blocking loss in the area of irregular neighborhoods known as the slip plane area.

4.2.4 Specification of Important Controls and Variables

Certain variables of the LAYOUT code are important in controlling the process of generating heliostat coordinates. These variables can change the look of a particular layout even though the same spacing coefficients are used and the imposed boundaries are not violated. They have to do with the initialization of the radius of the outside circle and its initial azimuthal separation. Further, the zone ratio (4/3 was chosen) is an optional variable as well as the minimum azimuthal spacing allowed before a new zone begins. Thus a large number of sets of collector field coordinates can be generated. Therefore obtaining a proper representative field is somewhat of an art, and the person producing the output should have considerable knowledge concerning the output desired as well as knowledge of the way to code works. Obviously, ridiculous initial values can be input for the variables mentioned above which would result in unacceptable layouts even though good data was obtained from RCELL and CELLAY.

All of the following FORTRAN variables can be found in Appendix B. The first is ZRATIO and is the ratio of heliostats from zone to zone. This variable is closely tied to RSYMIN which is the minimum azimuthal spacing in DMIR (heliostat width) which is allowed before a new zone is required. Trial and error led to the value of 4/3 for ZRATIO rather than other values such as 5/4 or 3/2. RSYMIN is chosen to be 2.1*0.85*0.9 = 1.6065 DMIR. The nominal azimuthal separation is 2.1 DMIR, and multiplying by 0.85 results in the smallest separation calculated in the RCELL run. The additional factor of 0.9 is added to allow for the fact that the deleted heliostat in the last circle of a zone increases the azimuthal spacing. In addition, thermal power requirements forced us to crowd the heliostats to allow for enough heliostat pedestal positions in the constrained land area. A denser heliostat field can be produced by allowing smaller spacings.

Two other variables which affect each layout are called RSYMAX and RA1. RSYMAX is the azimuthal separation of the outermost circle of heliostats, and RA1 is the radius in DMIR units of that circle measured from the tower. RA1 is defined by the imposed boundaries of this field, but RSYMAX may take on any value. Initially we set the value of RSYMAX to 2.1*1.15 = 2.415 DMIR, but this kind of initial azimuthal separation allowed for an undesirable slip plane in the inner most couple of circles. Therefore, after a few runs, the value of 2.1 was input and all slip planes were moved back a few circles and a desirable layout was obtained.

The above four variables are the important parameters in laying out a field once all data has been received from RCELL, CELLAY and outside sources. Due to the discrete nature of the generation of circle radii, an entire circle of heliostats may be lost or gained at the inner boundary of the collector field by only slight changes in these variables. This can have a large effect on the number of heliostats on the specified land area. Thus careful "fine tuning" must be performed to achieve a desirable layout.

4.2.5 Operation of Subroutines

A general breakdown on the operation of the subroutines of LAYOUT will be discussed in this section to reveal the procedure and logic of obtaining a

collector field layout. The first thing specified by the code concerning the circle radii is the radius of the outermost circle and its azimuthal spacing. Next, the CELLAY coefficients determine the radial spacing between the initial circle and the third circle given the radius and azimuthal spacing of the first circle. The second circle is then placed between the first and third circle using the CELLAY coefficients in the subroutine called HSTEP, which involves an iterative process.

The radii of succeeding circles are generated using the above process until a slip plane is encountered, which is determined by RSYMIN. When this occurs, the zone ratio of 4/3 is utilized, and then the radii of the next zone is computed. While this process is taking place, the mechanical limits (the closest distance allowed between adjacent heliostats) is checked at each circle radius which is generated. If mechanical limits are violated, the radius of the new circle is decreased until mechanical limits are satisfied. This process of calculating circle radii continues until the inner boundary of the field is encountered.

After all the radii are properly calculated taking into account the mechanical limits of the heliostats and slip planes, the location of heliostats on the circles needs to be determined. This involves only their azimuthal placement with respect to the tower since their radii are previously determined. The placement process takes place only for the east half of the field since there is east-west asymmetry. Starting in the north, heliostats are placed along a particular circle according to the particular subroutine called for that radius. This determines the correct azimuthal spacing along that circle. When the east radial road is encountered, heliostats that would be placed in the roadway are skipped. The placement process terminates for the particular circle in question when a boundary is encountered. This may be the east limit, the southern boundary, or the southern radial road should the circle happen to close all the way around to the south.

Roads and boundaries therefore come into play when the azimuthal component of a particular heliostat location coordinate is being generated. The deletes,

slip planes, and shifts discussed in 4.2.3 are taken into account by the subroutine that is called for a particular circle radius based upon its position within a zone of circles. In all, there are four possible kinds of azimuthal spacings on a given circle, and they are shown in Figure 4.2. Once the azimuthal placement of all heliostats on a circle are calculated, the (X,Y,Z) coordinates, along with the polar coordinates, are written to a data file. Then the next circle in question is treated in a like manner, until all coordinates have been generated and dumped to a disc file. This includes the symmetric western half of the field which is generated by a sign change in coordinates of the eastern half of the field.

4.2.6 Results

The final results were obtained after several iterations involving changes in the previously discussed control variables. Thermal power requirements and loss factors dictated the number of heliostats desired. This layout was generated for the Sandia/STMPO specified heliostat so that enough pedestal positions would be available for either the Martin Marietta or McDonnell Douglas heliostat to achieve specified performance. After the final layout output, a couple of variations were exercised to improve situations revealed by the individual heliostat /IH/ performance code. The azimuthal shift of heliostats in the first circle of a new zone was instituted after examination of shading and blocking performance output from the /IH/ code.

Blocking loss was more evenly distributed after this shift was instituted where mechanical limits were not violated. Other variations included output to cnhance the southern field. By putting more pedestal positions in the south, it was hoped that extreme flux gradients on the receiver could be alleviated. However, only moderate success was achieved by shifting an excessive number of efficient north heliostats to inefficient south sites. As the field boundaries of Figure 4-1 were violated and the cost was excessive (more heliostats were required) the attempt was abandoned.

With the University of Houston delivery of heliostat location coordinates, McDonnell Douglas proceeded to have the pedestal positions plotted, and chose the heliostat pedestal positions that were to be occupied by both types of heliostats to satisfy design point performance requirements.

Section 5
SPECIAL STUDIES FOR SFDI

5.1 PANEL POWER SUMMARY FOR ROCKETDYNE

The panel power summary output was made on 5/09/79 and a card delivery to Rocketdyne followed immediately.

This run utilized the cellwise performance model with the focal height of the receiver centerline above the plane of the heliostats set at 75.44 m (247.5 feet). The field boundary was trimmed to give 1910 heliostats. Receiver interception is obtained from a previous receiver study made on 4/19/79 using the SFDI receiver dimensions for the external cylindrical receiver with 24 panels. The cylinder radius is 3.505 m (23 ft in diameter), and the effective height is 13.716 m (45 ft).

The incident panel powers are reduced for heliostat reflection (82.1% net),[1] mean atmospheric transmission from the heliostats to the receiver (97.6%), shading and blocking which depends on time, and receiver interception which is assumed to be time independent. Cosine of incidence effects are also included and are considered to be the unavoidable losses. Special insolation data was input for this run using actual insolation records from Barstow. (See Figure 5-2 for the insolation summary and sample of times used to represent annual behavior.) Days are measured from vernal equinox and hours from local solar noon.

The absorbed panel power is obtained from the incident panel power (incident on the receiver surface) by a linear transformation.

$$P(abs) = a*P(inc) - b$$

---

[1] 82.1% net reflectivity = (86% specular reflectivity) X (97% field layout effectiveness) X (98.4% heliostat outage factor). Field layout effectiveness includes lost layout area due to collector field spoke roads. Heliostat outage factor accounts for the loss of one field controller (32 heliostats).

where a is the coefficient of receiver absorption and b is the loss estimate for convection and radiation under average operating conditions. For this study

$$a = 0.93 \text{ and,}$$

$$b = \begin{cases} 0.240 \text{ MW/panel for boiler panels, or} \\ 0.080 \text{ MW/panel for heater panels.} \end{cases}$$

There are six heater panels in the SFDI receiver. See Figure 5-1 for the numbering of panels and the location of the heater panels. The panel powers correspond to central nodes which are spaced 15° apart around the cylindrical receiver. The dimensionless panel gradients are given by the formula

$$G(i) = (P(i) - P(i-1))/(P(i) + P(i-1))$$

Consequently, the output value of the gradient is not centered on the panel, but represents an estimate of the gradient at panel i-1/2.

In December 1979, the STMPO office issued revised collector field design criteria which were to be applied to a field design based on the Martin Marietta heliostat (the selected heliostat supplier). The revisions to the criteria included:

1) Increase the heliostat reflectivity from 0.86 to 0.89.
2) Increase the receiver absorptivity from 0.93 to 0.95
3) Removal of the 32 heliostats which had been included in the initial criteria to offset an outage of a field controller.

The resulting collector field design contained 1818 heliostats. A summary of collector performance characteristics over a 1 year period is shown in Figures 5-2 - 5-13).

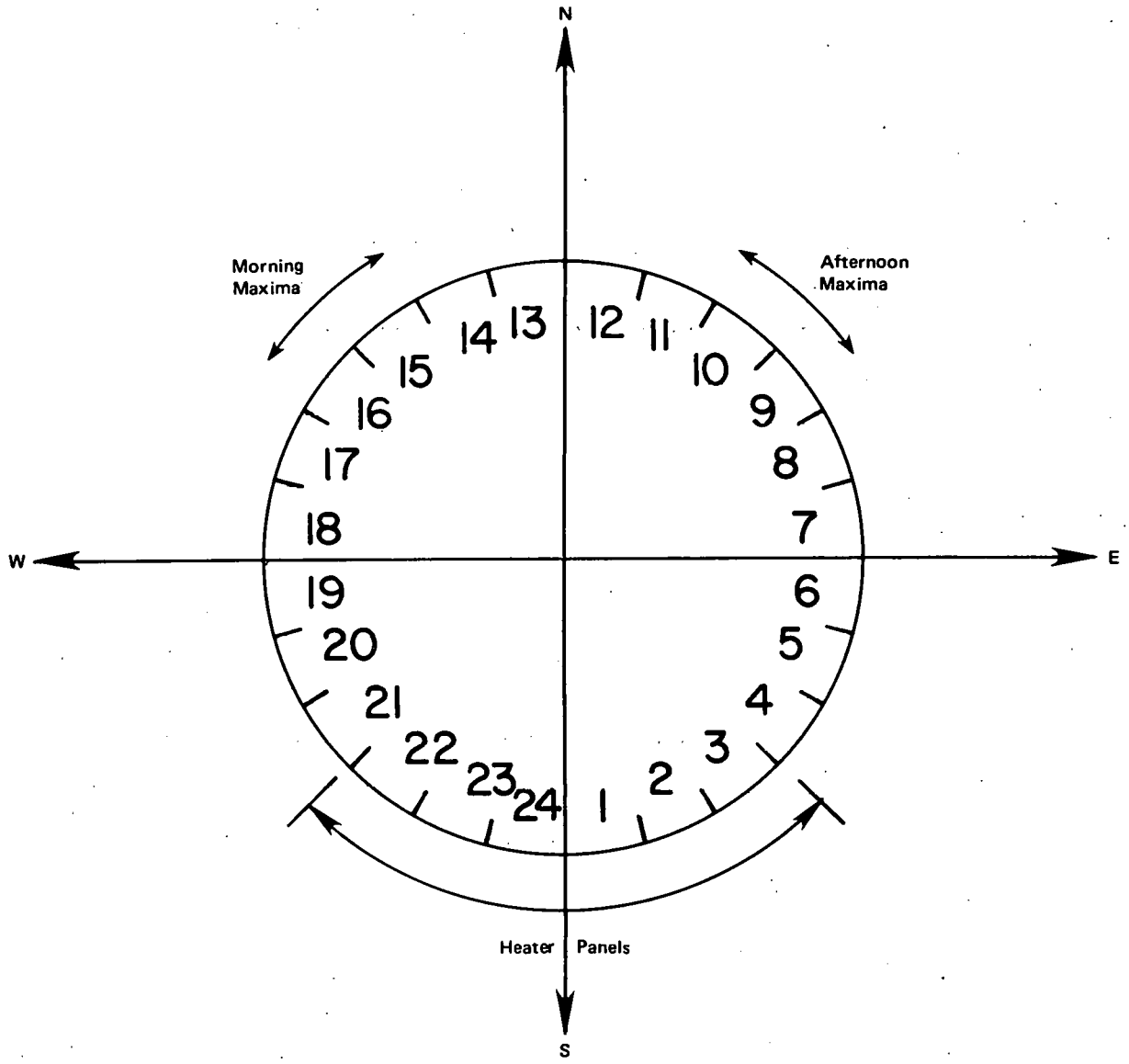

Figure 5-1. Panel Numbering System As Seen From Above.

Notice the six heater panels in the south. Panels are 15 degrees wide and are contoured to form a circle.

ANNUAL SUMMARY OF INSOLATION , UNIVERSITY OF HOUSTON , ANNUAL INSOLATION= 3.26160 MWH/M2

	HOUR =	0.	1.05	2.09	3.14	4.18	5.23	6.28	0.	0.	
DAY =	93	988.00	991.00	973.00	951.00	907.00	814.00	537.00	0.	0.	11.375
	HOUR =	0.	1.02	2.04	3.06	4.07	5.09	6.11	0.	0.	
DAY =	124	985.00	974.00	947.00	913.00	848.00	725.00	489.00	0.	0.	10.530
	HOUR =	0.	0.95	1.90	2.85	3.81	4.76	5.71	0.	0.	
DAY =	155	975.00	970.00	950.00	916.00	862.00	727.00	529.00	0.	0.	9.879
	HOUR =	0.	0.86	1.72	2.59	3.45	4.31	5.17	0.	0.	
DAY =	186	973.00	971.00	954.00	926.00	875.00	783.00	621.00	0.	0.	9.179
	HOUR =	0.	0.77	1.53	2.30	3.06	3.83	4.60	0.	0.	
DAY =	216	987.00	985.00	982.00	961.00	910.00	815.00	675.00	0.	0.	8.419
	HOUR =	0.	0.68	1.36	2.04	2.71	3.39	4.07	0.	0.	
DAY =	246	982.00	980.00	973.00	945.00	878.00	803.00	682.00	0.	0.	7.362
	HOUR =	0.	0.64	1.28	1.92	2.56	3.20	3.85	0.	0.	
DAY =	276	967.00	964.00	953.00	924.00	873.00	793.00	625.00	0.	0.	6.823

Figure 5-2. Insolation Data for Barstow Site at Times Used to Represent Yea

ANNUAL SUMMARY OF COSINES , UNIVERSITY OF HOUSTON

HOUR =	0.	1.05	2.09	3.14	4.18	5.23	6.28	0.	0.	
DAY = 93	0.8400	0.8339	0.8158	0.7865	0.7471	0.6996	0.6466	0.	0.	0.
HOUR =	0.	1.02	2.04	3.06	4.07	5.09	6.11	0.	0.	
DAY = 124	0.8429	0.8370	0.8195	0.7910	0.7526	0.7061	0.6538	0.	0.	0.
HOUR =	0.	0.95	1.90	2.85	3.81	4.76	5.71	0.	0.	
DAY = 155	0.8477	0.8424	0.8264	0.8004	0.7652	0.7220	0.6727	0.	0.	0.
HOUR =	0.	0.86	1.72	2.59	3.45	4.31	5.17	0.	0.	
DAY = 186	0.8484	0.8439	0.8305	0.8085	0.7785	0.7415	0.6987	0.	0.	0.
HOUR =	0.	0.77	1.53	2.30	3.06	3.83	4.60	0.	0.	
DAY = 216	0.8427	0.8392	0.8287	0.8115	0.7879	0.7585	0.7241	0.	0.	0.
HOUR =	0.	0.68	1.36	2.04	2.71	3.39	4.07	0.	0.	
DAY = 246	0.8343	0.8316	0.8236	0.8105	0.7925	0.7699	0.7431	0.	0.	0.
HOUR =	0.	0.64	1.28	1.92	2.56	3.20	3.85	0.	0.	
DAY = 276	0.8303	0.8279	0.8209	0.8094	0.7936	0.7737	0.7500	0.	0.	0.

Figure 5-3. Field Average of COSI with Daily and Annual Insolation-Weighted Averages. COSI is the cosine of the angle of incidence on the heliostat.

ANNUAL SUMMARY OF FMIRR , UNIVERSITY OF HOUSTON

HOUR =	0.	1.05	2.09	3.14	4.18	5.23	6.28	0.	0.	
DAY = 93	0.9909	0.9852	0.9822	0.9885	0.9849	0.9174	0.7507	0.	0.	0.
HOUR =	0.	1.02	2.04	3.06	4.07	5.09	6.11	0.	0.	
DAY = 124	0.9874	0.9843	0.9827	0.9887	0.9836	0.9135	0.7498	0.	0.	0.
HOUR =	0.	0.95	1.90	2.85	3.81	4.76	5.71	0.	0.	
DAY = 155	0.9836	0.9832	0.9852	0.9904	0.9816	0.9054	0.7418	0.	0.	0.
HOUR =	0.	0.86	1.72	2.59	3.45	4.31	5.17	0.	0.	
DAY = 186	0.9864	0.9867	0.9893	0.9912	0.9695	0.8879	0.7321	0.	0.	0.
HOUR =	0.	0.77	1.53	2.30	3.06	3.83	4.60	0.	0.	
DAY = 216	0.9912	0.9917	0.9912	0.9811	0.9460	0.8607	0.7208	0.	0.	0.
HOUR =	0.	0.68	1.36	2.04	2.71	3.39	4.07	0.	0.	
DAY = 246	0.9831	0.9825	0.9733	0.9554	0.9075	0.8226	0.7203	0.	0.	0.
HOUR =	0.	0.64	1.28	1.92	2.56	3.20	3.85	0.	0.	
DAY = 276	0.9717	0.9703	0.9602	0.9385	0.8898	0.8114	0.7201	0.	0.	0.

Figure 5-4. Field Averages of FMIRR. FMIRR is the effective fraction of the heliostat after shading and blocking losses.

ANNUAL SUMMARY OF FAREA , UNIVERSITY OF HOUSTON , ANNUAL TOTAL REFLECTED POWER/MIRROR

HOUR =	0.	1.05	2.09	3.14	4.18	5.23	6.28	0.	0.	
DAY = 93	0.8325	0.8220	0.8021	0.7777	0.7338	0.6291	0.4615	0.	0.	0.
HOUR =	0.	1.02	2.04	3.06	4.07	5.09	6.11	0.	0.	
DAY = 124	0.8327	0.8243	0.8060	0.7824	0.7381	0.6323	0.4657	0.	0.	0.
HOUR =	0.	0.95	1.90	2.85	3.81	4.76	5.71	0.	0.	
DAY = 155	0.8345	0.8289	0.8147	0.7929	0.7486	0.6406	0.4803	0.	0.	0.
HOUR =	0.	0.86	1.72	2.59	3.45	4.31	5.17	0.	0.	
DAY = 186	0.8373	0.8331	0.8218	0.8011	0.7510	0.6462	0.4957	0.	0.	0.
HOUR =	0.	0.77	1.53	2.30	3.06	3.83	4.60	0.	0.	
DAY = 216	0.8355	0.8323	0.8211	0.7945	0.7402	0.6408	0.5042	0.	0.	0.
HOUR =	0.	0.68	1.36	2.04	2.71	3.39	4.07	0.	0.	
DAY = 246	0.8190	0.8157	0.7994	0.7710	0.7123	0.6217	0.5207	0.	0.	0.
HOUR =	0.	0.64	1.28	1.92	2.56	3.20	3.85	0.	0.	
DAY = 276	0.8046	0.8011	0.7852	0.7555	0.6991	0.6166	0.5261	0.	0.	0.

Figure 5-5. Field Averages of FAREA. FAREA is daily total redirected power in kWh/m^2 and annual total redirected power in MWh/m^2. FAREA = FMIRR * FCOSI.

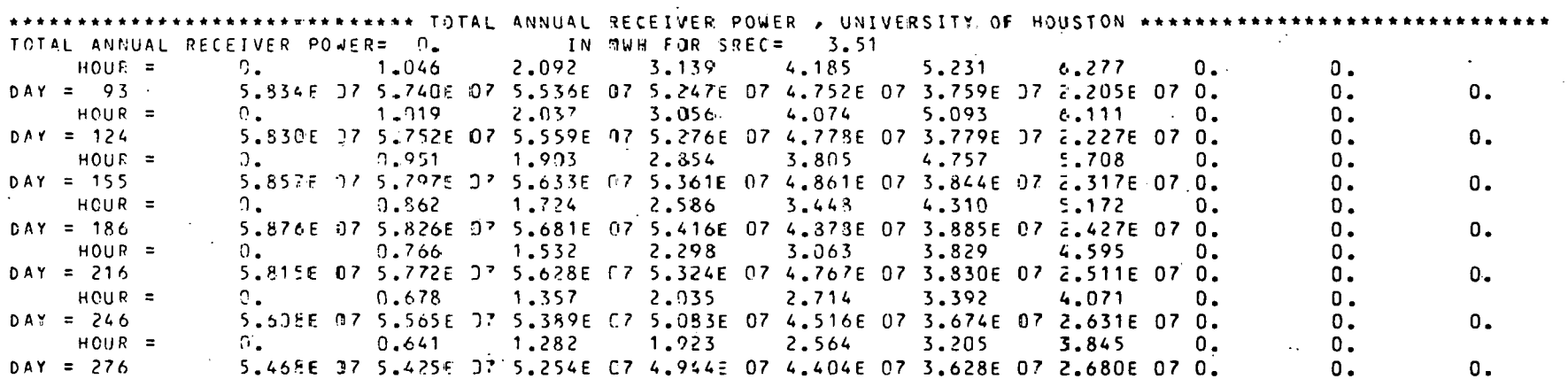

```
********** TOTAL ANNUAL RECEIVER POWER , UNIVERSITY OF HOUSTON **********
TOTAL ANNUAL RECEIVER POWER=  0.        IN MWH FOR SREC=   3.51
     HOUR =        0.          1.046       2.092       3.139       4.185       5.231       6.277       0.          0.
DAY =  93     5.834E 07   5.740E 07   5.536E 07   5.247E 07   4.752E 07   3.759E 07   2.205E 07   0.          0.          0.
     HOUR =        0.          1.019       2.037       3.056       4.074       5.093       6.111       0.          0.
DAY = 124     5.830E 07   5.752E 07   5.559E 07   5.276E 07   4.778E 07   3.779E 07   2.227E 07   0.          0.          0.
     HOUR =        0.          0.951       1.903       2.854       3.805       4.757       5.708       0.          0.
DAY = 155     5.857E 07   5.797E 07   5.633E 07   5.361E 07   4.861E 07   3.844E 07   2.317E 07   0.          0.          0.
     HOUR =        0.          0.862       1.724       2.586       3.448       4.310       5.172       0.          0.
DAY = 186     5.876E 07   5.826E 07   5.681E 07   5.416E 07   4.878E 07   3.885E 07   2.427E 07   0.          0.          0.
     HOUR =        0.          0.766       1.532       2.298       3.063       3.829       4.595       0.          0.
DAY = 216     5.815E 07   5.772E 07   5.628E 07   5.324E 07   4.767E 07   3.830E 07   2.511E 07   0.          0.          0.
     HOUR =        0.          0.678       1.357       2.035       2.714       3.392       4.071       0.          0.
DAY = 246     5.608E 07   5.565E 07   5.389E 07   5.083E 07   4.516E 07   3.674E 07   2.631E 07   0.          0.          0.
     HOUR =        0.          0.641       1.282       1.923       2.564       3.205       3.845       0.          0.
DAY = 276     5.468E 07   5.425E 07   5.254E 07   4.944E 07   4.404E 07   3.628E 07   2.680E 07   0.          0.          0.
```

(Power Data Contained in This Figure Based on University of Houston Insolation Model)

Figure 5-6. Total Incident Receiver Power for the Standard Set of Times Plus the Daily Total Energy in KWh and the Annual Total Energy in MWh.

ANNUAL SUMMARY OF SYSTEM EFFICIENCIES , UNIVERSITY OF HOUSTON

HOUR =	0.	1.05	2.09	3.14	4.18	5.23	6.28	0.	0.
DAY = 93	0.586	0.578	0.562	0.541	0.504	0.416	0.265	0.	0.
HOUR =	0.	1.02	2.04	3.06	4.07	5.09	6.11	0.	0.
DAY = 124	0.586	0.580	0.565	0.545	0.507	0.418	0.268	0.	0.
HOUR =	0.	0.95	1.90	2.85	3.81	4.76	5.71	0.	0.
DAY = 155	0.588	0.583	0.571	0.553	0.515	0.425	0.280	0.	0.
HOUR =	0.	0.86	1.72	2.59	3.45	4.31	5.17	0.	0.
DAY = 186	0.590	0.586	0.577	0.559	0.517	0.429	0.294	0.	0.
HOUR =	0.	0.77	1.53	2.30	3.06	3.83	4.60	0.	0.
DAY = 216	0.588	0.585	0.575	0.553	0.508	0.424	0.302	0.	0.
HOUR =	0.	0.68	1.36	2.04	2.71	3.39	4.07	0.	0.
DAY = 246	0.573	0.571	0.557	0.533	0.484	0.408	0.316	0.	0.
HOUR =	0.	0.64	1.28	1.92	2.56	3.20	3.85	0.	0.
DAY = 276	0.562	0.559	0.545	0.520	0.473	0.404	0.321	0.	0.

(Efficiency Data Contained in This Figure Based on University of Houston Insolation Model)

Figure 5-7. System Efficiences for Optical System Equal Total Receiver Power Divided by Total Insolation Incident on Heliostats.

ANNUAL SUMMARY OF SYSTEM EFFICIENCIES/COSI , UNIVERSITY OF HOUSTON

HOUR =	0.	1.05	2.09	3.14	4.18	5.23	6.28	0.	0.
DAY = 93	0.698	0.693	0.688	0.688	0.674	0.594	0.410	0.	0.
HOUR =	0.	1.02	2.04	3.06	4.07	5.09	6.11	0.	0.
DAY = 124	0.696	0.693	0.689	0.689	0.674	0.592	0.410	0.	0.
HOUR =	0.	0.95	1.90	2.85	3.81	4.76	5.71	0.	0.
DAY = 155	0.693	0.692	0.691	0.691	0.673	0.588	0.417	0.	0.
HOUR =	0.	0.86	1.72	2.59	3.45	4.31	5.17	0.	0.
DAY = 186	0.695	0.695	0.695	0.691	0.664	0.579	0.420	0.	0.
HOUR =	0.	0.77	1.53	2.30	3.06	3.83	4.60	0.	0.
DAY = 216	0.697	0.697	0.694	0.681	0.644	0.559	0.417	0.	0.
HOUR =	0.	0.68	1.36	2.04	2.71	3.39	4.07	0.	0.
DAY = 246	0.687	0.686	0.676	0.658	0.611	0.530	0.425	0.	0.
HOUR =	0.	0.64	1.28	1.92	2.56	3.20	3.85	0.	0.
DAY = 276	0.676	0.675	0.664	0.643	0.597	0.522	0.428	0.	0.

(Efficiency Data Contained in This Figure Based on University of Houston Insolation Model)

Figure 5-8. System Efficiencies/COSI Represent the Avoidable Losses

		(South)						(West)						(North)						(East)						(South)	
		(Panel Number)**																									
Day	Hours From Solar Noon	1	2	3	4	5	6	7	8	9	10	11	12	13	14	15	16	17	18	19	20	21	22	23	24	Total Incident Power	Sun Elevation Angle (deg)
	0	0.736	0.913	1.171	1.444	1.689	1.925	2.237	2.589	2.862	3.009	3.040	2.997	2.997	3.040	3.009	2.862	2.589	2.237	1.925	1.689	1.444	1.171	0.913	0.736	49.223	78.43
	1.05	0.722	0.877	1.112	1.355	1.568	1.768	2.041	2.364	2.629	2.797	2.875	2.900	2.973	3.091	3.128	3.027	2.775	2.416	2.081	1.814	1.534	1.228	0.941	0.741	48.752	72.12
	2.09	0.696	0.823	1.020	1.223	1.399	1.564	1.799	2.090	2.343	2.527	2.640	2.712	2.841	3.009	3.094	3.040	2.825	2.486	2.157	1.883	1.587	1.261	0.954	0.737	46.712	60.43
June 22	3.14	0.674	0.776	0.941	1.104	1.236	1.360	1.555	1.813	2.053	2.247	2.395	2.514	2.690	2.900	3.017	2.996	2.811	2.496	2.184	1.917	1.618	1.282	0.963	0.733	44.271	47.73
	4.18	0.631	0.715	0.848	0.969	1.053	1.123	1.258	1.467	1.688	1.893	2.069	2.227	2.432	2.660	2.802	2.801	2.637	2.350	2.061	1.810	1.526	1.210	0.909	0.962	39.832	34.89
	5.23	0.499	0.583	0.694	0.783	0.824	0.842	0.907	1.041	1.212	1.390	1.546	1.679	1.848	2.051	2.192	2.206	2.069	1.848	1.642	1.444	1.196	0.923	0.685	0.527	30.635	22.24
	6.28	0.247	0.304	0.373	0.418	0.421	0.398	0.398	0.439	0.518	0.633	0.750	0.834	0.914	1.023	1.115	1.134	1.034	0.870	0.749	0.664	0.558	0.438	0.328	0.253	14.810	10.00*
	0	0.717	0.890	1.144	1.414	1.661	1.903	2.224	2.587	2.870	3.030	3.070	3.031	3.031	3.070	3.030	2.870	2.587	2.224	1.903	1.661	1.414	1.144	0.890	0.717	49.080	74.99
	1.02	0.695	0.846	1.073	1.309	1.519	1.722	2.004	2.337	2.610	2.788	2.871	2.898	2.974	3.087	3.114	3.003	2.740	2.371	2.031	1.763	1.486	1.187	0.908	0.715	48.051	69.83
	2.04	0.665	0.786	0.975	1.172	1.345	1.513	1.754	2.051	2.313	2.503	2.620	2.692	2.817	2.978	3.055	2.991	2.768	2.423	2.090	1.817	1.527	1.210	0.914	0.705	45.685	59.20
May 21/	3.06	0.634	0.729	0.884	1.039	1.170	1.297	1.497	1.759	2.005	2.205	2.354	2.470	2.636	2.831	2.939	2.909	2.718	2.403	2.091	1.828	1.539	1.215	0.910	0.690	42.754	47.09
July 23	4.07	0.578	0.652	0.772	0.883	0.965	1.039	1.180	1.394	1.616	1.819	1.990	2.137	2.324	2.528	2.648	2.637	2.475	2.200	1.924	1.682	1.414	1.118	0.839	0.637	37.452	34.61
	5.09	0.438	0.507	0.601	0.675	0.712	0.734	0.806	0.942	1.111	1.278	1.415	1.530	1.680	1.858	1.979	1.981	1.857	1.662	1.466	1.273	1.044	0.806	0.601	0.465	27.420	22.16
	6.11	0.227	0.276	0.335	0.372	0.372	0.354	0.359	0.403	0.486	0.598	0.699	0.770	0.845	0.951	1.043	1.048	0.933	0.771	0.660	0.584	0.494	0.391	0.295	0.231	13.495	10.00*
	0	0.671	0.835	1.079	1.345	1.597	1.853	2.193	2.581	2.890	3.071	3.127	3.096	3.096	3.127	3.071	2.890	2.581	2.193	1.853	1.597	1.345	1.079	0.835	0.671	48.675	66.30
	0.95	0.657	0.799	1.015	1.248	1.465	1.690	1.999	2.364	2.670	2.872	2.970	3.001	3.073	3.174	3.179	3.038	2.743	2.349	1.987	1.708	1.428	1.134	0.864	0.678	48.105	62.98
	1.90	0.634	0.749	0.934	1.131	1.312	1.502	1.774	2.109	2.405	2.622	2.752	2.828	2.950	3.101	3.158	3.065	2.805	2.427	2.068	1.779	1.483	1.168	0.878	0.675	46.309	54.89
April 21/	2.85	0.601	0.690	0.838	0.993	1.134	1.285	1.518	1.820	2.106	2.336	2.498	2.614	2.773	2.955	3.045	2.988	2.762	2.415	2.077	1.797	1.499	1.177	0.876	0.661	43.455	44.56
Aug 23	3.81	0.554	0.619	0.732	0.842	0.934	1.038	1.222	1.483	1.748	1.978	2.156	2.296	2.472	2.666	2.768	2.732	2.542	2.238	1.936	1.680	1.406	1.107	0.826	0.619	38.597	33.29
	4.76	0.423	0.474	0.552	0.619	0.661	0.708	0.819	1.004	1.211	1.392	1.527	1.639	1.786	1.944	2.031	2.000	1.866	1.667	1.446	1.229	1.003	0.784	0.592	0.459	27.840	21.67
	5.71	0.252	0.282	0.315	0.329	0.326	0.331	0.375	0.469	0.603	0.742	0.840	0.908	1.000	1.122	1.195	1.151	1.019	0.873	0.750	0.639	0.527	0.418	0.325	0.263	15.056	10.00*
	0	0.621	0.778	1.065	1.280	1.541	1.818	2.089	2.608	2.946	3.151	3.222	3.198	3.198	3.222	3.151	2.946	2.608	2.189	1.818	1.541	1.280	1.015	0.778	0.621	48.730	54.76
	0.86	0.608	0.742	0.952	1.185	1.418	1.670	2.019	2.425	2.767	2.995	3.103	3.133	3.195	3.277	3.256	3.085	2.757	2.333	1.948	1.650	1.362	1.070	0.808	0.629	48.386	52.74
Equinox	1.72	0.586	0.693	0.871	1.071	1.271	1.493	1.813	2.197	2.537	2.781	2.920	2.991	3.099	3.229	3.255	3.124	2.825	2.414	2.029	1.722	1.419	1.107	0.825	0.627	46.893	47.28
(Spring	2.59	0.557	0.637	0.779	0.938	1.100	1.289	1.576	1.935	2.269	2.527	2.696	2.800	2.938	3.096	3.154	3.056	2.793	2.411	2.048	1.751	1.445	1.124	0.829	0.617	44.364	39.49
and Fall)	3.45	0.511	0.569	0.675	0.789	0.903	1.050	1.292	1.609	1.913	2.156	2.326	2.447	2.601	2.774	2.856	2.796	2.570	2.225	1.881	1.605	1.334	1.047	0.777	0.577	39.284	30.33
	4.31	0.411	0.447	0.519	0.593	0.663	0.758	0.934	1.184	1.420	1.603	1.739	1.853	2.010	2.166	2.225	2.185	2.038	1.770	1.478	1.249	1.047	0.836	0.631	0.470	30.231	20.38
	5.17	0.266	0.278	0.306	0.329	0.350	0.387	0.481	0.652	0.846	1.000	1.093	1.179	1.313	1.424	1.420	1.312	1.173	1.031	0.889	0.765	0.646	0.522	0.401	0.306	18.371	10.00*
	0	0.572	0.724	0.958	1.228	1.507	1.814	2.219	2.673	3.039	3.262	3.340	3.317	3.317	3.340	3.262	3.039	2.673	2.219	1.814	1.507	1.228	0.958	0.724	0.572	49.309	43.44
	0.77	0.560	0.688	0.896	1.138	1.391	1.679	2.072	2.520	2.896	3.139	3.249	3.268	3.313	3.380	3.342	3.149	2.796	2.344	1.931	1.610	1.310	1.014	0.755	0.581	49.023	42.19
Feb 21/	1.53	0.545	0.650	0.828	1.039	1.266	1.532	1.907	2.346	2.728	2.992	3.131	3.187	3.271	3.371	3.370	3.208	2.875	2.434	2.024	1.697	1.379	1.062	0.781	0.588	48.212	38.60
Oct 23	2.30	0.521	0.598	0.743	0.918	1.110	1.347	1.689	2.099	2.467	2.737	2.898	2.985	3.102	3.237	3.265	3.132	2.824	2.403	2.013	1.705	1.397	1.078	0.788	0.582	45.638	33.14
	3.06	0.471	0.526	0.634	0.765	0.914	1.109	1.404	1.758	2.077	2.321	2.487	2.602	2.739	2.892	2.955	2.861	2.584	2.190	1.834	1.562	1.291	1.001	0.732	0.537	40.246	26.30
	3.83	0.370	0.407	0.482	0.568	0.668	0.812	1.046	1.327	1.568	1.748	1.890	2.008	2.125	2.230	2.282	2.247	2.059	1.749	1.460	1.252	1.046	0.818	0.598	0.431	31.191	18.48
	4.60	0.244	0.257	0.291	0.334	0.385	0.469	0.636	0.861	1.048	1.170	1.269	1.366	1.485	1.548	1.496	1.406	1.284	1.092	0.908	0.789	0.688	0.564	0.420	0.298	20.308	10.00*
	0	0.522	0.667	0.893	1.161	1.446	1.762	2.074	2.627	2.995	3.217	3.296	3.274	3.274	3.296	3.217	2.995	2.627	2.174	1.762	1.446	1.161	0.893	0.667	0.522	48.068	34.77
	0.68	0.510	0.632	0.835	1.079	1.344	1.645	2.049	2.505	2.885	3.128	3.230	3.238	3.270	3.321	3.271	3.070	2.715	2.266	1.853	1.531	1.232	0.943	0.695	0.531	47.778	33.93
	1.36	0.494	0.594	0.771	0.987	1.227	1.509	1.890	2.327	2.701	2.954	3.082	3.125	3.199	3.282	3.259	3.074	2.730	2.294	1.896	1.580	1.278	0.980	0.715	0.533	46.479	31.49
Jan 21/	2.04	0.465	0.539	0.682	0.864	1.073	1.326	1.674	2.073	2.427	2.688	2.838	2.912	3.014	3.130	3.136	2.971	2.641	2.225	1.850	1.552	1.261	0.968	0.705	0.519	43.530	27.63
Nov 22	2.71	0.408	0.459	0.568	0.706	0.870	1.082	1.375	1.707	2.006	2.243	2.394	2.476	2.577	2.709	2.754	2.628	2.329	1.953	1.632	1.381	1.129	0.866	0.631	0.463	37.347	22.60
	3.39	0.327	0.362	0.437	0.532	0.649	0.817	1.059	1.320	1.552	1.753	1.916	2.015	2.074	2.145	2.191	2.119	1.880	1.570	1.328	1.153	0.962	0.738	0.530	0.379	29.806	16.65
	4.07	0.219	0.235	0.277	0.331	0.403	0.530	0.739	0.969	1.146	1.275	1.396	1.491	1.533	1.526	1.490	1.426	1.285	1.105	0.971	0.877	0.743	0.564	0.392	0.268	21.190	10.00*
	0	0.496	0.636	0.856	1.117	1.393	1.700	2.099	2.540	2.900	3.120	3.202	3.187	3.187	3.202	3.120	2.900	2.540	2.099	1.700	1.393	1.117	0.856	0.636	0.496	46.488	31.56
	0.64	0.482	0.601	0.799	1.039	1.300	1.594	1.985	2.427	2.797	3.035	3.137	3.149	3.181	3.225	3.165	2.960	2.610	2.173	1.775	1.465	1.179	0.901	0.662	0.503	46.144	30.85
	1.28	0.467	0.562	0.735	0.949	1.189	1.466	1.833	2.254	2.675	2.860	2.982	3.024	3.098	3.175	3.143	2.952	2.612	2.186	1.797	1.493	1.208	0.925	0.676	0.503	44.700	28.78
Dec 21	1.92	0.436	0.509	0.649	0.830	1.041	1.291	1.627	2.012	2.354	2.608	2.752	2.816	2.915	3.018	3.006	2.822	2.492	2.094	1.739	1.456	1.180	0.905	0.659	0.485	41.694	25.48
	2.56	0.387	0.440	0.549	0.692	0.683	1.075	1.360	1.682	1.982	2.227	2.379	2.447	2.533	2.653	2.680	2.536	2.238	1.885	1.582	1.331	1.075	0.817	0.593	0.436	36.441	21.12
	3.20	0.310	0.344	0.420	0.518	0.643	0.818	1.063	1.326	1.561	1.765	1.915	1.991	2.031	2.097	2.139	2.047	1.805	1.520	1.293	1.112	0.912	0.692	0.496	0.358	29.180	15.91
	3.85	0.203	0.218	0.259	0.312	0.386	0.513	0.704	0.899	1.057	1.190	1.313	1.399	1.420	1.409	1.392	1.327	1.177	1.002	0.876	0.787	0.665	0.509	0.358	0.248	19.662	10.00*

*Operation to a 10 deg sun elevation angle not required. Data provided for information only.
**Panel numbers are reversed from those shown in Figure 5-1.

Figure 5-9. Incident Panel Powers in MW/Panel and Total Incident Receiver Power for the Standard Set of Times Using Barstow Related Insolation

DAYS	HOUR	SOUTH TO	EAST TO	NORTH								
93	0.	0.000	0.237	0.269	0.094	0.186	0.151	0.170	0.163	0.110	0.055	0.011	-0.015
93	1.05	0.030	0.263	0.287	0.116	0.196	0.157	0.168	0.153	0.095	0.035	-0.013	-0.043
93	2.09	0.065	0.284	0.299	0.128	0.199	0.154	0.159	0.141	0.080	0.019	-0.030	-0.063
93	3.14	0.094	0.301	0.307	0.134	0.197	0.148	0.149	0.130	0.070	0.007	-0.044	-0.081
93	4.18	0.104	0.303	0.307	0.128	0.199	0.148	0.147	0.128	0.066	0.000	-0.057	-0.099
93	5.23	0.065	0.300	0.329	0.125	0.230	0.152	0.137	0.129	0.072	-0.006	-0.075	-0.119
93	6.28	0.029	0.336	0.346	-0.029	0.254	0.167	0.198	0.217	0.113	-0.021	-0.107	-0.140
124	0.	0.000	0.239	0.272	0.095	0.192	0.158	0.176	0.168	0.114	0.059	0.014	-0.014
124	1.02	0.031	0.264	0.289	0.116	0.201	0.162	0.174	0.159	0.100	0.039	-0.010	-0.041
124	2.04	0.066	0.287	0.301	0.129	0.203	0.159	0.165	0.146	0.085	0.023	-0.027	-0.061
124	3.06	0.097	0.305	0.310	0.135	0.201	0.153	0.155	0.136	0.074	0.011	-0.041	-0.078
124	4.07	0.110	0.307	0.309	0.128	0.204	0.153	0.151	0.130	0.069	0.005	-0.051	-0.093
124	5.09	0.068	0.295	0.325	0.123	0.241	0.168	0.145	0.126	0.072	-0.001	-0.071	-0.115
124	6.11	0.022	0.318	0.335	-0.047	0.251	0.170	0.207	0.240	0.141	-0.006	-0.112	-0.148
155	0.	0.000	0.245	0.279	0.098	0.205	0.173	0.191	0.181	0.124	0.066	0.019	-0.011
155	0.95	0.035	0.270	0.294	0.118	0.211	0.175	0.187	0.172	0.111	0.049	-0.002	-0.035
155	1.90	0.071	0.293	0.307	0.132	0.213	0.172	0.179	0.159	0.097	0.032	-0.020	-0.054
155	2.85	0.106	0.313	0.317	0.139	0.211	0.165	0.168	0.148	0.085	0.021	-0.032	-0.070
155	3.81	0.128	0.320	0.316	0.131	0.209	0.162	0.163	0.141	0.079	0.014	-0.041	-0.083
155	4.76	0.095	0.293	0.312	0.104	0.249	0.193	0.165	0.128	0.078	0.017	-0.049	-0.096
155	5.71	0.058	0.267	0.302	-0.051	0.285	0.219	0.199	0.192	0.149	0.044	-0.076	-0.140
186	0.	0.000	0.254	0.291	0.104	0.224	0.193	0.210	0.194	0.134	0.073	0.024	-0.008
186	0.86	0.039	0.280	0.306	0.124	0.227	0.192	0.203	0.185	0.122	0.059	0.007	-0.028
186	1.72	0.079	0.306	0.319	0.137	0.228	0.188	0.194	0.173	0.109	0.044	-0.009	-0.044
186	2.59	0.119	0.328	0.329	0.144	0.225	0.179	0.183	0.161	0.098	0.034	-0.020	-0.057
186	3.45	0.141	0.334	0.324	0.126	0.220	0.183	0.189	0.160	0.092	0.023	-0.032	-0.070
186	4.31	0.162	0.338	0.313	0.074	0.220	0.202	0.209	0.159	0.079	0.020	-0.030	-0.084
186	5.17	0.187	0.341	0.312	-0.056	0.247	0.205	0.191	0.162	0.136	0.094	0.003	-0.097
216	0.	0.	0.268	0.309	0.113	0.249	0.217	0.229	0.206	0.140	0.077	0.026	-0.008
216	0.77	0.044	0.297	0.323	0.131	0.248	0.211	0.219	0.195	0.129	0.064	0.012	-0.021
216	1.53	0.087	0.322	0.335	0.143	0.246	0.203	0.207	0.184	0.119	0.053	0.001	-0.033
216	2.30	0.129	0.343	0.341	0.142	0.236	0.192	0.199	0.179	0.113	0.045	-0.009	-0.046
216	3.06	0.156	0.353	0.343	0.128	0.229	0.188	0.202	0.184	0.112	0.036	-0.024	-0.060
216	3.83	0.187	0.382	0.352	0.090	0.225	0.187	0.211	0.186	0.098	0.017	-0.026	-0.055
216	4.60	0.276	0.437	0.346	-0.070	0.201	0.193	0.241	0.201	0.110	0.075	0.040	-0.050
246	0.	0.	0.282	0.326	0.117	0.270	0.234	0.240	0.211	0.143	0.078	0.027	-0.007
246	0.68	0.047	0.311	0.338	0.132	0.265	0.224	0.228	0.201	0.134	0.069	0.016	-0.017
246	1.36	0.090	0.335	0.346	0.137	0.257	0.213	0.216	0.193	0.130	0.063	0.007	-0.028
246	2.04	0.131	0.352	0.349	0.134	0.252	0.206	0.210	0.191	0.129	0.059	-0.002	-0.041
246	2.71	0.157	0.360	0.352	0.121	0.249	0.199	0.207	0.198	0.133	0.052	-0.018	-0.055
246	3.39	0.194	0.399	0.376	0.094	0.234	0.174	0.200	0.208	0.136	0.038	-0.024	-0.038
246	4.07	0.294	0.492	0.431	0.044	0.234	0.137	0.166	0.188	0.126	0.052	0.029	0.006
276	0.	0.000	0.289	0.333	0.116	0.274	0.236	0.242	0.213	0.146	0.080	0.028	-0.005
276	0.64	0.049	0.318	0.343	0.128	0.267	0.226	0.231	0.204	0.138	0.073	0.020	-0.015
276	1.28	0.091	0.340	0.349	0.129	0.259	0.218	0.222	0.198	0.134	0.068	0.011	-0.027
276	1.92	0.130	0.355	0.351	0.126	0.258	0.210	0.212	0.195	0.137	0.069	0.005	-0.038
276	2.56	0.150	0.361	0.359	0.122	0.266	0.207	0.204	0.194	0.139	0.061	-0.012	-0.051
276	3.20	0.189	0.393	0.380	0.097	0.258	0.188	0.193	0.200	0.143	0.049	-0.022	-0.036
276	3.85	0.287	0.473	0.418	0.032	0.235	0.145	0.173	0.201	0.144	0.056	0.014	0.009

Figure 5-10. Dimensionless Panel Gradients for the Standard Set of Times

DAYS	HOUR	NORTH TO WEST TO SOUTH											
93	0.	0.000	0.015	-0.011	-0.055	-0.110	-0.163	-0.170	-0.151	-0.186	-0.094	-0.269	-0.237
93	1.05	-0.028	-0.008	-0.030	-0.068	-0.118	-0.165	-0.165	-0.141	-0.175	-0.073	-0.257	-0.217
93	2.09	-0.051	-0.030	-0.048	-0.084	-0.129	-0.171	-0.164	-0.134	-0.165	-0.040	-0.235	-0.187
93	3.14	-0.074	-0.054	-0.071	-0.102	-0.142	-0.179	-0.161	-0.118	-0.143	0.002	-0.212	-0.159
93	4.18	-0.099	-0.083	-0.102	-0.132	-0.166	-0.187	-0.143	-0.083	-0.109	0.056	-0.191	-0.142
93	5.23	-0.111	-0.096	-0.127	-0.168	-0.192	-0.181	-0.102	-0.030	-0.074	0.122	-0.200	-0.180
93	6.28	-0.119	-0.139	-0.238	-0.302	-0.282	-0.184	0.003	0.108	-0.014	0.324	-0.251	-0.272
124	0.	0.000	0.014	-0.014	-0.059	-0.114	-0.168	-0.176	-0.158	-0.192	-0.095	-0.272	-0.239
124	1.02	-0.028	-0.010	-0.032	-0.072	-0.123	-0.173	-0.174	-0.148	-0.180	-0.071	-0.258	-0.218
124	2.04	-0.050	-0.030	-0.050	-0.088	-0.135	-0.179	-0.173	-0.141	-0.170	-0.040	-0.237	-0.188
124	3.06	-0.072	-0.053	-0.073	-0.107	-0.149	-0.188	-0.172	-0.128	-0.150	0.003	-0.213	-0.158
124	4.07	-0.094	-0.080	-0.102	-0.137	-0.174	-0.201	-0.161	-0.097	-0.116	0.062	-0.189	-0.138
124	5.09	-0.108	-0.092	-0.120	-0.169	-0.207	-0.207	-0.128	-0.044	-0.077	0.137	-0.194	-0.172
124	6.11	-0.118	-0.125	-0.216	-0.305	-0.313	-0.219	-0.028	0.100	-0.002	0.347	-0.237	-0.258
155	0.	-0.000	0.011	-0.019	-0.066	-0.124	-0.181	-0.191	-0.173	-0.205	-0.098	-0.279	-0.245
155	0.95	-0.026	-0.011	-0.037	-0.080	-0.134	-0.188	-0.194	-0.168	-0.196	-0.073	-0.262	-0.219
155	1.90	-0.046	-0.030	-0.054	-0.095	-0.147	-0.196	-0.195	-0.162	-0.186	-0.042	-0.242	-0.189
155	2.85	-0.065	-0.050	-0.074	-0.116	-0.165	-0.211	-0.201	-0.156	-0.170	0.005	-0.216	-0.156
155	3.81	-0.082	-0.070	-0.097	-0.141	-0.191	-0.233	-0.206	-0.137	-0.141	0.071	-0.187	-0.128
155	4.76	-0.098	-0.081	-0.108	-0.167	-0.230	-0.265	-0.201	-0.098	-0.101	0.170	-0.176	-0.136
155	5.71	-0.120	-0.101	-0.163	-0.286	-0.389	-0.405	-0.270	-0.030	0.020	0.576	-0.141	-0.148
186	0.	0.000	0.008	-0.024	-0.073	-0.134	-0.194	-0.210	-0.193	-0.224	-0.104	-0.291	-0.254
186	0.86	-0.021	-0.010	-0.039	-0.086	-0.146	-0.205	-0.218	-0.194	-0.219	-0.079	-0.274	-0.225
186	1.72	-0.038	-0.026	-0.054	-0.101	-0.160	-0.218	-0.226	-0.195	-0.215	-0.048	-0.254	-0.193
186	2.59	-0.052	-0.042	-0.071	-0.120	-0.179	-0.237	-0.240	-0.199	-0.207	0.001	-0.226	-0.155
186	3.45	-0.067	-0.057	-0.085	-0.135	-0.199	-0.261	-0.259	-0.197	-0.188	0.074	-0.195	-0.125
186	4.31	-0.092	-0.073	-0.093	-0.143	-0.220	-0.299	-0.286	-0.196	-0.176	0.193	-0.176	-0.103
186	5.17	-0.130	-0.095	-0.113	-0.218	-0.369	-0.493	-0.442	-0.251	-0.182	0.733	-0.126	-0.059
216	0.	0.	0.008	-0.026	-0.077	-0.140	-0.206	-0.229	-0.217	-0.249	-0.113	-0.309	-0.268
216	0.77	-0.015	-0.006	-0.037	-0.088	-0.153	-0.219	-0.241	-0.223	-0.250	-0.090	-0.293	-0.237
216	1.53	-0.028	-0.019	-0.049	-0.101	-0.167	-0.234	-0.255	-0.231	-0.251	-0.058	-0.272	-0.202
216	2.30	-0.042	-0.033	-0.063	-0.115	-0.181	-0.249	-0.270	-0.241	-0.252	-0.011	-0.246	-0.163
216	3.06	-0.056	-0.050	-0.077	-0.125	-0.191	-0.265	-0.292	-0.256	-0.251	0.063	-0.218	-0.131
216	3.83	-0.064	-0.069	-0.090	-0.126	-0.199	-0.296	-0.338	-0.288	-0.261	0.196	-0.204	-0.118
216	4.60	-0.100	-0.090	-0.100	-0.140	-0.260	-0.441	-0.525	-0.444	-0.414	0.742	-0.178	-0.069
246	0.	-0.000	0.007	-0.027	-0.078	-0.143	-0.211	-0.240	-0.234	-0.270	-0.117	-0.326	-0.282
246	0.68	-0.011	-0.003	-0.035	-0.088	-0.155	-0.225	-0.253	-0.243	-0.275	-0.097	-0.312	-0.250
246	1.36	-0.025	-0.015	-0.046	-0.099	-0.165	-0.235	-0.264	-0.252	-0.281	-0.068	-0.294	-0.216
246	2.04	-0.038	-0.028	-0.060	-0.113	-0.177	-0.245	-0.279	-0.267	-0.291	-0.024	-0.272	-0.178
246	2.71	-0.044	-0.038	-0.073	-0.125	-0.186	-0.256	-0.297	-0.287	-0.302	0.049	-0.249	-0.147
246	3.39	-0.032	-0.058	-0.102	-0.142	-0.193	-0.275	-0.346	-0.339	-0.332	0.195	-0.236	-0.132
246	4.07	-0.033	-0.079	-0.110	-0.133	-0.215	-0.371	-0.523	-0.552	-0.552	0.705	-0.236	-0.106
276	0.	0.	0.005	-0.028	-0.080	-0.146	-0.213	-0.242	-0.236	-0.274	-0.116	-0.333	-0.289
276	0.64	-0.011	-0.004	-0.036	-0.089	-0.157	-0.226	-0.254	-0.246	-0.284	-0.099	-0.321	-0.256
276	1.28	-0.026	-0.015	-0.046	-0.099	-0.165	-0.235	-0.264	-0.255	-0.291	-0.072	-0.305	-0.223
276	1.92	-0.037	-0.026	-0.059	-0.113	-0.177	-0.245	-0.278	-0.272	-0.305	-0.029	-0.283	-0.186
276	2.56	-0.038	-0.031	-0.073	-0.132	-0.189	-0.252	-0.292	-0.292	-0.320	0.041	-0.264	-0.159
276	3.20	-0.023	-0.044	-0.093	-0.143	-0.195	-0.273	-0.347	-0.355	-0.362	0.189	-0.248	-0.138
276	3.85	-0.018	-0.035	-0.119	-0.146	-0.206	-0.332	-0.486	-0.547	-0.550	0.629	-0.244	-0.100

Figure 5-10. Dimensionless Panel Gradients for the Standard Set of Times (Continued)

ANNUAL SUMMARY OF RECEIVER ASYMMETRY RATIOS , UNIVERSITY OF HOUSTON

HOUR =	0.	1.05	2.09	3.14	4.18	5.23	6.28	0.	0.
DAY = 93	4.417	4.608	4.679	4.708	4.690	4.753	5.355	0.	0.
HOUR =	0.	1.02	2.04	3.06	4.07	5.09	6.11	0.	0.
DAY = 124	4.601	4.780	4.856	4.890	4.845	4.884	5.421	0.	0.
HOUR =	0.	0.95	1.90	2.85	3.81	4.76	5.71	0.	0.
DAY = 155	5.066	5.224	5.316	5.380	5.326	5.174	7.363	0.	0.
HOUR =	0.	0.86	1.72	2.59	3.45	4.31	5.17	0.	0.
DAY = 186	5.728	5.882	6.028	6.118	6.061	5.978	12.353	0.	0.
HOUR =	0.	0.77	1.53	2.30	3.06	3.83	4.60	0.	0.
DAY = 216	6.574	6.698	6.826	6.914	6.972	7.030	13.904	0.	0.
HOUR =	0.	0.68	1.36	2.04	2.71	3.39	4.07	0.	0.
DAY = 246	7.248	7.356	7.449	7.621	7.695	7.918	13.794	0.	0.
HOUR =	0.	0.64	1.28	1.92	2.56	3.20	3.85	0.	0.
DAY = 276	7.484	7.605	7.703	7.873	8.003	8.224	12.401	0.	0.

Figure 5-11. Receiver Asymmetry Ratios for the Standard Set of Times

ANNUAL SUMMARY OF RECEIVER PANEL MAXIMA IN KW OVER PANEL NUMBER OF MAXIMA , UNIVERSITY OF HOUSTON

HOUR =	0.	1.05	2.09	3.14	4.18	5.23	6.28	0.	0.
DAY = 93	2.72	2.79	2.77	2.70	2.52	1.99	1.15	0.	0.
	14.08	10.24	9.89	9.65	9.51	9.41	9.34	0.	0.
HOUR =	0.	1.02	2.04	3.06	4.07	5.09	6.11	0.	0.
DAY = 124	2.75	2.83	2.81	2.74	2.54	2.02	1.20	0.	0.
	11.00	10.30	9.95	9.72	9.59	9.49	9.46	0.	0.
HOUR =	0.	0.95	1.90	2.85	3.81	4.76	5.71	0.	0.
DAY = 155	2.85	2.92	2.91	2.84	2.63	2.07	1.27	0.	0.
	13.85	10.47	10.12	9.89	9.76	9.76	9.87	0.	0.
HOUR =	0.	0.86	1.72	2.59	3.45	4.31	5.17	0.	0.
DAY = 186	2.95	3.00	3.00	2.92	2.67	2.11	1.32	0.	0.
	13.75	10.70	10.33	10.13	9.92	9.90	10.53	0.	0.
HOUR =	0.	0.77	1.53	2.30	3.06	3.83	4.60	0.	0.
DAY = 216	3.00	3.03	3.00	2.89	2.63	2.06	1.33	0.	0.
	11.27	10.86	10.52	10.33	10.10	9.91	10.95	0.	0.
HOUR =	0.	0.68	1.36	2.04	2.71	3.39	4.07	0.	0.
DAY = 246	2.92	2.93	2.89	2.78	2.50	1.98	1.33	0.	0.
	13.72	11.00	10.71	10.46	10.24	10.11	11.65	0.	0.
HOUR =	0.	0.64	1.28	1.92	2.56	3.20	3.85	0.	0.
DAY = 276	2.86	2.87	2.82	2.71	2.43	1.94	1.35	0.	0.
	13.66	11.08	10.80	10.61	10.34	10.19	11.84	0.	0.

(Power Values Shown in This Figure are Based on the University of Houston Insolation Model)

Figure 5-12. Panel Maxima Over Interpolated Panel Number of Maxima for Standard Set of Times

ANNUAL SUMMARY OF RECEIVER PANEL MINIMA IN KW OVER PANEL NUMBER OF MINIMA , UNIVERSITY OF HOUSTON

HOUR =	0.	1.05	2.09	3.14	4.18	5.23	6.28	0.	0.
DAY = 93	0.62	0.60	0.59	0.57	0.54	0.42	0.22	0.	0.
	24.50	24.39	24.25	24.14	24.08	24.25	24.42	0.	0.
HOUR =	0.	1.02	2.04	3.06	4.07	5.09	6.11	0.	0.
DAY = 124	0.60	0.59	0.58	0.56	0.53	0.41	0.22	0.	0.
	24.50	24.39	24.25	24.13	24.06	24.23	24.43	0.	0.
HOUR =	0.	0.95	1.90	2.85	3.81	4.76	5.71	0.	0.
DAY = 155	0.56	0.56	0.55	0.53	0.49	0.40	0.17	0.	0.
	24.50	24.37	24.24	24.10	24.00	24.09	20.11	0.	0.
HOUR =	0.	0.86	1.72	2.59	3.45	4.31	5.17	0.	0.
DAY = 186	0.52	0.51	0.50	0.48	0.44	0.35	0.11	0.	0.
	24.50	24.37	24.22	24.07	23.97	23.88	20.65	0.	0.
HOUR =	0.	0.77	1.53	2.30	3.06	3.83	4.60	0.	0.
DAY = 216	0.46	0.45	0.44	0.42	0.38	0.29	0.10	0.	0.
	24.50	24.36	24.21	24.06	23.95	23.88	20.81	0.	0.
HOUR =	0.	0.68	1.36	2.04	2.71	3.39	4.07	0.	0.
DAY = 246	0.40	0.40	0.39	0.37	0.32	0.25	0.10	0.	0.
	24.50	24.36	24.22	24.08	23.98	23.90	20.91	0.	0.
HOUR =	0.	0.64	1.28	1.92	2.56	3.20	3.85	0.	0.
DAY = 276	0.38	0.38	0.37	0.34	0.30	0.24	0.11	0.	0.
	24.50	24.35	24.22	24.09	24.02	23.92	20.95	0.	0.

(Power Values Shown in This Figure are Based on the University of Houston Insolation Model)

Figure 5-13. Panel Minima Over Interpolated Panel Number of Minima for Standard Set of Times

5.2 DEFINITION OF THE HELIOSTAT AIMING STRATEGY

5.2.1 Introduction

A heliostat aiming strategy requiring a multiplicity of heliostat aim points on the receiver is required to keep the peak flux within the prescribed limits. In addition to preventing excessive power density on the receiver, the aiming strategy should result in a uniform flux profile as well as prevent excessive spillage. On an external cylindrical receiver, these aim points are defined by vertical shifts away from the centerline belt of the receiver. In order to minimize the increase of spillage relative to the one point "aim at the belt" strategy, the magnitude of the shift is governed by the size of the heliostat image at the receiver.

The aim points are calculated on a cellwise basis on order 2.1 cells for the pilot plant. These aim points depend upon the size of the heliostat image at the receiver. If the image is relatively small, it may be shifted up or down by several meters without an excessive increase in spillage. If the image is large, even a small vertical shift may introduce excessive spillage.

The image size at the receiver is governed by three basic components. First is the sun size, whose image size varies with the slant range. The second is the heliostat size when projected to the receiver. The last item can be influenced by canting of the segments as well as segment curvature.

All heliostats at the Barstow plant will be canted to a focal length of 410 meters. However, the curvature will be temperature dependent. This means the image size will also change with temperature, and consequently, so will the distance available for shifting an image up or down without incurring excessive spillage.

The three components mentioned above are combined in such a way as to produce an estimate of image size for each cell in the collector field. This is done in such a fashion that, when the image radius is subtracted from one half the available receiver height after cosine foreshortening as viewed from the cell, the result is an appropriate shift from aiming at the belt which will not appreciably increase the existing spillage.

The definition of an aiming strategy on a cellwise basis is the important step in satisfying the goals previously stated. Once a particular strategy has been chosen, the individual heliostat aim points can be processed by interpolating from the cellwise output.

5.2.2 Estimation of Image Size

The way in which aim points are computed is based upon an estimate of image size. As mentioned before, the sun size, guidance error function and the heliostat segment size at the receiver determine image size. The image radius estimate is obtained only for the vertical direction and is then subtracted from half the height of the cylindrical receiver which has been foreshortened by projecting it onto the image plane. If the result is positive, this is the amount the image may be shifted up (or down) on the image plane before the top (or bottom) part of the image moves off the receiver. If the result is zero or negative, then there is no room for a shift.

Let SIGMA be the angular standard deviation of the guidance error function, G, and let ALPHA be the limb angle of the sun. These are combined via a sum of squares to get a result representative of the sun size and the two sigma point of G. (*represents multiplication, ** exponentiation)

```
ALPHAD = (ALPHA**2 + 4.0 * SIGMA**2)**.5
```

ALPHAD is then multiplied by the slant range SLRNG to obtain the image size from a point mirror, or in our case, from a point on the mirror. This is call RIM for "Radius of the Image".

```
RIM = ALPHAD * SLRNG
```

Next, the vertices of all segments of the heliostat are traced to the image plane. The worst vertical segment aberration is located by summing the vertical values of the four impact points of each segment and finding the maximum value (the worst aberration):

```
YABBER = Max((y1 + y2 + y3 + y4)/4.)
```

Next we must calculate the vertical segment size at the image plane for this worst case. This is done by taking the RMS value of the vertex impact points of the worst segment as measured from the aberration displacement:

```
YSEG = (((y1-y0)**2+(y2-y0)**2+(y3-y0)**2+(y4-y0)**2)/4.)**.5
```

In the above equation y0 = YABBER. YSEG can be shown to be equal to the following:

```
YSEG = ((y1**2 + y2**2 + y3**2 + y4**2 - y0**2)/4.)**.5
```

Thus the final value for RIM is given by:

```
RIM = ALPHAD * SLRNG + YABBER + YSEG
```

where ALPHAD represents the RMS combination of the two sigma value of the guidance error function and the limb angle of the sun.

5.2.3 Preliminary Studies

An initial delivery of time-dependent aim points for the University of Houston's standard set of annual days and times was made to McDonnell Douglas. These aim points revealed the change in aims versus time, which was caused by heliostat orientation and aberrations. From this information a determination can be made as to how many aim points each heliostat needs on an annual basis to satisfy the aiming strategy goals.

The next output delivered was a set of flux profiles on the receiver at noon on vernal equinox. In addition, a flux profile was delivered which used the aim points of noon for the time of 3:45 P.M. on vernal equinox.

The next concern was the temperature dependent curvature of the heliostat segments and the resulting effect on the image size, and therefore, the effect on the magnitude of the aim point shifts. The delivery to MDAC displayed the effect of heliostat segment curvature on image size for three different times with two different temperatures for each time.

The ambient temperature variations at the Barstow site will have some effect on the curvature of the heliostat segments. The manner in which the glass facets are mounted will allow the temperature to govern the curvature in the longest dimensions, while the short dimension will remain essentially flat at all temperatures. The equation defining the curved surface assumes the temperature effect to produce a spherical surface. An equation has been obtained which defines the radius of curvature of a segment as a function of temperature for the Martin heliostat.

Let R be the radius of curvature and let T be the ambient temperature in degrees Celcius.

$$R = 16230./(T + 2.2)$$

This gives the radius of curvature in meters. A spherical mirror has an effective focal length equal to one half the radius of curvature when the mirror width is much less than the radius of curvature.

The investigation to reveal the effects of temperature on image formation was undertaken in order to study the changes in the magnitude of the aim point shifts. Six runs were made for three instances in time and two different temperatures.

(1) DAY 124	(23 July)	HOUR 3.0	T = 100.0F, 120.0F
(2) DAY 186	(22 Sept)	HOUR 0.0	T = 90.9F, 80.9F
(3) DAY 246	(23 Nov)	HOUR 2.0	T = 59.2F, 49.2F

When this output was examined, the effect of time (and therefore aberrations) was seen to affect the image size more than temperature. With these preliminary studies done, the aiming strategy was decided upon, and the aim points were generated in a straight forward manner.

5.2.4 Delivery of Final Aim Points

The final aiming strategy involved only three solar positions (noon and two afternoon times) and therefore three aim points per heliostat. Of course, due to the symmetry of the field, the actual number of aim points for each

heliostat is five. The days and times for the three solar positions are as follows (day 0 is March 21st):

(1) DAY 124 (23 July) HOUR 4.074
(2) DAY 186 (22 Sept) HOUR 0.000
(3) DAY 246 (23 Nov) HOUR 2.714

Image size estimates were determined for these times for an ambient temperature of 78°F. The algorithm discussed in section 5.2.2 was used on a cellwise basis. Then the IH (Individual Heliostat) programs were used to interpolate the cellwise aiming data and assign aim points to each heliostat for the three solar positions. The delivery was made with cards, each card having the heliostat location coordinate and the three aim points.

5.3 RECEIVER FLUX DISTRIBUTION

The final design heat flux distribution was calculated on the basis of a three point aim strategy with the folllowing shift ratios being applied:

35% aimed above the equator
30% aimed at the equator
35% aimed below the equator

The high, middle, and low aim points were distributed uniformly throughout each of the field control segments and in compliance with the segment "pecking" order which is the sequence of heliostats moving between track and standby in response to operator commands. In this way, the results of increasing or decreasing the number of heliostats tracking the receiver or a loss of a portion of the field due to cloud passage will increase or decrease the amplitude of the flux without significantly changing the flux distribution. It should be emphasized however that the actual high and low aim point locations are uniquely defined for each heliostat based on the size of the particular image.

The calculated heat flux on the receiver surface at 4.074 PM (sun time) on July 23 is shown in Figure 5-14. The figure shows that a uniform vertical flux distribution would occur over the north, east, and south facing receiver panels. Some profile waviness would be experienced on the southwest facing panels.

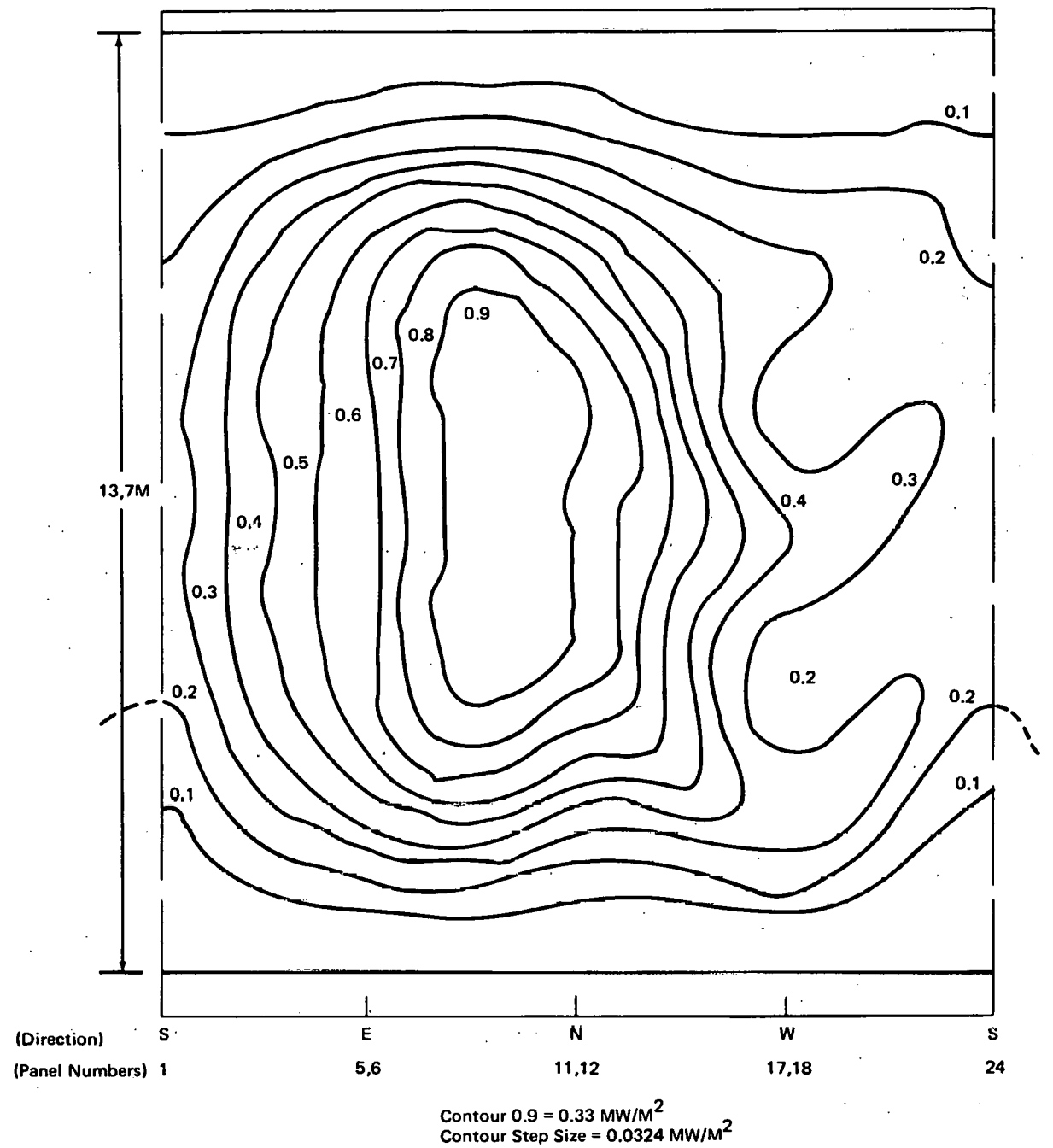

Figure 5-14. Receiver Flux Distribution at 4.074 PM on July 23

These irregularities will be investigated from a receiver panel control system standpoint. If control problems are anticipated as a result of this power profile, modifications to the current aim strategy will be made. Any such modifications however will not be made until actual "as built" heliostat drive system and reflective surface error budgets have been established.

5.4 STARTUP STUDY

5.4.1 Introduction

The purpose of the startup study is to provide the receiver designer a profile of power levels on the 24 receiver panels as a function of time during the sunrise and sunset period of the day. During these times the insolation level is changing most rapidly and shading efficiency among the heliostats as the solar elevation increases is changing most rapidly. Thus, except for possible cloud passages, this time period represents the most rapidly changing power levels on the receiver. An examination of previous performance simulations shows that this time period is represented by a solar elevation range of 2 degrees to approximately 16 degrees.

The individual heliostat computer code is used for the startup study. This code interpolates from a cell structured node file to get power levels on the receiver. The code system is described in detail in Section 3 and Appendix C. For this and other performance studies a cell structure is used which tightly fits the pilot plant field boundary. This provides a minimum cell size and maximizes the computational resolution. The cell size is given by (order 2.1)

$$\frac{\sqrt{2.1}}{2} \quad (75.438\text{m}) = 54.66\text{m}.$$

For this cell size 15 columns (West to East) and 13 rows of cells (North to South) are required. The tower is in column 8, row 9 (numbering W to E and N to S).

The node file formed for this study is based on the Sandia defined heliostat which has a glass area of 450 ft^2. Further design characteristics of the heliostat are given in Table 5-1. The node file was formed on day 124 with the sun at 10.0 degrees elevation.

The insolation output by the insolation model code for the start up period was compared to the 1976 Barstow data. It was found that the profile of insolation versus time from the Barstow data was faithfully reproduced by the model,

Table 5-1. Design Heliostat Physical Characteristics

Glass area	41.81 m^2 (450 ft^2)
Mount axis	az - el
Design Width (D_H)	6.9977 m
Minimum clearance radius	5.3749 m
Number of segments	12
Segment surface shape	flat
Segment width	3.048 m
Segment height	1.143 m
Canting focal length	400 m
Image degradation	2.83 mr (RMS)

but the insolation levels were not the same. Without weather data the computer model insolation was higher than the 1976 data and with weather data the model was lower. It was decided to run the startup studies with the computer model, no weather, and apply a correction factor to curve fit the Barstow data. Thus, the insolation levels in the startup study are based on actual data. It is a simple matter to scale the data to other insolation values since incident power level scales in direct proportion to insolation level.

The startup data can be generated for any day in the year. It has been run for several days that were requested by the SFDI. The results for July 21st (day 124, one month after summer solstice) are given in the next section.

5.4.2 Startup Power Levels for July 21

A summary of the startup data is given in Table 5-2. The times were chosen to start at 2.0 degrees solar elevation and increment approximately every 2 degrees until reaching 16 degrees. The negative value given at the top of the absorbed power level column indicates that there was not sufficient incident

Table 5-2. Startup Receiver Total Power Levels on Day 124 (July 21)

Curve Number	Time (A.M. Solar time) (hrs:min)	Solar Elevation (deg)	Direct Normal Insolation (W/m^2)	Incident Power (MW)	Absorbed Power (MW)
1	5:11.4	2.00	199.8	2.70	-2.29
2	5:22.2	3.97	376.3	6.44	1.19
3	5:32.4	5.96	483.9	9.91	4.41
4	5:42.6	7.97	556.1	13.27	7.54
5	5:53.4	10.00	608.2	16.54	10.58
6	6:3.6	12.04	648.1	19.54	13.37
7	6:14.4	14.09	679.7	22.30	15.94
8	6:24.6	16.16	705.6	24.75	18.22

power with the sun at 2.0 degrees to overcome radiative and convective losses characteristic of normal operating receiver temperature.

The distribution of absorbed power on the receiver as calculated for all twenty-four panels is given as a function of time in Figure 5-15. The heat loss model used in this analysis is identical to the model assumed for the receiver during normal operation (960°F outlet steam temperature). The anomalously high absorbed power level on panels 1-3 and 22-24 arises because these are preheater panels operating at a lower temperature than the remaining boiler panels. Observe the suppressed baseline - several values are negative as noted above.

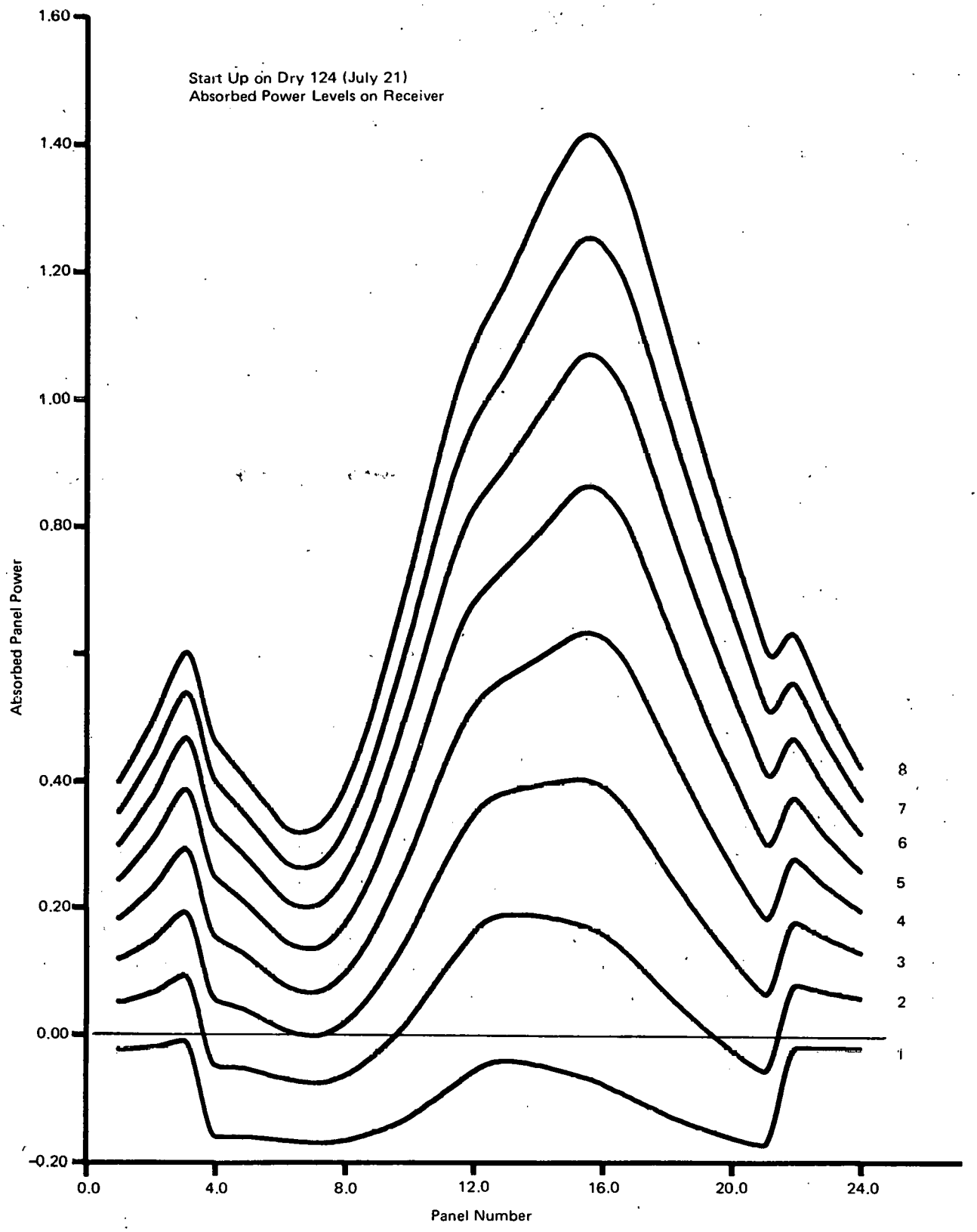

Figure 5-15. Absorbed Panel Powers on Receiver During Startup (July 21)
Number 1-8 refer to Table 5-2.

5.5 CLOUD STUDY

5.5.1 Introduction

A cloud transit study has been performed to determine the power levels and, more importantly, the rate of change of power level on the twenty-four panels of the receiver as various selected cloud fields are passed across the pilot plant collector field. The cloud fields were selected from actual data taken at the Barstow site. The results for five cloud events have been processed and sent to the SFDI.

The cloud field data was prepared by B. Robert Johnson, member of the Chemistry and Physics Laboratory of the Aerospace Corporation. The form of the data will be described in section 5.5.2. The data is based on measurements taken by Randall, Whitson, and Johnson (1) of the insolation at a site near the pilot plant site over a region in size comparable to the pilot plant. The measurements and preparation of the cloud field data are described by the same authors in reference (2).

Emphasis is placed in this study on the effect of clouds over a time period of several minutes. The results of this study can then be extrapolated to longer periods of time based on the Aerospace data correlation studies documented in reference (2). These extrapolated results are used directly in the receiver structural and control system design and analysis.

5.5.2 Computational Basis for the Cloud Study

The cellwise codes are used to perform the cloud study. The cell structure is the same as that described in Section 5.4. To make the cellwise cloud simulation as representative of the actual field as possible the cell structure was imposed over the actual pilot plant collector field layout to determine the exact number of heliostats falling in each cell. This number of heliostats per cell matrix is used in all cloud simulation runs.

This cell structure has more than adequate resolution in comparison to the dimensions and resolution present in the cloud field data base. A cloud field is typically 731 m wide and 3000 m long. Data for the cloud fields are taken by four sensors spaced across the width of the field. The length of the

cloud field is determined by the cloud drift velocity and time period for the selected data (typically 10 min).

In the computer simulation the cloud field is passed across the collector field in small spatial increments (typically 50 m) and the incident power level on each of the twenty-four panels is determined at each increment. Thus, the simulation produces a listing of power level as a function of cloud field position with respect to the collector field. The user of the data can use it to represent any cloud drift velocity. The time period between successive cloud field increments (between the output power levels) is the spatial increment divided by the drift velocity. The cloud field can be passed across the field in any direction, and many directions can be handled in each computer run. The cloud field begins typically 500 m from the tower so that full power is on the receiver. The width of the cloud field is centered with the width of the collector field and the movement is along the length of the cloud field. The increments continue until the cloud field clears the collector field and full power is back on the receiver. This process is shown in Figure 5-16.

In the computer code the cloud field is represented by a subroutine which, when given an X and a Y coordinate in the cloud field, returns an effective value of transmission from zero (totally opaque) to one (completely clear). These values are derived from the actual insolation data as the cloud passed over the sensors and an interpolation routine. (Ref. 2 page 2-31.)

The simulation is implemented by forming a node file for the day and time of day that the simulation is to be done. It is assumed that the cloud simulation time is short enough that solar position and insolation do not change appreciably during the cloud transit. The power on each panel from each cell in the field is formed. For each spatial cloud field increment the coordinate of each cell is formed and based on cloud direction the cell's coordinates are transformed to the cloud coordinates. The cloud subroutine is called and returns the effective cloud transmission. The transmission is multiplied by the fraction of power on the panel due to that cell and the powers are summed over cells to form the total power on each panel. The result is the total power on each panel that reflects the effective cloud transmission available

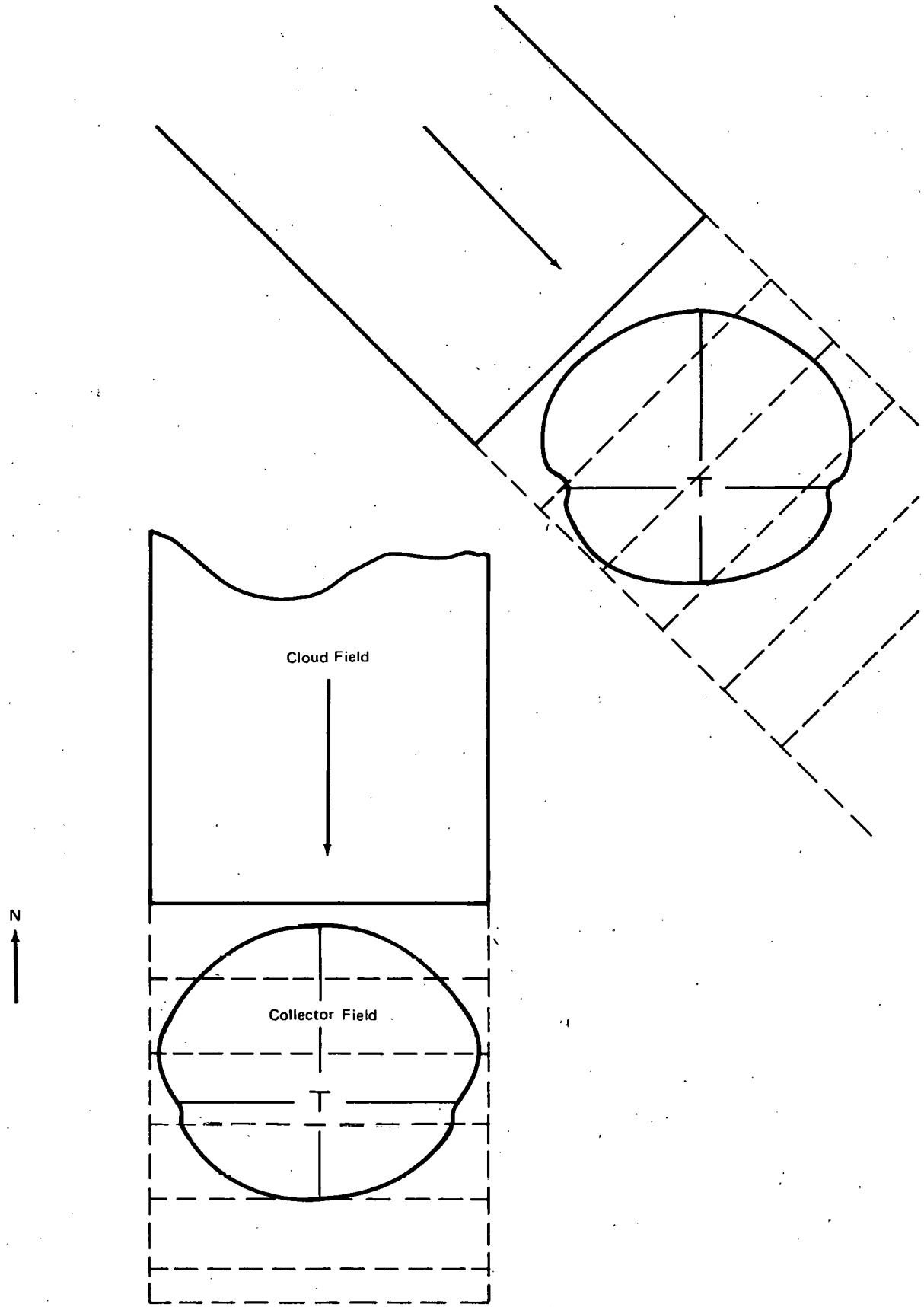

Figure 5-16. Cloud Field Transit Geometry

to each cell in the field. The cloud is incremented across the collector field by simply adding the spatial increment to the cloud field Y coordinate, then doing the loop over cells again.

The results from an example cloud transit simulation is given in the next section.

5.5.3 Cloud Transit on an Equinox Afternoon

An equinox day (day 186) at 3:30 P.M. has been chosen as a typical day and time to run the simulation. The cloud field used is shown in a contour plot in Figure 5-17. This cloud field is derived from data taken over a nine-minute period on August 8, 1978, and is identified as cloud field No. 1. The cloud drift velocity was 5.5 m/sec. The cloud was moving from Northeast to Southwest. A convenient advantage of the simulation is the ability to move the cloud at any direction, at any desired velocity, at any time in the year, and with any desired insolation level. Since we use the effective cloud transmittance, the actual insolation level when the cloud passed is normalized out.

The results of the cloud transit on an equinox day (March 21 or September 21) at 3:27 P.M. are shown in Table 5-3. The cloud field is moving from the Northwest to the Southeast. The cloud field starts 500 meters from the tower and increments in the direction of the tower in 50 meter increments. The total distance the cloud has moved is shown in the left column. The insolation level at this time is 938.522 W/m^2. The total clear day power level incident on the receiver is 44.414 MW. The power level in MW for each panel is shown to the right of the cloud field displacement. Panel numbers 1 to 12 are shown on the first line (left to right) and 13 to 24 on the second line with the total receiver power level on the far right. The cloud field begins to influence the power level by the time it moves 100 meters (now 400 m from the tower). The cloud field is fully over the collector field when it has moved 850 meters. The total power level has dropped to its lowest value, 9.4 MW or about 21% of the peak power. The leading areas of the cloud are fairly opaque. The following areas are less opaque and the reductions in power level appear to be less severe.

Label	Transmission
1	0.05
2	0.15
3	0.25
4	0.35
5	0.45
6	0.55
7	0.65
8	0.75
9	0.85
10	0.95

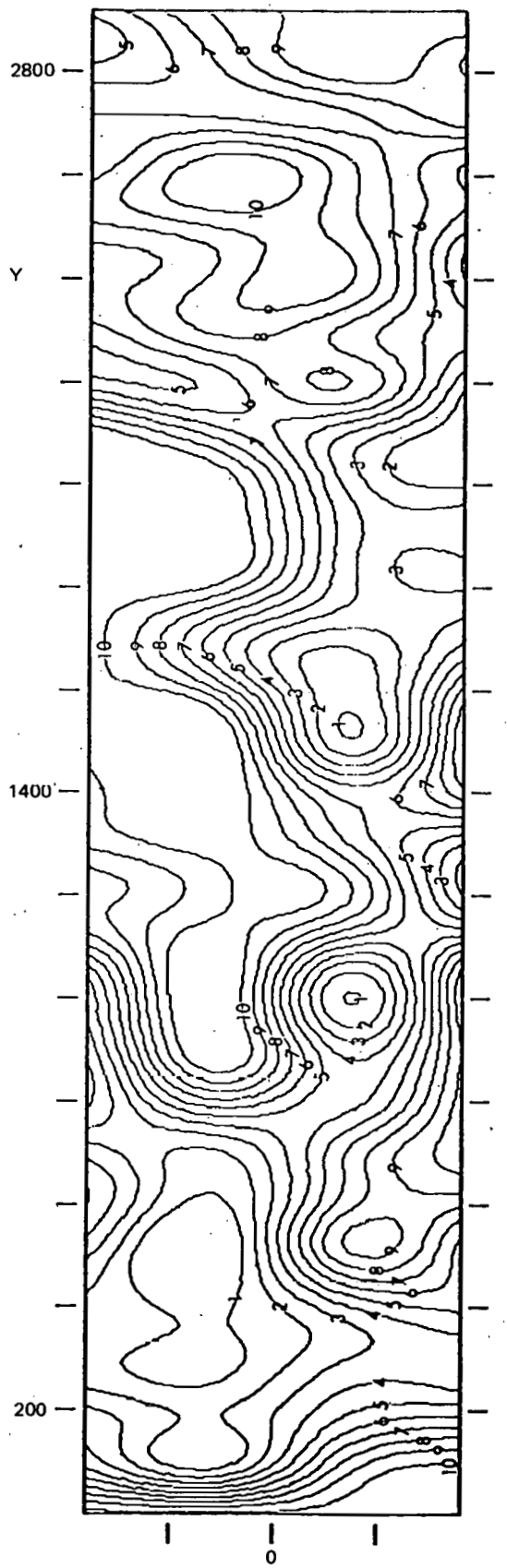

Figure 5-17. Contour Plot of Cloud Field Number 1

Table 5-3. Panel Power Levels During a Cloud Transit
(Page 1 of 3)

CLOUD TRANSIT SIMULATION
DAY 186 TIME 3.45 HOURS CASE NO.(CLOUD TYPE) 1 DIRECTION 45.0 DEG NW-SE
SPACIAL INCREMENT 50.0 METERS STARTING DISTANCE FROM TOWER 500.0 METERS

0.	0.737	1.000	1.397	1.658	1.858	2.144	2.528	2.901	3.107	3.086	2.907	2.726	
	2.573	2.454	2.443	2.247	1.820	1.478	1.166	0.942	0.976	0.921	0.720	0.627	44.414
50.0	0.737	1.000	1.397	1.658	1.858	2.144	2.528	2.901	3.107	3.086	2.907	2.726	
	2.573	2.454	2.443	2.247	1.820	1.478	1.166	0.942	0.976	0.921	0.720	0.627	44.414
100.0	0.737	1.000	1.397	1.658	1.858	2.144	2.528	2.901	3.107	3.086	2.907	2.725	
	2.571	2.452	2.441	2.245	1.818	1.477	1.166	0.941	0.976	0.921	0.720	0.627	44.402
150.0	0.737	1.000	1.397	1.658	1.858	2.144	2.528	2.901	3.107	3.085	2.903	2.716	
	2.552	2.419	2.400	2.208	1.794	1.465	1.161	0.940	0.976	0.921	0.720	0.627	44.217
200.0	0.737	1.000	1.397	1.658	1.858	2.144	2.528	2.900	3.105	3.078	2.885	2.671	
	2.466	2.292	2.258	2.091	1.722	1.431	1.148	0.936	0.975	0.920	0.720	0.627	43.550
250.0	0.737	1.000	1.397	1.658	1.858	2.144	2.528	2.899	3.100	3.061	2.839	2.570	
	2.291	2.057	2.019	1.904	1.609	1.379	1.129	0.931	0.974	0.920	0.720	0.627	42.351
300.0	0.737	1.000	1.397	1.658	1.858	2.144	2.527	2.896	3.089	3.027	2.756	2.405	
	2.032	1.744	1.719	1.672	1.465	1.308	1.102	0.922	0.971	0.920	0.720	0.627	40.697
350.0	0.737	1.000	1.397	1.658	1.858	2.144	2.525	2.887	3.062	2.961	2.614	2.160	
	1.696	1.373	1.379	1.402	1.283	1.209	1.060	0.908	0.967	0.919	0.720	0.627	38.548
400.0	0.737	1.000	1.397	1.658	1.858	2.143	2.519	2.866	3.002	2.816	2.346	1.781	
	1.262	0.957	1.018	1.103	1.050	1.066	0.996	0.886	0.961	0.917	0.719	0.627	35.685
450.0	0.737	1.000	1.397	1.658	1.858	2.139	2.505	2.820	2.876	2.542	1.910	1.279	
	0.812	0.593	0.702	0.817	0.800	0.890	0.896	0.849	0.950	0.915	0.719	0.627	32.291
500.0	0.737	1.000	1.397	1.658	1.856	2.131	2.475	2.727	2.629	2.098	1.366	0.791	
	0.491	0.395	0.499	0.602	0.611	0.704	0.747	0.770	0.918	0.908	0.718	0.627	28.855
550.0	0.735	0.999	1.397	1.657	1.847	2.097	2.358	2.409	2.077	1.459	0.864	0.501	
	0.349	0.321	0.415	0.499	0.510	0.560	0.589	0.647	0.819	0.854	0.707	0.623	25.294
600.0	0.714	0.989	1.371	1.624	1.789	1.946	2.009	1.843	1.425	0.942	0.578	0.374	
	0.280	0.280	0.392	0.486	0.489	0.492	0.478	0.512	0.674	0.752	0.664	0.595	21.700
650.0	0.660	0.924	1.259	1.481	1.593	1.614	1.498	1.259	0.942	0.646	0.418	0.274	
	0.218	0.257	0.405	0.531	0.535	0.497	0.429	0.409	0.523	0.609	0.576	0.535	18.095
700.0	0.562	0.782	1.043	1.193	1.227	1.157	1.008	0.833	0.648	0.458	0.290	0.190	
	0.177	0.258	0.443	0.610	0.635	0.557	0.427	0.353	0.407	0.466	0.456	0.447	14.627
750.0	0.440	0.597	0.763	0.824	0.801	0.730	0.646	0.553	0.437	0.309	0.205	0.154	
	0.167	0.276	0.497	0.711	0.772	0.662	0.468	0.335	0.334	0.358	0.346	0.347	11.732
800.0	0.331	0.431	0.515	0.510	0.460	0.419	0.389	0.350	0.288	0.224	0.175	0.151	
	0.182	0.313	0.564	0.816	0.910	0.792	0.564	0.369	0.301	0.286	0.266	0.263	9.869
850.0	0.250	0.323	0.374	0.353	0.304	0.269	0.250	0.238	0.222	0.201	0.177	0.172	
	0.224	0.372	0.637	0.896	1.000	0.908	0.695	0.472	0.343	0.262	0.211	0.200	9.350
900.0	0.193	0.250	0.293	0.280	0.240	0.207	0.193	0.199	0.208	0.208	0.208	0.232	
	0.309	0.463	0.718	0.941	1.011	0.964	0.812	0.615	0.476	0.326	0.204	0.161	9.711
950.0	0.164	0.191	0.225	0.213	0.180	0.159	0.163	0.185	0.214	0.245	0.283	0.343	
	0.448	0.604	0.827	0.974	0.973	0.951	0.855	0.728	0.653	0.483	0.276	0.170	10.506
1000.0	0.188	0.173	0.198	0.178	0.143	0.131	0.144	0.181	0.238	0.310	0.391	0.497	
	0.647	0.812	0.978	1.022	0.942	0.896	0.815	0.749	0.774	0.659	0.416	0.244	11.725
1050.0	0.277	0.237	0.255	0.214	0.157	0.135	0.150	0.205	0.295	0.402	0.519	0.678	
	0.889	1.071	1.160	1.086	0.918	0.824	0.746	0.698	0.773	0.744	0.549	0.360	13.343
1100.0	0.392	0.368	0.376	0.293	0.195	0.151	0.168	0.252	0.378	0.517	0.673	0.900	
	1.177	1.356	1.351	1.143	0.871	0.740	0.680	0.650	0.714	0.712	0.588	0.447	15.091
1150.0	0.462	0.487	0.484	0.360	0.225	0.167	0.205	0.325	0.482	0.655	0.879	1.190	
	1.303	1.633	1.521	1.184	0.817	0.648	0.594	0.600	0.678	0.666	0.551	0.457	16.774
1200.0	0.461	0.517	0.522	0.393	0.253	0.203	0.267	0.419	0.614	0.858	1.174	1.539	
	1.820	1.865	1.659	1.231	0.794	0.577	0.503	0.513	0.626	0.643	0.523	0.430	18.404
1250.0	0.425	0.475	0.499	0.397	0.281	0.262	0.364	0.564	0.832	1.166	1.536	1.880	
	2.069	2.021	1.769	1.295	0.800	0.546	0.452	0.429	0.528	0.576	0.499	0.410	20.077
1300.0	0.395	0.440	0.475	0.401	0.325	0.350	0.514	0.800	1.164	1.547	1.877	2.121	

Table 5-3. Panel Power Levels During a Cloud Transit
(Page 2 of 3)

	2.200	2.087	1.845	1.373	0.834	0.553	0.432	0.383	0.449	0.479	0.428	0.377	21.851
1350.0	0.367	0.431	0.489	0.449	0.420	0.512	0.770	1.151	1.561	1.894	2.103	2.231	
	2.242	2.116	1.907	1.475	0.933	0.597	0.411	0.336	0.401	0.417	0.351	0.326	23.891
1400.0	0.339	0.429	0.547	0.571	0.604	0.778	1.122	1.542	1.912	2.139	2.231	2.276	
	2.255	2.148	1.982	1.613	1.102	0.692	0.411	0.276	0.323	0.357	0.305	0.288	26.240
1450.0	0.323	0.452	0.649	0.767	0.882	1.119	1.485	1.869	2.154	2.292	2.315	2.312	
	2.272	2.188	2.073	1.765	1.292	0.832	0.475	0.259	0.233	0.256	0.245	0.257	28.765
1500.0	0.303	0.494	0.767	0.988	1.186	1.448	1.780	2.102	2.323	2.406	2.388	2.353	
	2.302	2.230	2.150	1.877	1.425	0.970	0.597	0.326	0.221	0.177	0.159	0.200	31.170
1550.0	0.256	0.491	0.830	1.147	1.417	1.691	1.992	2.276	2.463	2.507	2.446	2.385	
	2.328	2.248	2.172	1.895	1.441	1.045	0.720	0.453	0.324	0.201	0.112	0.137	32.975
1600.0	0.204	0.428	0.809	1.195	1.522	1.824	2.126	2.399	2.564	2.575	2.488	2.421	
	2.354	2.234	2.120	1.804	1.337	1.023	0.779	0.570	0.497	0.340	0.158	0.121	33.891
1650.0	0.210	0.383	0.773	1.187	1.544	1.876	2.201	2.479	2.632	2.633	2.550	2.484	
	2.384	2.192	2.002	1.631	1.157	0.919	0.748	0.614	0.640	0.524	0.292	0.187	34.241
1700.0	0.307	0.445	0.830	1.226	1.574	1.913	2.244	2.521	2.679	2.703	2.637	2.551	
	2.391	2.121	1.847	1.423	0.962	0.776	0.659	0.578	0.683	0.647	0.440	0.313	34.469
1750.0	0.459	0.614	0.994	1.341	1.637	1.943	2.258	2.545	2.737	2.796	2.723	2.587	
	2.360	2.020	1.669	1.207	0.768	0.625	0.564	0.511	0.632	0.657	0.522	0.435	34.605
1800.0	0.588	0.803	1.183	1.474	1.704	1.964	2.270	2.589	2.822	2.887	2.775	2.575	
	2.276	1.868	1.469	0.999	0.581	0.481	0.476	0.459	0.560	0.588	0.509	0.490	34.390
1850.0	0.632	0.914	1.300	1.556	1.740	1.975	2.301	2.662	2.914	2.952	2.788	2.525	
	2.156	1.697	1.286	0.843	0.456	0.365	0.370	0.396	0.512	0.528	0.449	0.469	33.792
1900.0	0.599	0.905	1.301	1.560	1.743	1.994	2.357	2.744	2.988	2.991	2.776	2.450	
	2.023	1.553	1.170	0.784	0.442	0.312	0.270	0.287	0.425	0.480	0.409	0.423	32.985
1950.0	0.533	0.827	1.228	1.516	1.735	2.025	2.417	2.806	3.027	2.992	2.724	2.341	
	1.896	1.477	1.159	0.829	0.508	0.329	0.232	0.191	0.278	0.363	0.358	0.379	32.171
2000.0	0.457	0.743	1.135	1.453	1.723	2.050	2.455	2.834	3.025	2.940	2.617	2.211	
	1.817	1.494	1.246	0.939	0.603	0.383	0.249	0.168	0.173	0.212	0.243	0.303	31.470
2050.0	0.355	0.640	1.019	1.369	1.689	2.049	2.465	2.827	2.970	2.813	2.453	2.095	
	1.828	1.621	1.406	1.085	0.719	0.448	0.275	0.181	0.156	0.138	0.129	0.195	30.926
2100.0	0.239	0.495	0.872	1.260	1.623	2.007	2.416	2.731	2.807	2.623	2.327	2.096	
	1.962	1.829	1.606	1.246	0.843	0.518	0.310	0.198	0.166	0.133	0.091	0.115	30.511
2150.0	0.152	0.356	0.715	1.129	1.526	1.921	2.296	2.550	2.601	2.490	2.346	2.249	
	2.169	2.028	1.778	1.374	0.923	0.575	0.360	0.232	0.185	0.142	0.093	0.083	30.274
2200.0	0.115	0.271	0.585	0.985	1.386	1.764	2.099	2.349	2.480	2.518	2.503	2.450	
	2.331	2.125	1.851	1.420	0.937	0.601	0.397	0.275	0.240	0.180	0.107	0.077	30.046
2250.0	0.113	0.226	0.487	0.836	1.206	1.568	1.922	2.262	2.537	2.688	2.688	2.582	
	2.383	2.111	1.829	1.404	0.917	0.606	0.413	0.295	0.298	0.250	0.149	0.098	29.871
2300.0	0.143	0.215	0.435	0.721	1.048	1.429	1.878	2.352	2.730	2.882	2.801	2.605	
	2.335	2.022	1.756	1.371	0.906	0.613	0.424	0.301	0.323	0.300	0.204	0.148	29.942
2350.0	0.206	0.268	0.467	0.695	0.991	1.419	1.979	2.538	2.912	2.986	2.808	2.533	
	2.206	1.881	1.662	1.347	0.922	0.631	0.431	0.305	0.330	0.313	0.232	0.200	30.261
2400.0	0.278	0.382	0.602	0.819	1.107	1.565	2.156	2.698	3.006	3.002	2.756	2.413	
	2.040	1.731	1.585	1.352	0.971	0.671	0.437	0.298	0.328	0.317	0.239	0.231	30.984
2450.0	0.333	0.500	0.785	1.044	1.345	1.786	2.324	2.794	3.028	2.958	2.637	2.234	
	1.859	1.621	1.565	1.406	1.065	0.747	0.462	0.284	0.306	0.310	0.245	0.248	31.885
2500.0	0.362	0.578	0.929	1.247	1.562	1.963	2.427	2.825	2.985	2.821	2.411	1.994	
	1.715	1.605	1.625	1.508	1.196	0.856	0.530	0.299	0.276	0.277	0.235	0.255	32.482
2550.0	0.367	0.611	0.998	1.353	1.677	2.048	2.459	2.784	2.843	2.568	2.122	1.786	
	1.665	1.680	1.742	1.629	1.310	0.963	0.642	0.379	0.289	0.242	0.203	0.242	32.601
2600.0	0.346	0.602	0.993	1.358	1.683	2.032	2.391	2.625	2.574	2.249	1.884	1.708	
	1.719	1.787	1.863	1.728	1.366	1.033	0.747	0.508	0.396	0.275	0.183	0.212	32.265
2650.0	0.318	0.558	0.934	1.296	1.617	1.934	2.219	2.356	2.253	1.998	1.801	1.774	
	1.837	1.896	1.961	1.805	1.413	1.072	0.783	0.592	0.550	0.414	0.235	0.206	31.824
2700.0	0.323	0.512	0.866	1.207	1.500	1.769	1.977	2.062	2.007	1.909	1.867	1.905	

Table 5-3. Panel Power Levels During a Cloud Transit
(Page 3 of 3)

	1.960	2.000	2.052	1.887	1.490	1.112	0.785	0.588	0.619	0.558	0.363	0.267	31.584
2750.0	0.386	0.526	0.840	1.120	1.347	1.556	1.724	1.842	1.914	1.961	1.986	2.021	
	2.056	2.084	2.129	1.952	1.542	1.157	0.822	0.585	0.593	0.580	0.455	0.364	31.541
2800.0	0.465	0.610	0.871	1.059	1.206	1.369	1.560	1.776	1.967	2.071	2.082	2.094	
	2.117	2.122	2.148	1.948	1.518	1.168	0.869	0.637	0.609	0.555	0.447	0.408	31.676
2850.0	0.505	0.682	0.921	1.048	1.137	1.292	1.544	1.845	2.079	2.166	2.149	2.151	
	2.158	2.122	2.109	1.887	1.458	1.142	0.875	0.681	0.687	0.603	0.439	0.405	32.086
2900.0	0.514	0.698	0.965	1.098	1.180	1.355	1.646	1.960	2.172	2.244	2.233	2.224	
	2.186	2.098	2.052	1.831	1.422	1.117	0.856	0.681	0.730	0.678	0.494	0.424	32.858
2950.0	0.514	0.725	1.026	1.196	1.302	1.488	1.765	2.049	2.251	2.344	2.339	2.279	
	2.159	2.025	1.988	1.797	1.417	1.116	0.850	0.666	0.718	0.698	0.545	0.472	33.760
3000.0	0.597	0.802	1.122	1.311	1.429	1.602	1.849	2.133	2.367	2.470	2.405	2.249	
	2.055	1.906	1.910	1.769	1.414	1.130	0.865	0.665	0.699	0.679	0.550	0.503	34.480
3050.0	0.630	0.870	1.204	1.392	1.503	1.667	1.933	2.264	2.516	2.550	2.364	2.121	
	1.905	1.786	1.847	1.753	1.416	1.151	0.884	0.677	0.700	0.665	0.532	0.503	34.834
3100.0	0.628	0.881	1.229	1.421	1.538	1.732	2.053	2.402	2.591	2.497	2.200	1.934	
	1.786	1.758	1.862	1.795	1.483	1.196	0.898	0.683	0.704	0.666	0.522	0.494	34.953
3150.0	0.617	0.868	1.232	1.445	1.587	1.821	2.161	2.460	2.526	2.318	1.996	1.798	
	1.777	1.849	1.966	1.895	1.595	1.262	0.934	0.695	0.688	0.651	0.519	0.489	35.149
3200.0	0.607	0.873	1.252	1.494	1.665	1.902	2.185	2.364	2.317	2.088	1.863	1.801	
	1.878	1.989	2.106	2.011	1.677	1.334	1.011	0.754	0.697	0.624	0.499	0.474	35.466
3250.0	0.582	0.867	1.250	1.517	1.699	1.887	2.061	2.150	2.093	1.955	1.865	1.910	
	2.020	2.112	2.215	2.088	1.712	1.383	1.076	0.837	0.782	0.663	0.487	0.442	35.651
3300.0	0.544	0.800	1.167	1.436	1.609	1.751	1.874	1.964	1.988	1.977	2.001	2.105	
	2.213	2.264	2.321	2.157	1.755	1.415	1.099	0.876	0.876	0.769	0.538	0.438	35.937
3350.0	0.535	0.723	1.060	1.298	1.443	1.576	1.722	1.869	1.989	2.004	2.173	2.281	
	2.350	2.355	2.380	2.199	1.792	1.438	1.112	0.880	0.900	0.836	0.621	0.488	36.102
3400.0	0.576	0.727	1.016	1.195	1.306	1.446	1.639	1.861	2.075	2.254	2.374	2.451	
	2.460	2.420	2.421	2.229	1.816	1.460	1.137	0.898	0.901	0.840	0.655	0.541	36.700
3450.0	0.630	0.802	1.063	1.192	1.269	1.413	1.651	1.969	2.305	2.562	2.658	2.640	
	2.548	2.449	2.443	2.247	1.820	1.478	1.166	0.935	0.937	0.853	0.655	0.560	38.245
3500.0	0.657	0.859	1.141	1.267	1.330	1.478	1.762	2.166	2.559	2.782	2.782	2.684	
	2.561	2.452	2.443	2.247	1.820	1.478	1.166	0.941	0.971	0.895	0.672	0.569	39.684
3550.0	0.670	0.876	1.188	1.341	1.426	1.610	1.960	2.411	2.784	2.925	2.844	2.705	
	2.568	2.453	2.443	2.247	1.820	1.478	1.166	0.941	0.975	0.915	0.703	0.590	41.042
3600.0	0.689	0.900	1.232	1.410	1.528	1.764	2.165	2.622	2.942	3.010	2.879	2.717	
	2.571	2.454	2.443	2.247	1.820	1.478	1.166	0.942	0.976	0.920	0.715	0.610	42.200
3650.0	0.721	0.955	1.310	1.523	1.689	1.975	2.394	2.817	3.066	3.069	2.901	2.724	
	2.572	2.454	2.443	2.247	1.820	1.478	1.166	0.942	0.976	0.920	0.719	0.623	43.504
3700.0	0.733	0.984	1.362	1.597	1.782	2.072	2.476	2.872	3.094	3.081	2.906	2.725	
	2.573	2.454	2.443	2.247	1.820	1.478	1.166	0.942	0.976	0.921	0.720	0.626	44.050
3750.0	0.737	0.997	1.392	1.648	1.845	2.133	2.521	2.897	3.106	3.085	2.907	2.726	
	2.573	2.454	2.443	2.247	1.820	1.478	1.166	0.942	0.976	0.921	0.720	0.627	44.360
3800.0	0.737	1.000	1.397	1.658	1.858	2.144	2.528	2.901	3.107	3.086	2.907	2.726	
	2.573	2.454	2.443	2.247	1.820	1.478	1.166	0.942	0.976	0.921	0.720	0.627	44.414
3850.0	0.737	1.000	1.397	1.658	1.858	2.144	2.528	2.901	3.107	3.086	2.907	2.726	
	2.573	2.454	2.443	2.247	1.820	1.478	1.166	0.942	0.976	0.921	0.720	0.627	44.414

EOF

?

Each of the 5 cloud fields characterized in Table 5-4 was directed across the heliostat field from each of 5 directions (N, NW, W, SW, S). Tabulations similar to Table 5-3 were provided to the SFDI for each of the 25 cases. Punched card format was utilized to facilitate further analysis by the SFDI.

5.5.4 Summary of Transit Data for Five Cloud Fields

A summary of pertinent information on the five cloud fields used in this study is given in Table 5-4. The direction and drift velocity were provided from the data reduction done by Randall, Johnson and Whitson (2). The width of the field is determined by sensor placement and cloud direction. The length of the field is determined by the period of observation (approximately 10 minutes) and cloud drift velocity. The cloud type and sky cover are taken from the U.S. Weather Bureau hourly meteorological observations for Daggett, California. The cloud type given in the table was either reported at the time of the observation or was reported on that day. Even though there was no definite report on July 8, 1979 the cloud velocity and sky cover imply that cirrus clouds were present.

An additional examination of the cloud data has been carried out by the University of Houston, Energy Laboratory and a portion of the result of that work will be given here. This work was designed and carried out by the Energy Laboratory and is not a formal part of the SFDI effort.

For each cloud transit the incident power level on each group of 3 panels, hereafter called superpanels, and total incident power are plotted as a function of time. Panels 1, 2 and 3 are superpanel 1, panels 4, 5 and 6 comprise superpanel 2, etc. The rates of change of the power levels are plotted, and at each point in time the worst panel-to-panel gradient present on the receiver is determined and plotted. The rates of change of the total power level is divided up into twenty equal intervals and the number of occurrences counted during the cloud transit. The percent of occurrence is plotted as a function of rate of change.

Table 5-4. Cloud Field Characteristics

No.	1	2	3	4	5
Date	8/8/78	8/26/78	3/29/79	4/26/79	7/8/79
Actual Direction of Motion	NE-SW	W-E	W-E	SW-NE	W-E
Velocity (m/s)	5.5	30.5	6.7	7.3	41.0
Field Dimensions (m)	730 X2985	657 X16581	645 X3648	730 X3979	645 X22385
Probable Cloud Type	Towering Cumulus	Cirrus	Alto-Cumulus	Alto-Cumulus	Not Available
Total Sky Cover (1/10)	4-3	7-5	5	0-1	8
Total Opaque Sky Cover (1/10)	4-3	3-2	5	0-1	3

The results of this analysis are given for cloud case No. 3 in reference (3). The results for case No. 1 are given in Figs. 5-18 to 5-21. To avoid looking at the effect of forcing the front of the cloud field to be clear, the data is analyzed only for the period of time the cloud field is fully over the collector field.

Figure 5-18 is a plot of the incident power level on each superpanel and the total incident power level as a function of time. The superpanel numbers are indicated. In a qualitative sense the panel power variations are substantially out of phase. This is in contrast to cases 2 and 5 for high altitude, fast moving cirrus clouds where the variations in panel power were much more in phase. Figure 5-19 illustrates the rate of change of the total power level which obviously depends on both the amplitude and phase of the individual panel variations.

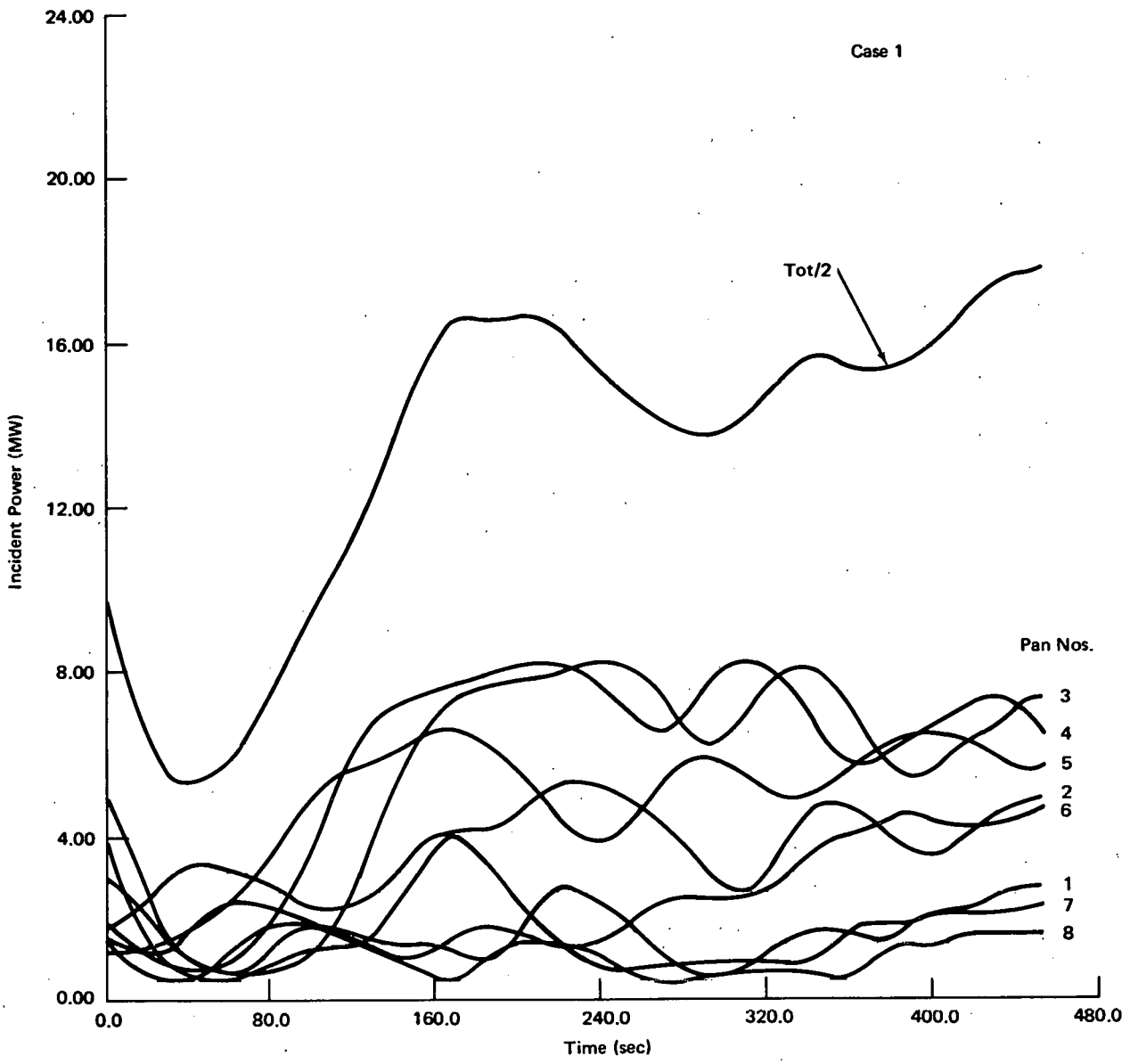

Figure 5-18. Incident Power Level on Each Superpanel and Total Power Level as a Function of Time

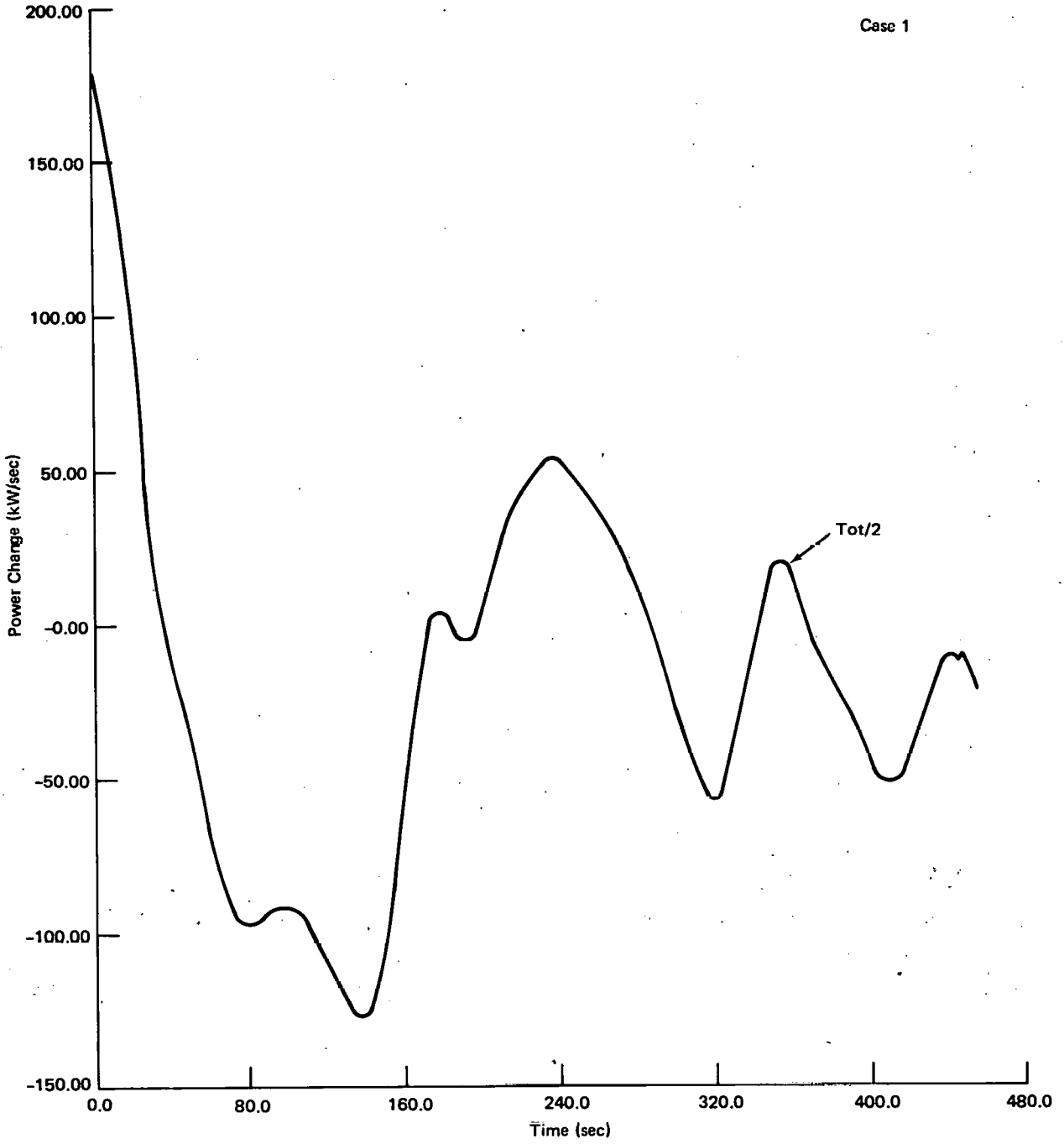

Figure 5-19. Rate of Change of the Total Power as a Function of Time

To get some idea of the changes occurring in the panel gradients the maximum gradient between any two of the twenty four panels is plotted in Figure 5-20 as a function of time. The variations are rather rapid and depend on phase and power levels on the panels. For a more in depth examination of this data it would be valuable to look for gradient reversals from the gradients occurring during normal operation. The distribution of rates of change of total power is shown in Fig. 5-21. Although most variations are around 100 kw/sec, variations two to three times that can occur. It is interesting to contrast this with the distribution for case 4 shown in Figs. 5-22 and 5-23. The case 4 cloud field was more like an impulse function with one fairly opaque area. The rates of change of power level were much less severe. This points out, as might be expected, that a series of broken clouds can induce much more severe input power level variations than one isolated cloud.

A summary of the examination of the cloud transit data is given in Table 5-5. In the third column is tabulated the worst panel gradient occurring at any time on any two panels. The fourth column is the total power level at the time that gradient occurred. The fifth column is the highest rate of change of total incident power and the last column is the intervals of rates of power change that occur more than 10% of the time during the transit. It is interesting to compare the fast moving, high altitude cirrus clouds (cases 2 and 5) to the slower moving cumulus clouds (cases 1, 3, and 4). Although moving five to six times as fast as the cumulus clouds, the cirrus clouds did not seriously impact the panel gradients and the rates of change of power level were only two to three times those for the cumulus clouds. As a matter of fact, looking at the panel gradients and distribution of rates of change of power level, one might somewhat subjectively conclude that case 3 had the worst impact on the collector field.

Some additional simulation runs were made to access the effect of direction of cloud propagation. The cloud field (case 3) was directed across the collector field in 45 degree increments from North to South (N-S) to South to North (S-N). A summary of the overall characteristics of these runs is

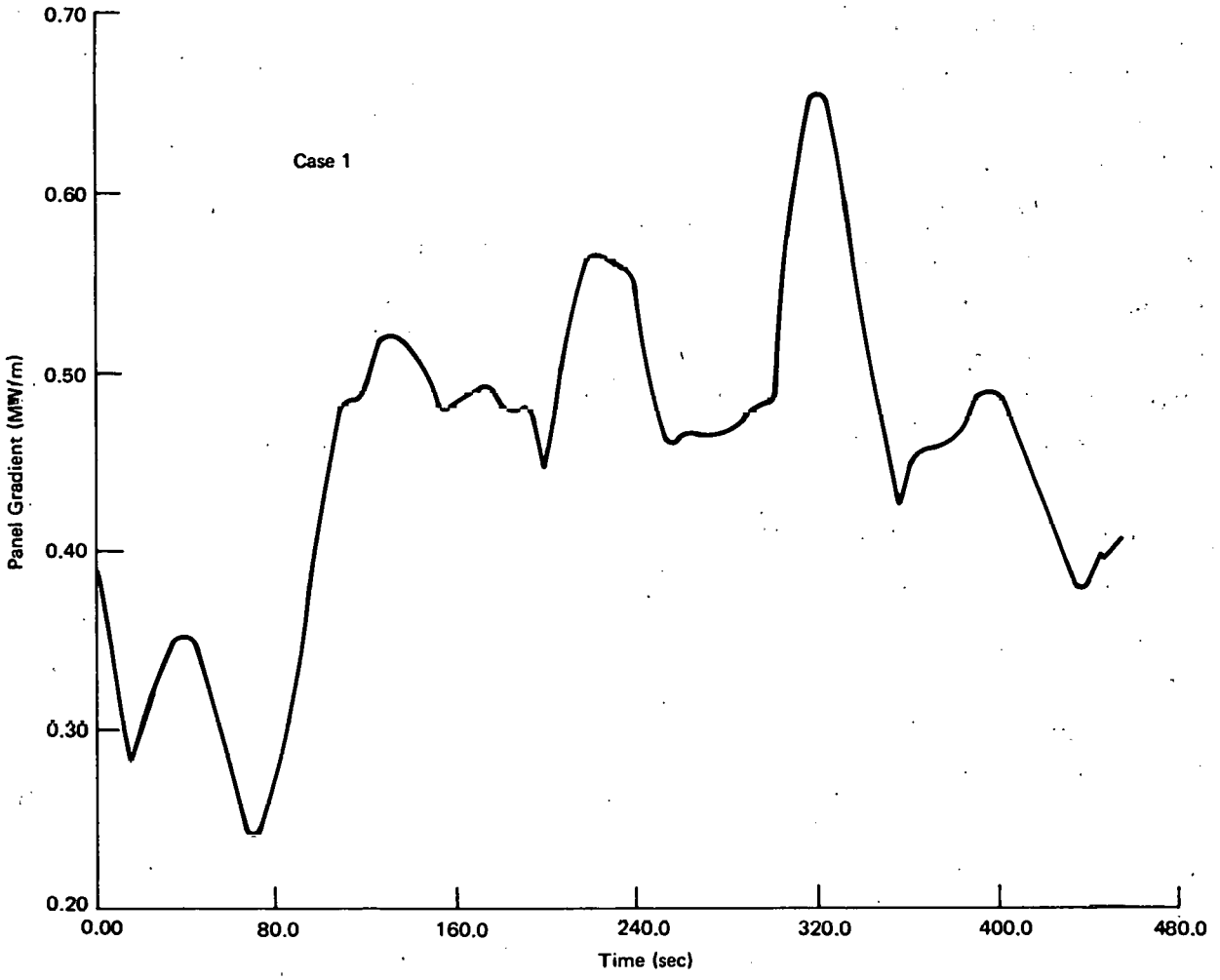

Figure 5-20. Maximum Panel Gradient as a Function of Time

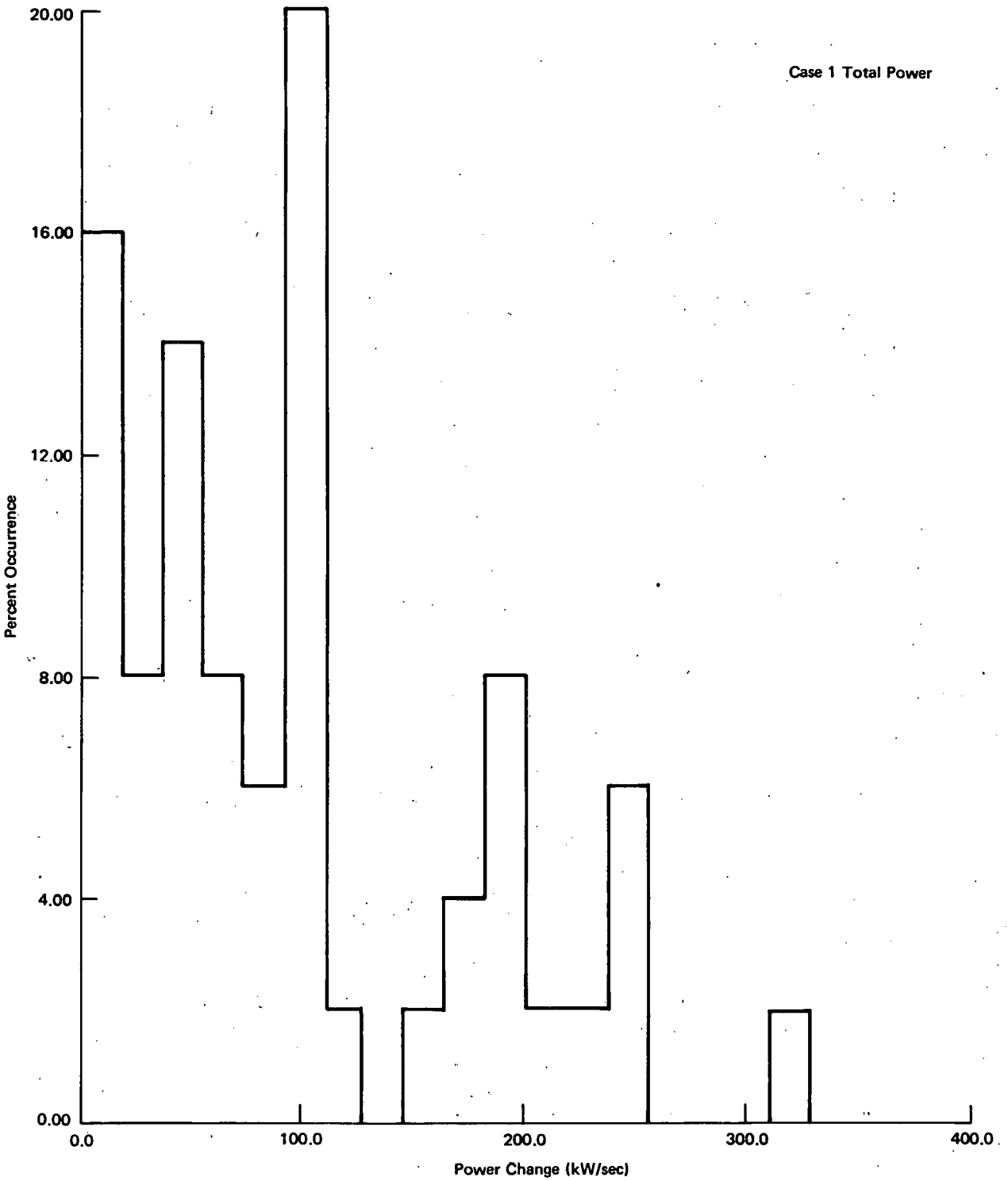

Figure 5-21. Distribution of the Rate of Change of Total Power

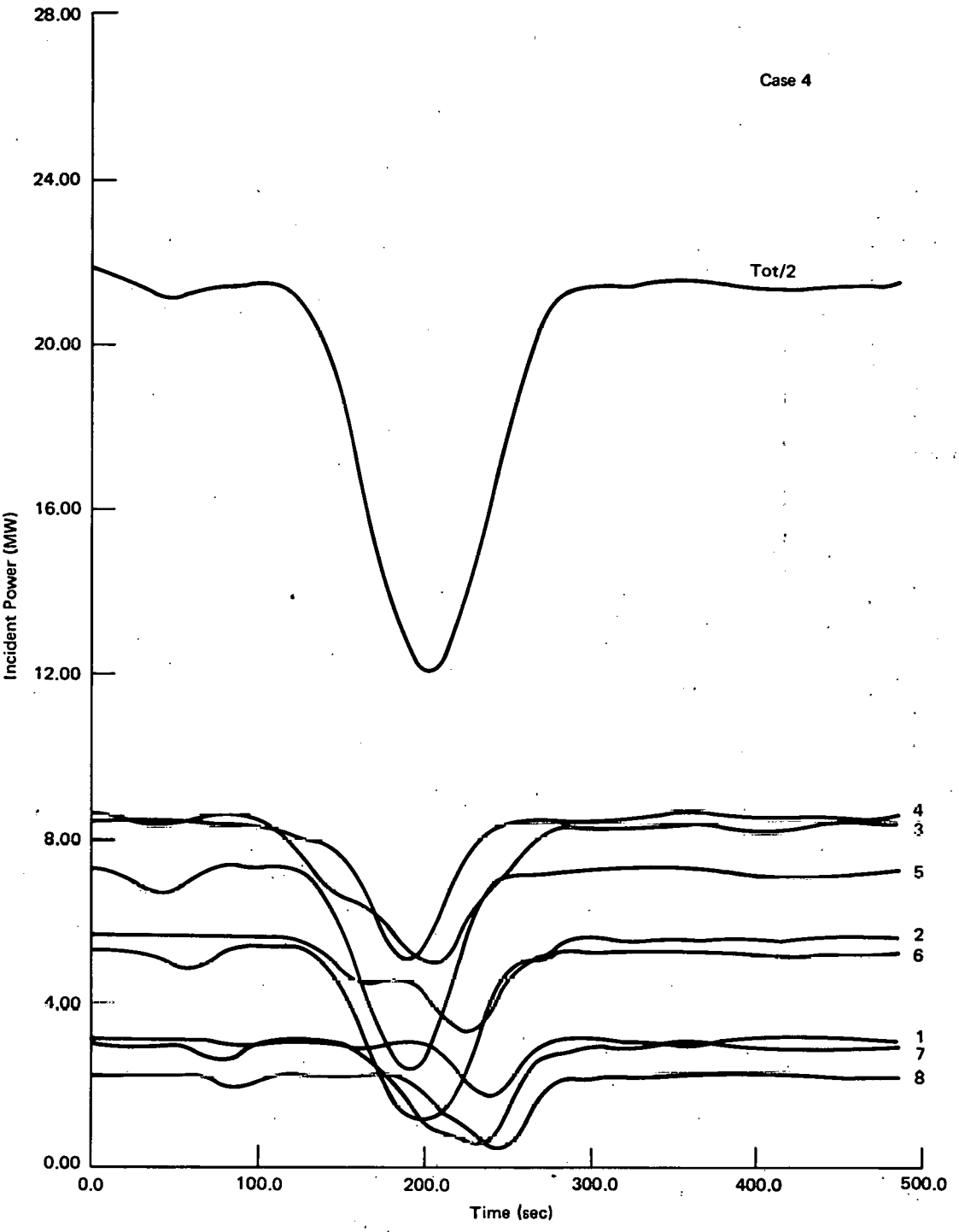

Figure 5-22. Incident Power Level as a Function of Time for Case 4

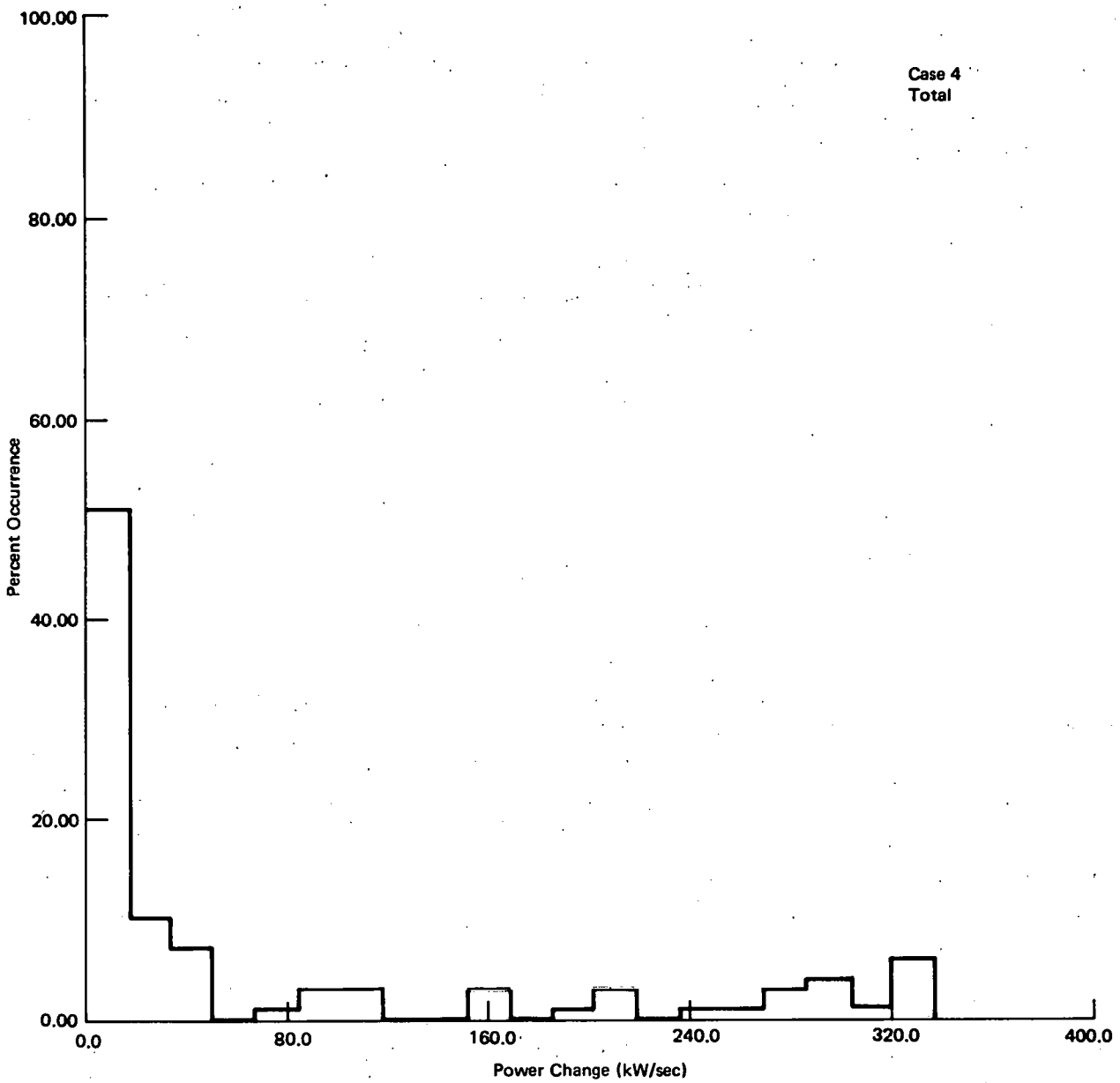

Figure 5-23. Distribution of Rates of Change of Total Incident Power for Case 4

Table 5-5. Summary of Cloud Simulation Results

Case No.	Drift Velocity (m/sec)	Max. Panel Gradient (MW/m)	Total Incid Power At Max Grad (MW)	Maximum Power Change (KW/sec)	Ranges of Power Change Occurring More than 10% (KW/sec)
1	5.5(NW-SE)	0.66	29.0	253	0-18, 36-55 91-109
2A	30.5(W-E)	0.48	43.8	860	176-220 220-264
3A	6.7(N-S)	0.79	23.6	483	0-30, 60-90 417 447
4	7.3(N-S)	0.54	32.2	336	0.17, 17-34
5	41.0(N-S)	0.42	36.8	1097	0-55, 55-110 110-165, 165-219

is given in Table 5-6. The sensitivity to direction, at least for these parameters shows little difference except with respect to the distribution of rates of change of power.

Table 5-6. Summary of Simulation Data for One Cloud Propagating in Five Directions

Case No.	Direction	Max Panel Gradient (MW/m)	Total Incid Power @ Max Grad. (MW)	Max Power Change (KW/sec)	Ranges of Power Change Occurring More than 10% (KW/sec)
3A	N-S	0.79	23.6	595.5	0-30, 60-90, 417-447
3B	NW-SE	0.76	27.6	572.7	57-86, 344-372
3C	W-E	0.80	21.0	624.6	0-31
3D	SW-NE	0.81	19.2	535.6	80-170
3E	S-N	0.78	28.7	594.6	None

Thus, it appears that the direction of approach of a specific cloud field can significantly affect the rates of power change. In the events tabulated in Table 5-6 high rates of power change occur most frequently when the cloud transit is from north to south.

5.6 DIURNAL PERFORMANCE OF HELIOSTATS

The individual heliostat (IH) program provides a very powerful tool for investigating the detailed shading and blocking performance of the heliostat field. One use of this code will be to compute average annual performance factors for each heliostat (shading and blocking, cosine, and interception).

This will allow detailed comparison with the desired optimized performance for each heliostat as a detailed check on the overall layout procedure. It is planned to generate this data on the as-built configuration late in the Phase II program activities.

The run itself will be rather time consuming due to the quantity of data being generated. It will be an expanded version of the current Individual Heliostat (IH) code which prints all of the intermediate performance values (cosine, blocking and shadowing, etc.) for each heliostat for selected times throughout the year. The final output will form a collector field performance data book (200-300 pages) which will be provided as a permanent collector field performance record. Information pertaining to the basic format of the Individual Heliostat code is contained in Appendix C and Section 3.

REFERENCES

1. Randall, C. M., Whitson, M. E., Jr., Johnson, B. R., "Measurements of Insolation Variation Over a Solar Collector Field," Aerospace Corp. Report, No. ATR-79 (7747)-2, Dec., 1978.

2. Randall, C. M., Johnson, B. R., Whitson, M. E., Jr., "Measurements of Typical Insolation Variation at Daggett, California," Aerospace Corp. Report No. ATR-80 (7747)-1, Vol. 1, Mar. 1980.

3. Laurence, C. L., "Short Term Effect of Cloud Transition for the Barstow Central Receiver Pilot Plant," Proceedings of the 1980 Annual Meeting, American Section of the International Solar Energy Society, Vol. 3.1, p. 586, 1980.

THIS PAGE

WAS INTENTIONALLY

LEFT BLANK

Appendix A
METHOD FOR COST/PERFORMANCE OPTIMIZATION OF COLLECTOR FIELD DESIGN

The process of heliostat layout for a central receiver system is based on minimizing the overall system cost per kilowatt of thermal power provided at the base of the tower. A "figure of merit" is defined as

$$F = C_S/E_T \tag{1}$$

where E_T is the total annual thermal energy available at the base of the tower for an average year, and C_S is the total system cost necessary to produce the energy E_T. The turbine-generator subsystem and the thermal storage subsystem are not included. The optimization computer codes contain cost models for the land, heliostats, wiring, receiver, tower, riser/downcomer, and feed pumps. Virtually all factors affecting system optical and thermal performance, from the solar disk profile and incident isolation levels to the absorption and convection losses in the receiver are modeled in the computer code. These include cosine effects, heliostat surface shape, surface irregularities, tracking errors, inter-heliostat shading and blocking, atmospheric absorption between heliostat and receiver, interception losses at the receiver, receiver absorptivity, and receiver thermal losses.

To obtain reasonable computation times the collector field must be reduced from a continuum into discrete cells. The optimization computations are carried out on a cell by cell basis. In the course of these studies three different cell sizes were used. Cells are sized in proportion to the tower focal height so that the elevation angle from the center of a cell to the center of the receiver is the same for any system whose cells are of the same order. The cell size is given by

$$D = \sqrt{\frac{n}{4}}\, H_T \tag{2}$$

where n is the order and H_T is the tower focal height (distance from the plane of the heliostat axes to the body center of the receiver). For the optimization study of the commercial plant large cells of order 5 were required. In this study there are fourteen rows of cells North to South with the tower in the 9th row from the North and there are fifteen columns of cells West to East with the tower in the center column. In later performance analysis and start-up studies for the pilot plant, smaller cell sizes were used to provide greater resolution.

In preparation for an optimizer run two sets of data must first be computed. The first is a node file. This represents the fraction of the redirected power from a representative heliostat at the center of each cell to each node of the receiver. From this node file the fraction of power intercepted by the receiver from each cell can be determined. The fractions are called interception fractions or FINTs and are the ratio of energy at the receiver coming from the collectors to that energy actually incident on the receiver for each cell. The theory behind the programs required for these computations has been published by Lipps and Walzel (2-4). Unless otherwise specified the method of heliostat image formation presented in reference (3), i.e. a two-dimensional Hermite function expansion of the heliostat flux density integral, is being used. Experience has shown that for large systems with moderate concentration the FINTs do not vary significantly as a function of solar position except at very low sun angles. Also, the deviation from the mean over long periods of time in the year is small. Of course, there is no interest in a design optimized at low sun angles since very little energy will be available at these times. Node files intended for design purposes are usually run at noon on an equinox day. The formation of a node file requires a complete description of the heliostat geometry, segment focusing, segment canting and associated focal lengths.

As can be seen in reference 3, page 241, the computer codes actually form the spatial moments of the flux distributions. These moments are convolved with the moments of the limb darkened sun and with the moments of a Gaussian distribution of a specified standard deviation to simulate the effect of mirror surface irregularities and tracking errors. The resulting Hermite polynomials define the heliostat image at the receiver plane. The formation of node files

which are generated from these polynomials usually requires considerable computer time and must be repeated as necessary to access the impact of heliostat design changes.

The second set of data required by the optimizer consists of annualized cell performance as a function of heliostat spacing. This data is based on cosine effects, and the shading and blocking losses. The shading and blocking theory has been published by Lipps and Vant-Hull (5). The shading and blocking data base contains four variations of both radial and azimuthal heliostat spacing. A set of curve fit coefficients is input to the program which defines a nominal set of radial and azimuthal heliostat spacings as a function of tower elevation and cell azimuth angle. The program varies the radial spacing by ±5% and ±15% and the azimuthal spacing by ±5% and ±15%. The ensuing calculations provide a set of 16 numerical values for the cell efficiency $\lambda_c(R_c,Z_c)$ defined as

$$\lambda_c = \lambda_c(R_c,Z_c) = E_c/S_oA_c \tag{3}$$

where R_c is the radial spacing parameter in cell c, Z_c is the azimuthal spacing parameter in cell c, E_c is the annual total thermal energy which is redirected by the heliostats of cell c, A_c is the total area of glass in cell c, and S_o is the mean annual direct beam insolation available at the site. The purpose of the optimizer is to select the optimum spacings in each cell based on cost and performance parameters.

With the interception data available from the image formation codes and cell performance data available from the shading and blocking codes, the optimization process is based on the following formulation. The annual thermal energy delivered to the base of the tower can be represented by

$$E_T = a\left(\sum_c \eta_c\lambda_c f_c\phi_c\right) S_oA_L - b \tag{4}$$

where a represents linear system losses (receiver absorptivity, heliostat reflectivity, etc.), b represents receiver thermal losses, η_c is the receiver interception fraction for a representative heliostat in cell c including

atmospheric absorption effects, A_L is the area of a cell, $f_c\phi_c$ is the fraction of ground covered by glass in cell c, ϕ_c is the fraction of land used in cell c (for fractional cells only), λ_c is the cell efficiency defined above and S_o is the annual total direct solar beam energy per square meter at normal incidence.

Note that

$$A_c = f_c\phi_c A_L \tag{5}$$

and

$$f_c = a_c/R_c Z_c \tag{6}$$

where

$$a_c = A_H/D_H^2\gamma_c = 2A_H/D_H^2 \tag{7}$$

with $\gamma = 1/2$ for radial stagger neighborhoods. R_c and Z_c are in units of heliostat widths. D_H is the heliostat width and A_H is the reflective area of the heliostat.

Two cases will now be considered, the first with a simple cost model for the purpose of illustrating the theory and the second for a cost model including land and wiring which reflects the current capability of the optimized design system.

The simplest possible cost model includes only a fixed cost and the area dependent heliostat cost and is given by

$$C_S = C_o + C_h A_G \tag{8}$$

where C_h is the prorated cost of heliostats per meter squared, and

$$A_G = \left(\sum_c f_c\phi_c\right) A_L \tag{9}$$

gives the total area of glass in the collector field. In this case the optimization process varies the set $V \doteq \{(R_c, Z_c, \phi_c) | c = 1 \ldots N\}$ for given values of $a, b, S_o, A_L, \eta_c, C_o$ and C_h.

Consider variations of the figure of merit, F, with respect to each of the variables in the set V. Assuming that the optimum occurs within the allowed range of all the variables,

$$\delta F = \delta C_S / E_T - C_S \delta E_T / E_T^2 = 0 \tag{10}$$

resulting in

$$\delta E_T = \delta C_S / F \tag{11}$$

at the optimum point. Since we are minimizing a function with respect to three variables, the variations in (11) hold for all three.

Thus, δ in (11) can be δ_{ϕ_c}, δ_{R_c}, δ_{Z_c}. As will become apparent later it is convenient to introduce a change of variables, suggested by (6), the fraction of ground covered. Thinking of f_c as a variable (a set of hyperbolas in R,Z space) we write (6) more generally as

$$f = a_c / RZ \tag{12}$$

and forming an orthogonal variable to f_c

$$t = \frac{1}{2}(R^2 - Z^2) \tag{13}$$

Pertinent differentials for this transformation are

$$df = -a_c (dR / R^2 Z + dZ / RZ^2) \tag{14}$$

$$dt = R\,dR - Z\,dZ \tag{15}$$

$$dR = \left(Rdt - a_c Z\, df/f^2\right) \Big/ (R^2 + Z^2) \tag{16}$$

$$-dZ = \left(Zdt + a_c R\, df/f^2\right)/(R^2 + Z^2) \tag{17}$$

Before transforming variables in the simple case of (8) we have

$$\delta_{\phi_c} C_S = C_h f_c A_L \tag{18}$$

$$\delta_{R_c} C_S = -C_h f_c \phi_c A_L / R_c \tag{19}$$

$$\delta_{Z_c} C_S = -C_h f_c \phi_c A_L / Z_c \tag{20}$$

$$\delta_{\phi_c} E_T = a n_c \lambda_c f_c S_o A_L \tag{21}$$

$$\delta_{R_c} E_T = a n_c (R_c \partial_R \lambda_c - \lambda_c)\, f_c \phi_c S_o A_L / R_c \tag{22}$$

$$\delta_{Z_c} E_T = a n_c (Z_c \partial_Z \lambda_c - \lambda_c)\, f_c \phi_c S_o A_L / Z_c \tag{23}$$

With the change in parameters given by (12) and (13)

$$\lambda_c(R,Z) = \lambda_c(f,t) \tag{24}$$

and the optimizing condition (11) becomes

$$\delta_{f_c} E_T = \delta_{f_c} C_S / F \tag{25}$$

and

$$\delta_{t_c} E_T = \delta_{t_c} C_S / E \tag{26}$$

In terms of (f,t) and using (14) to (23) we have

$$\delta_{t_c} C_S = 0 \tag{27}$$

$$\delta_{t_c} E_T = a n_c (\partial_t \lambda_c)\ f_c \phi_c S_o A_L \tag{28}$$

and

$$\delta_{f_c} C_S = C_h \phi_c A_L = C_h A_L \tag{29}$$

$$\delta_{f_c} E_T = a n_c (f_c \partial_f \lambda_c + \lambda_c)\ S_o A_L \tag{30}$$

From (26), (27) and (28) we have

$$\partial_t \lambda_c = 0 \tag{31}$$

and from (25), (29) and (30)

$$(f_c \partial_f \lambda_c + \lambda_c) n_c = \tilde{\mu} = C_h / (F_a S_o) \tag{32}$$

where $\tilde{\mu}$ is the cell matching parameter and must be input to the optimizer. Equations (31) and (32) are the fundamental optimizing conditions for the cost model given in (8). In the optimizer, all values of cell spacing satisfying (31) and (32) are determined for each cell. The intersection of these values is determined with an interpolation procedure and satisfies both (31) and (32). This set of cell spacings is the optimized set. Notice that $\tilde{\mu}$ depends on the figure of merit F which must be estimated before the optimum

value can be determined, so that the whole solution process must be repeated to converge F_i (input) to F_o (output). Fortunately, convergence is quite rapid.

The extent of the field is determined by the variations with respect to ϕ_c. The trim variable ϕ_c is limited to the range $0 \leq \phi_c \leq 1$. $\phi_c = 0$ if cell c is outside of the optimum field and $\phi_c = 1$ if cell c is inside of the optimum field. However, $0 < \phi_c < 1$ if the cell c is a boundary cell. For boundary cells only,

$$F = (\delta_{\phi_c} C_S)/(\delta_{\phi_c} E_T) = C_h/a\eta_c\lambda_c S_o \tag{33}$$

so that

$$\eta_c\lambda_c = C_h/(FaS_o) \tag{34}$$

if c is a boundary cell. The exterior cells are discarded. This condition can also be written in terms of $\tilde{\mu}$.

Cell c is an interior cell and contributes to the optimum collector field, if

$$\rho_T = \eta_c\lambda_c/\tilde{\mu} \geq 1 \tag{35}$$

This is impossible for cells with a small receiver interception factor η_c, which occurs if the cell has a large slant range or a poor receiver incidence angle (e.g., for a cylindrical receiver because the cell is too near the tower). Hence the inequality $\rho_T \geq 1$ trims the collector field and provides both the outer and inner boundary. The effect of forcing the field to be larger or smaller than that indicated by the optimized figure of merit can be observed by varying the value of ρ_T. When the resulting figure of merit is plotted as a function of annually produced energy the result is a parabola with a minimum of $\rho_T = 1$.

The cost model given by (8) is not sufficient for actual collector field design and has been presented for the purposes of an illustration. The actual design process, reflecting the current capability of the RCELL code, takes into account the cost of land, wiring (cabling, trenching, etc.), operations, and maintenance. The analysis process and the resulting equations are similar to that presented above, although slightly more complex.

The cost model including land and wiring is represented by

$$C_S = C_o + C_h A_L \sum_c \phi_c \psi_c \tag{36}$$

where

$$\psi_c = \alpha + f_c + (\beta_1 r_c + \beta_2 R_c + \beta_3 Z_c)\, f_c \tag{37}$$

$$\alpha = C_l / C_h \tag{38}$$

and

$$\beta_i = C_{wi}\, (A_L/A_H)(D_H/C_h A_L) = C_{wi}/(C_h R_H D_H) \tag{39}$$

where

R_H = A_H/D_H^2, the actual reflective area compared to an ideal square heliostat

D_H = width of heliostat

R_c = radial spacing parameter for heliostat field in cell c in units of D_H.

Z_c = azimuthal spacing parameter

r_c = radial distance from tower to cell c in units of D_H.

C_l = cost of land in $\$/m^2$

C_h = cost of heliostats in $\$/m^2$

C_{wi} = cost of ith wires in \$/m/heliostat

For this cost model the optimum conditions are still represented by (11) with

$$\delta = \delta_{f_c}, \delta_{t_c}, \text{ and } \delta_{\phi_c}$$

Equation (4) can be re-written as

$$e = \sum_c \eta_c \lambda_c f_c \phi_c = (E_T + b)/(aS_o A_L) \tag{40}$$

with

$$g = C_S/C_h A_L \tag{41}$$

and as previously

$$\mu = C_h/(FaS_o) \tag{42}$$

After differentiation we can drop factors of ϕ_c, so that

$$\partial_{f_c} e = \eta_c(\lambda_c + f_c \partial_f \lambda_c) \tag{43}$$

$$\partial_{t_c} e = \eta_c(\partial_t \lambda_c)\, f_c \tag{44}$$

$$\partial_{\phi_c} e = \eta_c \lambda_c f_c \tag{45}$$

$$\partial_{f_c} g = 1 + \beta_1 r_c + \beta_2 R_c + \beta_3 Z_c + (\beta_2 \partial_f R_c + \beta_3 \partial_f Z_c)\, f_c \tag{46}$$

$$\partial_{t_c} g = (\beta_2 \partial_t R_c + \beta_3 \partial_t Z_c)\, f_c \tag{47}$$

$$\partial_{\phi_c} g = \alpha + f_c(1 + \beta_1 r_c + \beta_2 R_c + \beta_3 Z_c) \tag{48}$$

The above equations comply with the optimum conditions as shown in equations (49) and (50), which depend on cost parameters occurring in equation (36) for the cost model.

$$\eta_c(\lambda_c + f_c \partial_f \lambda_c) = \tilde{\mu} \partial_{f_c} g \tag{49}$$

$$\partial_t \lambda_c = \tilde{\mu}(\beta_2 \partial_t R_c + \beta_3 \partial_t Z_c)/\eta_c \tag{50}$$

Evaluating the partial derivatives on the right hand side of (49) and (50) and using (42) the final expressions for the two optimum conditions are

$$(\lambda_c + f_v \partial_f \lambda_c) = (C_h/FS_0)\ \{1+\beta_1 r_c+\beta_2 R_c+\beta_3 Z_c - a(\beta_2 Z_c+\beta_3 R_c)/f_c(R_c^2+Z_c^2)\}\eta_c^{-1} \tag{51}$$

and

$$\partial_t \lambda_c = (C_h/FS_0)\ (\beta_2 R_c - \beta_3 Z_c)\ \eta_c^{-1}/(R_c^2 + Z_c^2). \tag{52}$$

Notice that $\beta_i = 0$ gives the previous results, i.e., a result independent of wiring cost.

The boundary condition is given by

$$\eta_c \lambda_c = \tilde{\mu}(\alpha/f_c + 1 + \beta_1 r_c + \beta_2 R_c + \beta_3 Z_c) \tag{53}$$

for boundary cells. The interior of the field satisfied the condition,

$$\rho_T = \eta_c \lambda_c/[(\alpha/f_c + 1 + \beta_1 r_c + \beta_2 R_c + \beta_3 Z_c)\tilde{\mu}] \geq 1 \tag{54}$$

These relations degenerate to the previous case if land and wiring have no cost, i.e.,

$$\alpha = \beta_1 = \beta_2 = \beta_3 = 0$$

The RCELL program outputs a set of coordinates for each cell in the field that satisfy equations (51) and (52) and the energy quantities given by RCELL are for a field whose boundaries are chosen by values of ρ_T. The best figure of merit occurring at $\rho_T = 1$. Once these spacings are determined, they can be used directly but it is more convenient to form a two dimensional curve fit, thus reducing the set of heliostat spacings, R_c, Z_c to a set of curve fit coefficients, C_i where i is usually 6. This process forms a smoothing function to give approximate values at locations other than at cell centers. It is also very convenient for scaling purposes. The best curve fits are obtained when the tower elevation angle, θ, and cell azimuth angle, ϕ, are used as independent variables, although usually the variation on ϕ is small and can be neglected. Typically, the form of the curve fit used is

$$R(\theta,\phi) \text{ or } Z(\theta,\phi) = \frac{C_1}{\theta} + C_2 + C_3\theta + \left(\frac{C_4}{\theta} + C_5 + C_6\theta\right) \cos\phi \qquad (55)$$

The azimuthal spacing, Z, is only a slowly varying function of θ, and the radial spacing, R, has little dependence on ϕ. Thus, the most important curve fit coefficients are C_1, C_2, and C_3 for the radial spacing. The curve fit routines are built into the optimizer code so that the coefficients are output at the end of each optimizer run. These coefficients are used by CELLAY and LAYOUT subroutines to determine actual heliostat locations in a collector field.

REFERENCES

1. Lipps, F.W. and Vant-Hull, L.L., "A Cellwise Method for the Optimization of Large Central Receiver Systems," Solar Energy, 20, p. 505 (1978).

2. Lipps, F.W., "Four Different Views of the Heliostat Flux Density Integral", Solar Energy, 18, p. 555 (1976).

3. Walzel, M.D., Lipps, F.W., and Vant-Hull, L.L., "A Solar Flux Density Calculation For a Solar Tower Concentrator Using a Two-Dimensional Hermite Function Expansion," Solar Energy, 19, p. 239 (1977).

4. Lipps, F.W. and Walzel, M.D., "An Analytic Evaluation of the Flux Density Due to Sunlight Reflected from a Flat Mirror having a Polygonal Boundary," Solar Energy, 21, p. 113 (1978).

5. Lipps, F.W., and Vant-Hull, L.L., "Shading and Blocking Geometry for a Solar Tower Concentrator with Rectangular Mirrors," ASME Proceedings, 74-WA/501-11, p. 2. (1974).

Appendix B

LAYOUT OF A HELIOSTAT FIELD VIA THE INDIVIDUAL HELIOSTAT /IH/ CODE

This appendix documents the code used to develop the coordinates of the heliostat locations for the Barstow pilot plant. One module will be discussed in detail. It is the package of routines called INPUTS, which contains six subroutines and consists of 336 lines of code.

The fact that code maintenance and utilization demands periodic code changes is recognized. This commentary is written using the code as it existed on July 23, 1979. The discussion will reveal the theory of the layout procedure, the details of this code, and the logic of the design of the Barstow pilot plant.

```
1*#RUNH-500 /IH/INPUTS;/IH/R-LAY;/IH/R-YEAR;/IH/R-FIELD;/IH/R-SABI;
2*#/IH/R-ANNUAL=(CORE=60,OPTZ,BCD,ULIB) UH/SLIBB/UH,R #AIMS"09";
3*#TRIM"17";HELIOS1"10";HSELCG1497/PPNODE2"14";CARD.F"30"
4C#HSELCG1122/PPSTNODE"14";CARD.F"30";PLOTD"11"
```

These lines are for a Honeywell timesharing run on the 66/60. In a batch stream, the * in the first column is treated as a comment card and those lines have no effect. However, they do have some information pertaining to the utilization of the /IH/ system of code. There are six packages of subroutines: INPUTS, LAY, YEAR, FIELD, SABI, and ANNUAL. 60K of core is called for as well as a library. The object programs are in BCD, and OPTZ calls for optimal compiling, although the "R-" designates a file containing object code. The library asked for with read permission is UH/SLIBB/UH and contains some handy, arbitrary function least squares routines. Next come the various file codes for I/O in addition to the standard "05" and "06". "09" is a file called AIMS and contains the aim points for representative heliostats in a matrix of cells covering the collector field. Individual heliostat aim points are interpolated from this matrix. "17" is a file called TRIM and contains the collector field

boundary via a list of x,y coordinates obtained from RCELL on an optimization run. "10" is a file called HELIOS1 and contains the heliostat coordinates generated by LAY. "14" is a file containing nodal interception fractions on the receiver for each cell in the field. Individual heliostat interception factors are generated from the cellwise interception factors calculated from this file. "30" is a file containing receiver panel powers that may or may not be written during the course of a run. "11" is a file which can, upon the user's option, have various outputs written to it for future plotting on our "22" Complot plotter.

```
5C
6C      TG -- VERSION OF LAYOUT PROGRAMS              M.D.WALZEL      08/22/79
7C
8C      VARIABLE DIMENSIONS                           F.W.LIPPS       08/26/77
9C      INDIVIDUAL HELIOSTAT PROGRAM                  W.A.HOLLEY      03/15/78
10C
11C
12      PARAMETER MAXH= 2400                ;*MAX NUMBER OF HELIOSTATS
13      PARAMETER MAXF= 2400                ;*MAX SIZE OF HELIOSTAT SUBFIELD
14      PARAMETER MAX2= MAXF/2              ;*HALF FIELD DIMENSIONS
15      PARAMETER IGREC=  22, JGREC= 24     ;*FOR PANEL(IGREC,JGREC)
16      PARAMETER NXD=13,NYD=15             ;*FOR OUTPUT CELL STRUCTURE
17C     PARAMETER NXD=14,NYD=15             ;*FOR OUTPUT CELL STRUCTURE
18      PARAMETER NS   =  8                 ;*NO. OF SECTORS AROUND COLL.FIELD
19      PARAMETER NSP = NS + 1
```

Parameter statements are used when a change is required in integer constants which are needed to dimension arrays. They can be passed along in subroutine arguments to control loops and equations as well as dimension variable arrays in subroutines. MAXH is the maximum number of heliostats that can be dealt with, while MAXF and MAX2 are related as shown if a subsection of the field is desired for evaluation. IGREC and JGREC dimension the matrix of nodes on the receiver while NXD and NYD dimension the cell structure of the collector field. NS and NSP allow the number of sectors or "pie slices" of the field to be varied for a circle-sector style of output.

```
20      DIMENSION PANEL(IGREC,JGREC),FLREC(IGREC,JGREC),FLRECP(JGREC)
21      DIMENSION NH(131),NHT(131)
22      DIMENSION AIMTRX(NXD,NYD),CFINT(NXD,NYD)
23      DIMENSION ACELL(NXD,NYD),AI(JGREC),AJ(JGREC)
24      DIMENSION FCOSI(MAXF),FMIRR(MAXF),FAREA(MAXF),FINT(MAXF)
25      DIMENSION ERGM1(MAX2),ERGM2(MAX2),RTPOW(MAX2)
```

```
      DIMENSION XC(MAXH),YC(MAXH),ZC(MAXH),AZ(MAXH)
      DIMENSION FSAB(MAXF),ASAB(MAXF)
      DIMENSION ENHEL(130,NS),FGRND(131,NSF)
```

These are the dimension statements for the /IH/ system. Note the parameters used to dimension many of the arrays. The array names will be discussed as they occur in the code.

```
      COMMON /CELL/ HT,DA,AC,NTOWI,NTOWJ
      COMMON /SITE/ XLAT,VR,HS,CMW,RATMOS,PATMOS,PGRND,ZGRND,RINSOL
      COMMON /ATMOS/ILAT,PPS(3,12),APW(3,12),ATF(3,12)
      COMMON /TIME/ JDVEQ,ESUNO,HYEARS,IMAX,JMAX,NSKIP
      COMMON /TIMEX/IDAYS,IHORS,NDAY1,HOURO,HOUR1,HOUR2,DHOUR
      COMMON /FINT/ COFNT(8)
      COMMON /XLOSS/KPANL,PREPAN,BOILER,HEATER
      COMMON /TOWER/HTX,HCYLNT,RRECT,HCYLN,WCYLN,OFSET,REFLT,ABSOR,
     &        FRLOS,NPANLS,INODE1,INODE2,JNODE1,JNODE2
      COMMON /RECVR/ICYLN,IAIMS,NFLAT,APERHT,APERWD,KSHAPE,IAPER,ANGREC
      COMMON /CALCX/JDISK,ISUMS,KANNU,ICLDF,ICNTR,IAXIS,KTAPE,IPSEC,
     &        NFILES
      COMMON /GRPLS/ASDCS(7,10),ASDIN(7,10)
      COMMON /GRP01/KVEC(8)
      COMMON /GRP7/ NBOR,NGON,NGONP,NGHF,IPSAB,SRATIO
      COMMON /GRPB/ANG1,ANG2,IROW1,IROW2,IFIELD,IPWAV,
     &        ANP1,ANP2,NCIR,AZD,IDEL(20,2),ADEL(20,50)
      COMMON /GROPT/ITRIM,IPRNT,IFILE,IFAIM,ICOOR,IDATA
      COMMON /ZONE3/ DMECH,RSYMIN,RSYMAX,SLIP,HALFAZ
C
C   *0*0*0 NEW GROUPS BELOW 0*0*0*
C
      COMMON /GRLAY/ NC,HX,HGLASS,HTD,EXCLRD,ZRATIO
      COMMON /BOUND/ STHRD,ESTRD,RTHRD,RSOTH,CSOTH,ELIMT,WLIMT
      COMMON /HELI2/ UMIR,VMIR,SLOT
```

These are the common groups in the /IH/ system. Some of the group names are descriptive. Note that vectors and arrays that are in common statements are dimensioned there. The variables in the common statements will be dealt with as they occur in the code.

```
C
C          INPUT DATA
      DATA KVEC/272,122,152,182,212,242,272,162/
C
```

KVEC is a vector containing the days of the year chosen for annual simulation. The numbers are integers representing days after vernal equinox.

```
58        TIMIT = 0.
59        CALL PTIME(XTIME2)
60C
```

PTIME is a Honeywell system subroutine for timing code which will return the time of execution in the variable XTIME2. Later, another call to PTIME will result in another value of the time, and the difference is the CPU time required for execution between the two calls. TIMIT keeps a running total of time elapsed.

```
61COLLECTOR FIELD
62        PGRND = .0040       ;*GRADE IN %/100 FOR COLLECTOR FIELD
63        ZGRND = .0          ;*DIRECTION OF UPGRADE IN DEGREES
```

PGRND and ZGRND have to do with the magnitude and direction of the slope of the land. When ZGRND is zero degrees, the direction of the upgrade is due south.

```
64        NTOWI = 9           ;*TOWER ROW FOR NODE FILE
65        NTOWJ = 8           ;*TOWER COLUMN FOR NODE FILE
```

In the cell structure of the collector field, the tower occupies one of the cells of the matrices dimensioned NXD (number of rows) by NYD (number of columns). NTOWI and NTOWJ locate the position of the tower within the grid of cells.

```
66        NC    = 36          ;*MAXIMIUM NUMBER OF CIRCLES IN LAYOUT
67        NGON  = 4           ;*NUMBER OF SIDES FOR HELIOSTAT
68        IAXIS = 1           ;*ALT-AZ IS 1  R-PROLL IS 2  AZ-PROLL IS 3
69C                             POLAR IS 4  RECEIVER IS 5
```

NC is the maximum number of circles of heliostats about the tower allowed in the layout. For a Barstow sized plant, there are usually about 25-35 circles in a layout. NGON can take on the value of 4, 6 or 8 and is utilized by the shading and blocking program to calculate losses for a heliostat that is rectangular, hexagonal, or octagonal. IAXIS is the choice of mounting system for the heliostats and is usually elevation-azimuthal.

```
70       IPSAB = 1          ;*IS 0 FOR NO S&B OUTPUT 1 FOR S&B MATRICES
71C                              2 FOR BOUNDARY VECTORS 3 FOR PICTURES.
72C                             -1 FOR NO S&B CALC
```

IPSAB is the switch that controls the shading and blocking calculations and output. When IPSAB is equal to -1, no S&B calculations take place. When the values, 0, 1, 2, or 3 are chosen, S&B calculation takes place with the output shown. The option IPSAB = 3 is no longer operative, however.

```
73       NCIR  = 3            ;*NUMBER OF CIRCLES SCANNED BY SABI
74C                              IS NCIR*DMIR/ROW SPACING + 2  7/2/79
```

The shading and blocking program for the /IH/ system scans neighbors in circles behind and before the heliostat under consideration. The number of circles scanned is given by NCIR and the formula in the comment card. Note that more circles than ±2 can be considered for shading and blocking events when the circles are in close proximity.

```
75       ZRATIO = 4./3.              ;* RATIO OF HELIOS FROM ZONE TO ZONE
76       SRATIO= 2.*ZRATIO  ;*MULTIPLIER FOR AZD TO CONTROL AZIMUTHAL
77C                           ANGLES SCANNED BY SABI
```

ZRATIO sets the ratio of heliostats from one zone to another in the layout. As the radius of succeeding circles becomes smaller, the heliostats are squeezed together azimuthally. When a minimum azimuthal distance is achieved, some heliostats must be removed for the construction of the next circle. Therefore, where there were four heliostats within a fixed azimuthal range, there will be three for the next circle. Within a zone, all heliostats have the same azimuthal angle between them as measured from the tower, unless special slides and slips have been instituted for the purpose of reducing shading and blocking. SRATIO is used by the shading and blocking routine to govern the azimuthal angle over which neighbors are scanned for possible shading and blocking, much as NCIR controls the number of circles (or radial distance) to be scanned.

```
78       IPSEC = 0          ;*IS 0 FOR NO SECTOR OUTPUT 1 FOR OUTPUT
79       ICNTR = 1          ;*IS 1 TO PLOT & AVER, 0 NOT TO PLOT 2 NO AVER
80C                              3 TO PLOT AVERAGE AND SHIFT BY AVERAGE
```

IPSEC is an output control. A sector is a pie-slice shaped region of the field, of which there are typically eight. ICNTR is a variable in calls to the contour routine which outputs and contours various matrices.

```
81C
82C        * * * BEGINNING OF INPUT DATA FOR LAYOUT * * *
83C
84C                  LINEAR DIMENSIONS ARE CONVERTED FROM FEET TO METERS
85C                  STD CONVERSION IS 2.54 CM/IN OR .3048 M/FT
86C
```

Most dimensions for the Barstow Pilot Plant were given to us in feet instead of meters. To retain our use of the metric system, and still reveal the dimensions as presented to us, most linear dimensions are in feet with the 0.3048 multiplier. Many of the parameters that follow are used exclusively to size and control the layout of the collector field.

```
87        HT     =  247.5 * .3048      ;*FOCAL HEIGHT OF TOWER IN METERS
88        DA      = HT*SQRT(2.10/4.)     ;*CELL SIZE FOR NODE FILE
89C       DA      = HT*SQRT(3./4.)     ;*CELL SIZE FOR NODE FILE
```

HT is the centerline elevation of the receiver above the plane of heliostat centers. DA is the distance between cell centers of the collector field. The order of the cell is denoted by the numerator within the SQRT function. Order 2.1 cells were judged appropriate for a collector field matrix dimensioned 13 x 15 with the tower at cell (9, 8) given the acreage and shape of the Barstow site.

```
90   DMIR   = 33.00 * .3048         ;*WIDTH OF SANDIA HELIOSTSAT IN METERS
91   HGLASS= 450.0 * .3048**2      ;*SANDIA GLASS/HELIOS IN M2 (450 SQ.FEET)
92   EXMIR = 17.67                 ;*EXCLUSION RADIUS FOR HELIOSTAT (FEET)
```

DMIR is the width of the nominal heliostat specified by S.T.M.P.O to be used in designing the collector field layout. HGLASS is the area of reflector area and EXMIR is the free turning radius of the specified heliostat.

```
93        STHRD = (35.0+EXMIR)*.3048 ;* WIDTH/2 OF SOUTH ROAD IN METERS
94        ESTRD = (10.0+EXMIR)*.3048 ;* WIDTH/2 OF EAST ROAD
95        RTHRD = (10.0+EXMIR)*.3048 ;* WIDTH/2 OF NORTH ROAD
```

STHRD is the half width of the radial south road as far as heliostat pedestal positions are concerned. Thus, STHRD is set to 35 feet plus EXMIR for a south road 70 feet wide without interference. Similarly, the clearance required for the east (and the west) and north radial roads is twenty feet. (See Figure 4.1).

```
96        RSOTH = ((2150.-(1408.-10.)-5.-1.)+643.-EXMIR)*.3048
97        CSOTH =  (642.+1.) * .3048          ;* CENTER OF SOUTH CIRCLE
```

The southern boundary of the field (the fence line) is defined by a circle offset to the north of the tower location by 642 feet. Since the field is sloped downward to the north on a 0.4% grade, the center point about which the circles of heliostats are constructed is located one foot to the south of the tower. Thus the collector field circles are true circles in the sloped ground plane, but are slightly elliptical in the level plane. Therefore a foot is added such that the center of the southern perimeter circle, CSOTH, is 643 feet north of the center of the collector field circles. RSOTH is the radius of the southern boundary circle and is determined the following way. The field, when measured from the center of the northern perimeter road to the center of the southern perimeter road due south, is 2150 feet. The perimeter roads are 10 feet wide, and there is a gap of 5 feet between the fence and the edge of the road. The distance from the tower to the north fence is 1408 feet. If we reduce 1408 by 10 feet, the result is the distance from the tower to the center of the north perimeter road. If we subtract this from 2150, the result is the distance (due south) from the tower to the center of the southern perimeter road. Next we subtract 5 feet to get the distance from the tower to the inside edge of the southern perimeter road, and finally, subtract one foot to get the distance from the center of the collector field circles to the inside edge of the southern perimeter road. Next we subtract EXMIR, the heliostat exclusion radius and add back in 643 feet (the value of CSOTH). The result gives a radius for the southern boundary outside of which no heliostat pedestal may be placed. This offset circle terminates on the south side of the east and west radial roads.

```
98        RNRTH = (1408.-15.-EXMIR+1.)*.3048;*RADIUS OF NORTH CIRCLE
99        ELIMT = (1290.-EXMIR-5.-15.0)*.3048  ;* EAST LIMIT
100       WLIMT = (1290.-EXMIR-20.-15.0)*.3048  ;* WEST LIMIT
```

The northern fence line is circular, centered at the tower and is 1408 feet away as mentioned above. To obtain the greatest allowable collector field circle, RNRTH, we subtract 15 feet for the 10 foot road and 5 foot gap. Next we subtract EXMIR and then add one foot to obtain the radius of the northern-most circle. The east and west limits are boundaries beginning at the north side

of the east and west radial roads and proceeding due north. The distance from the tower to the fence line due east (or west) is 1290 feet. From this we subtract EXMIR and 15 feet for the heliostat exclusion radius and the ten foot perimeter road and five foot gap, respectively. For the east limit, ELIMT, we subtract an extra five feet for existing obstructions, and on WLIMT, and extra 20 feet is subtracted for existing obstructions. Thus heliostat pedestal positions begin at radius RNRTH, and terminate into ELIMT and WLIMT. Succeeding collector field circles terminate on the east and west boundaries or the southern boundary circle, or if their radii are sufficiently small, they close around entirely to the south, terminating on the southern radial road, STHRD.

```
101       DMECH = 2.*(EXMIR*.3048) / DMIR       ;* MECH LIM IN DMIR
102       EXCLRD = (219.0+EXMIR)*.3048  ;* EXCLUSION RADIUS IN METERS
```

DMECH is the diameter of the mechanical limit exclusion circle in units of DMIR, the heliostat width. EXCLRD is the exclusion radius for heliostats about the tower. No heliostat pedestal positions are allowed within 219 + 17.67 = 236.67 feet of the tower.

```
103       ITRIM =-2             ;*2 GIVES TRIM 1 GIVES TRFC 0 GIVES ISECT
104                             ;* -1 GIVES GEOMETRIC BOUNDRY
105                             ;* -2 GIVES GEOMETRIC BOUNDRY MINUS TRIM LIST
106       IPRNT = 0             ;*IS 1 TO PRINT COORDS AND 0 NOT
107       IFILE = 0             ;*IS 1 TO WRITE COORDS TO FILE AND 0 NOT
100       IDATA = 0             ;*IS 1 TO WRITE PDATA TO FILE AND 0 NOT
109       IFAIM = 0             ;*IS 1 TO READ AIMTRX AND 0 FOR DATA
110       ICOOR = 1             ;*IS 1 TO CALL COORDS SUBROUTINE AND 0 NOT
```

The variables above are used to choose I/O options and manage the flow of control within the program. ITRIM is a variable which provides for five different trim options to determine the point at which the collector field circles terminate. When ITRIM is set to 2, the subroutine TRIM is called which accepts data from a previous optimization run to determine the field boundary. When ITRIM is set to +1, a function subroutine TRFC is called which determines the southern boundary upon which the collector field circles terminate. When ITRIM is 0, a data statement defining the vector ISECT is utilized. This vector contains the trim angle for each circle of heliostats. One must know the circle radii from a previous layout run to choose the trim angles and use this option effectively. When ITRIM is -1, the geometric trim using the

information described previously is used. This option is chosen when the land area is already specified. When ITRIM is -2, a list of removals from the resulting heliostat coordinates is invoked by calling the function subroutine ISKIP. IPRNT controls the output of coordinates to file code 06, while IFILE controls the output of coordinates to file code 10. IDATA controls the output of certain matrices to file code 11, IFAIM controls the input of data from file code 09. ICOOR will cause the generation of individual heliostat coordinates if set to 1, and will bypass this function if set to 0. The collector field circle radii are generated nonetheless.

```
111       NC     = 130          ;*MAX NUMBER OF CIRCLES IN LAYOUT .LE. 130
```

NC is the maximum number of circles allowed in a layout. Numbers in this range of 130 have been obtained for a commercial size plant, while the current design for the Barstow plant has 30 circles of heliostats.

```
112       RSYMIN = 2.1*.85*   .9          ;*MIN. AZIMUTHAL SPACING IN DMIR
113       RSYMAX = 2.1*1.00          ;*MAX. AZIMUTHAL SPACING IN DMIR
```

RSYMIN is the minimum azimuthal spacing allowed and is measured along the arc in units of DMIR. RSYMAX is the starting (rather than maximum as the comment reads) azimuthal spacing in DMIR of only the outermost circle. For succeeding circles of smaller radius, the azimuthal spacing also becomes smaller. When it is less than RSYMIN, a new zone is constructed with the ratio of heliostats from one circle to the next circle in the new zone being defined previously by ZRATIO, or 4/3 for the Barstow plant. The new maximum azimuthal spacing for the next zone is therefore defined by ZRATIO and the value of the azimuthal spacing of the circle just before RSYMIN was violated, and not by RSYMAX.

```
114       AHELI  = DMIR**2              ;*AREA OF SQUARE HELIOS IN M2
115       RHELI  = HGLASS/AHELI
116       RA1    =  RNRTH   / DMIR          ;*RADIUS OF OUTER CIRCLE IN DMIR
117C
```

AHELI is the area in square meters of the regions bounded by the perimeter of the heliostat. RHELI is the ratio of actual reflector area to AHELI. RHELI is less than one mainly due to the slot of the inverting heliostat. RA1 is the radius of the outermost circle in units of DMIR rather than meters as RNRTH.

```
118C  INPUTS TO DEFINE A COLLECTOR SUBFIELD FOR PROCESSING
119       IFIELD = 0          ;*IS 1 TO CALL SUBFLD, 0 NOT TO
120       ANG1 = -.625        ;*FIRST AZIMUTH (PI UNITS) FOR SUBFLD
121       ANG2 = .625         ;*SECND AZIMUTH (PI UNITS) FOR SUBFLD
122C                             SUBFLD SELECTS HELIOS FOR RUNSTREAM
123       IROW1 = 1           ;*OUTER CIRCLE TO END COLLECTOR SUBFIELD
124       IROW2 =  0          ;*INNER CIRCLE TO END COLLECTOR SUBFIELD
125       ANP1 = -.00         ;*FIRST  AZIMUTH PRINT CONTROL
126       ANP2 = .00          ;*SECOND AZIMUTH PRINT CONTROL
127C                             AZIMUTH NEG. TO WEST POS. TO EAST
128       IPWAV = 1           ;* 1 OUTPUT ONLY WEIGHTED AVE. OF
129C                          ;*MIRROR FRACTIONS 0 NOT TO OUTPUT
130C
```

These lines define a subsection of the field. IFIELD controls the access to the processor, while ANG1, ANG2, IROW1, and IROW2 define the sector and circles to be processed if IFIELD = 1. If IROW2 = 0, all circles are processed. IPWAV is a switch governing output for the collector subfield under investigation.

```
131       CALL WREAD (20,1,100)
132       CALL WREAD (21,1,400)
```

WREAD is a subroutine which reads a file and writes to filecode 06. Here the filecodes being read are 20 and 21, and the line numbers are from 1 to 100 and from 1 to 400 respectively. This allows the reproduction of certain source files within the output of the code.

```
133       CALL LAYOUT(DMIR,AHELI,RHELI,RA1,NH,NHT,XC,YC,ZC,AZ,
134      &                NXD,NYD,AIMTRX,NS,NSP,FGRND,ENHEL)
```

LAYOUT is the routine that generates the collector field layout. Upon return from this routine, the collector field coordinates have been written to filecode 10 if ICOOR is set to one. If ICOOR is set to zero, then only a preliminary layout will be generated. This subroutine will be discussed in more detail later.

```
135C
136       XTIME1 = XTIME2
137       CALL PTIME(XTIME2)
138       XTIME  = XTIME2 - XTIME1
139       TIMIT  = TIMIT + XTIME
140       WRITE(6,9000)XTIME,TIMIT
141  9000 FORMAT(1HO,'$ $ $ $ CPU TIME=',F14.8,' HOURS * * * * ',
142      &            'TOTAL CPU TIME=',F14.8,' HOURS'//)
143C
```

PTIME is a Honeywell system subroutine that reports time during execution. By placing calls in appropriate sections, the CPU time consumed by various portions of the code can be monitored (refer to lines 58-60). This particular output will reveal the time required to layout the field.

At this point, the layout is complete and the following code (lines 144-243) has to do with performance simulation via the individual heliostat system of code. For completeness the code is revealed below without comment except that which is contained within the code as in-line comments.

```
144C TIME CONTROLS
145       JDVEQ = 2442859    ;*JULIAN DAY OF VERNAL EQUINOX FOR 1976
146       XLAT  = 35.        ;*LATITUDE OF SITE IN DEGREES
147       ILAT = 0           ;* 0 TURNS OFF WEATHER  MODEL
148C                          ;* 1 GIVES MODEL FOR LAT. = 25
149C                          ;* 2 GIVES MODEL FOR LAT. = 35
150C                          ;* 3 GIVES MODEL FOR LAT. = 45
151       NSKIP = 30         ;*NUMBER OF DAYS SKIPPED BETWEEN CALCULATIONS
152       JMAX  = 1          ;*NUMBER OF SAMPLE DAYS
153       IMAX  = 7          ;*NUMBER OF SAMPLE HOURS
154       ESUNO = 10.0       ;*ELEVATION OF STARTUP IN DEGREES
155       IDAYS = 0          ;*IS 0 TO NDAY1 1 TO JMAX DAYS 2 TO 7 DAYS
156       NDAY1 =  186       ;*DAYS AFTER VERNAL EQUINOX
157       IHORS =    0       ;*2 FOR PM HOURS 1 FOR GIVEN HOURS 0 FOR HOURO
158                          ;* -1 FOR AM, -2 FOR PM STARTUP OPTIONS
159C                         ;*-1 FOR SOLAR ELEVATION EQUAL TO ESUMO
160       HOUR1 = -6.650     ;*THE INITIAL HOUR IF IHORS = 1
161       HOUR2 = -5.620     ;*THE FINAL HOUR IF IHORS = 1
162       HOURO =  3.448     ;*THE HOUR FOR IHORS =0
163       DHOUR = 0.1721     ;*HOURS BETWEEN CALCULATIONS FOR IHORS=-1 OR 0
164C
```

```
165C HELIOSTAT CONTROLS FOR PERFORMANCE STUDY
166C      DMIR  = 23.597* .3048        ;*WIDTH OF MDAC HELIOSTSAT IN METERS
167C      HGLASS= 479.0 * .3048**2     ;*MDAC GLASS/HELIOS IN M2 (479 SQ.FEET)
168C      DMIR  = 22.246* .3048        ;*WIDTH OF MARTIN HELIOSTSAT IN METERS
169C      HGLASS= 430.0 * .3048**2     ;*MARTIN GLASS/HELIOS IN M2 (430 SQ.FEET)
170       DMIR = 6.9976885  ;*WIDTH OF HELIOSTSAT IN METERS (SANDIA 450)
171       UMIR = DMIR       ;*
172       VMIR = DMIR       ;*
173       SLOT = 0.         ;*
174       DMIR = SQRT((UMIR**2 + VMIR**2)/2.)
175       HGLASS = 41.8063680;* M2 = 450 SQ. FEET (SANDIA 450)
176C      AHELI = DMIR**2             ;*AREA OF SQUARE HELIOS IN M2
177       AHELI = (UMIR-SLOT)*VMIR
178       RHELI = HGLASS/DMIR**2
179       RA1   =  RNRTH  / DMIR        ;*RADIUS OF OUTER CIRCLE IN DMIR
180       NFLAT =12                    ;* EQUALS NUMBER OF SEGMENTS/HELIOS
181C
182C ANNUAL STATISTICS
183       KTAPE = 1         ;*  1 TO READ FILE (14) FROM RECEIVER STUDY
184       NFILES = 2        ;*0<NFILES<3  ---  IS THE # OF NODE FILES
185C                          TO BE READ --- FILE CODES 14 AND 24 --- 14 IF
186C                          NFILES IS SET TO 1  ---  SLAVE TO KTAPE
187       KANNU = 2         ;*  1 TO DO PANEL POWER ANNUAL 0 NOT
188       ICYLN = -1        ;* -1 FOR CYLN REC. -2 FOR FLAT REC. 0 TO BYPASS
189       ICLDF = 0         ;*  1 TO DO CLOUD FRONT STUDY 0 OTHERWISE
190       ISUMS = 1         ;*  1 TO SUM OVER HOURS 0 OTHERWISE
191       IAPER = 0         ;*  1 FOR APERTURE STUDY 0 NOT
192       JDISK =  0        ;*  -1 FOR HALF FIELD NODE FILE 0 FOR WHOLE
193C
194CONSTANTS FOR ATMOSPHERE
195       VR    = 50.       ;*VISUAL RANGE IN KMS
196       HS    =550.       ;*ELEVATION OF SITE IN METERS
197       CMW = 1.44        ;*CENTIMETERS OF ATMOSPHERIC WATER VAPOR
198       REARTH = 6370.    ;*RADIUS OF EARTH IN KILOMETERS
199       HATMOS = 8.430    ;*HEIGHT OF ATMOSPHERE IN KILOMETERS
200       PATMOS = (1.0 - .0065*HS / 288.)**5.2568   ;*PRESSURE IN ATMOS
201       RATMOS = REARTH/(HATMOS * PATMOS)
202       RINSOL = 1.00     ;* INSOLATION MODEL CORRECTION FACTOR
203C
204CYLINDRICAL RECIEVER
205       INODE1 = 2        ;*LOOP PARAMETERS TO CONTROL RECEIVER NODES
206       INODE2 = 21       ;*IN THE VERTICAL DIRECTION - FOR RCFINT&RCFLUX
207       JNODE1 = 1        ;*LOOP PARAMETER FOR AZIMUTHAL OR HORIZONTAL
208       JNODE2 = 24       ;*DIRECTION (USUALLY JNODE2= NO. OF PANELS)
209       HCYLNT = 15.0876  ;*TOTAL HEIGHT OF CYLN OR FLAT FROM NODE FILE
210       HCYLN = HCYLNT*(INODE2-INODE1+1)/FLOAT(IGREC)  ;*HEIGHT OF RECVR
211       RRECT =   3.5052  ;*TOTAL RADIUS OF CYLN OR HALF WIDTH OF FLAT
212       WCYLN =   3.5052  ;*RADIUS OF CYLN OR HALF WIDTH OF FLAT
213C                           OR RADIUS OF CYLINDER ACCORDING TO ICYLN
214       OFSET = 0.0       ;*OFFSET FOR FLAT RECEIVER
215       ABSOR = .93       ;* RECEIVER ABSORBTIVITY
216       OUTAGE = 1900./1932.  ;*PERCENT HELIOSTATS NOT ACTIVE
217       SLIPAG = 1.0  ;* .958/.987   HELIOSTATS LOST BY LAYOUT
218       REFLE = .86       ;*REFLECTIVITY AND DUST
219C                                 AND CORRECTION FOR ACTUAL IH S&B
```

```
      SNSHAD= 1.0          ;*SENSOR SHADOW, 1.0 OR .98
      REFLT = REFLE*OUTAGE*SLIPAG*SNSHAD
      FRLOS = ABSOR*REFLT
      KPANL = 1            ;*FIRST PANEL FOR FINT (NOT USED NOW )
      PREPAN = 3           ;*HALF NUMBER OF PRE-HEAT PANELS IN PANPOW
      BOILER = 240.0E3     ;*RADIATIVE&CONVECTIVE LOSSES IN WATTS/PANEL
      HEATER =  80.0E3     ;*RADIATIVE&CONVECTIVE LOSSES IN WATTS/PANEL
C
      CALL YEAR(IGREC,JGREC,PANEL,FLREC,FLRECP,MAXH,MAXF,FCOSI,
     &          FMIRR,FINT,FAREA,RTPOW,ERGM1,ERGM2,FSAB,ASAB,NH,NHT,
     &          XC,YC,ZC,AZ,NXD,NYD,AIMTRX,CFINT,ACELL,AI,AJ,
     &          DMIR,AHELI,RHELI,RA1,
     &          TIMIT,XTIME2,NS)
C
      XTIME1 = XTIME2
      CALL PTIME(XTIME2)
      XTIME  = XTIME2 - XTIME1
      TIMIT  = TIMIT + XTIME
      WRITE(6,9000)XTIME,TIMIT
C
      STOP
      END
C
C
      FUNCTION ISKIP(I,J)
      DIMENSION JSKIP(31,15)
      DATA JSKIP                                    ;*REMOVALS
     & /31*0,                                       ;*FOR CIRCLE # 1
     & 8,26,66,68,70,45,47,53,65,67,69,             ;*FOR CIRCLE # 2
     & 1,3,5,7,9,13,17,21,                          ;*FOR CIRCLE # 2
     & 2,4,6,10,12,14,18,22,30,3*0,                 ;*FOR CIRCLE # 2
     & 76,78,80,82,77,79,81,24*0,                   ;*FOR CIRCLE # 3
     & 85,30*0,                                     ;*FOR CIRCLE # 4
     & 68,70,67,69,27*0,                            ;*FOR CIRCLE # 5
     & 70,72,69,71,27*0,                            ;*FOR CIRCLE # 6
     & 74,76,73,75,27*0,                            ;*FOR CIRCLE # 7
     & 76,78,75,77,27*0,                            ;*FOR CIRCLE # 8
     & 82,84,81,83,27*0,                            ;*FOR CIRCLE # 9
     & 86,88,85,87,27*0,                            ;*FOR CIRCLE # 10
     & 92,94,91,93,27*0,                            ;*FOR CIRCLE # 11
     & 74,76,73,75,27*0,                            ;*FOR CIRCLE # 12
     & 80,82,79,81,27*0,                            ;*FOR CIRCLE # 13
     & 86,88,90,85,87,89,25*0,                      ;*FOR CIRCLE # 14
     & 31*0/                                        ;*FOR CIRCLE # 15
      ISKIP = JSKIP(I,J)
      RETURN
      END
C
C
```

ISKIP is a function subroutine designed to remove certain heliostats from the list of coordinates that have been generated for each circle. Circle #1 is the outermost circle. The first index of the augment, I, determines the heliostat to be removed. The second argument, J, determines on which circle the heliostat is located. The matrix JSKIP is loaded with integers which designate the heliostat to be removed. If ISKIP (I,J) is zero, no heliostat is removed. If JSKIP (I,J) is some other positive integer, that heliostat is removed. For a particular circle the heliostats are numbered with the evens to the west and the odds to the east. Heliostats one and two are next to the north radial road and the count continues around to the south for both halves of the field.

Obviously, to intelligently remove certain heliostats, the coordinates must have been previously generated and inspected. The JSKIP matrix has to have the first dimension be at least as big as the most heliostats removed in any circle. The second dimension is related to the circle number, and need not include all the circles, but must start with circle #1.

```
269       FUNCTION RSFC(ETA,CNSAZM)
270       EXTERNAL POLYNM
271       DIMENSION CELAYC(4,3), RS(4), AZ(4), COFLST(25), WKSPC(25,25)
272       COMMON /ZONE3/ DMECH,RSYMIN,RSYMAX,SLTP,HALFAZ
273       RFUNC(C1,C2,C3,THETA) = C1/THETA+C2+C3*THETA
```

RSFC is a function subroutine which determines the radial separation between heliostats of the same azimuth, i.e., the distance between every other circle for the radial stagger configuration. ETA and CNSAZM are two inputs to the routine via the argument list. ETA is the tower elevation angle in radians at the point in the field under consideration. CNSAZM is the constrained azimuthal spacing for the circle under consideration. Only the first circle has its azimuthal spacing as a chosen variable. Afterwards, all angular azimuthal spacings are the same within a zone and increase by ZRATIO in succeeding zones. The radial spacing function RSFC, therefore, determines the circle after next, given the current tower elevation angle and the current azimuthal spacing.

POLYNM is the name of a function subroutine used in the call to the arbitrary least squares routine. The variables in the dimension statement of line 271 will be discussed as they occur in the routine. Group common /ZONE3/ is included, and the statement function RFUNC is defined in line 273.

```
274       DATA ((CELAYC(I,J),J=1,3),I=1,4)
275      &/7.6256948E+01,-6.3566463E-01,2.0852482E-02,
276      & 4.9358923E+01,3.3424066E-01,7.6399559E-03,
277      & 5.2074868E+01,-1.1602792E-01,1.2732010E-02,
278      & 5.0780993E+01,3.5846674E-02,6.1396681E-03/
279       DATA (AZ(I),I=1,4) /1.785,1.995,2.205,2.415/
```

The data statements above load the coefficients for spacings from the program CELAY in CELAYC (I,J) and the azimuthal spacings, AZ. For each of the four azimuthal spacings (in units of DMIR) defined in the vector AZ, there are three coefficients for the appropriate radial spacing in the matrix CELAYC. Each of the four sets of coefficients results in radial and azimuthal spacings which have the same annual shading and blocking losses for a particular point in the collector field.

```
280       RAD = 180./3.1415926535
281       THETA = ETA * RAD
```

RAD is a variable to convert from radians to degrees and vice versa. THETA is the value of ETA in degrees.

```
282       AITRMX = AZ(4)
283       AITRMN = AZ(1)
284C       IF(THETA .LT. 20.0) AITRMN = AZ(2)
```

AITRMX and AITRMN are the maximum and minimum values for the constrained azimuth, CNSAZM, that will be allowed. By defining them as shown in lines 282-283, we are assured that the values of RSFC will be interpolated and not extrapolated. Line 284 was used when there was no value for the radial spacing that would give the correct annual shading and blocking losses for the azimuthal value of AZ(1) when the tower elevation was less than 20 degrees. This means one is using an extrapolated value for the radial spacing when the azimuth is smaller than AZ(2) and when THETA is less than 20 degrees.

```
285       NUMPTS = 4
286       NUMCON = 4
287       M = NUMCON + 1
288       DO 100 IAZ = 1,4
289   100 RS(IAZ) = RFUNC(CELAYC(IAZ,1), CELAYC(IAZ,2), CELAYC(IAZ,3),
290      & THETA)
291C*** LSQF AND VALF COME FROM UH/SLIBB/UH
292       CALL LSQF(AZ,RS,NUMPTS,M,POLYNM,COFLST,WKSPC)
```

NUMPTS and NUMCON are the number of points and constants desired for the arbitrary function least squares fit in line 292. The 100 loop of lines 288 and 289 use the coefficients of CELAYC and the function RFUNC to evaluate the radial spacing at each of the four values of the azimuthal spacing. The call to the subroutine LSQF of the UH/SLIBB/UH library results in a fit of the RS dependent values to the four AZ independent values, using the fitting function POLYMN.

```
293       IF( CNSAZM .GT. AITRMX ) CNSAZM = AITRMX
294       IF( CNSAZM .LT. AITRMN ) CNSAZM = AITRMN
295       RSFC = VALF(CNSAZM,COFLST,M,POLYNM)
296       RETURN
297       END
298C
299C
300C
301C
```

If the input value of CNSAZM is out of range, it is modified in lines 293-294. Finally, the functional fit POLYMN of AZ versus RS is evaluated at AZ=CNSAZM by the call to VALF. This value is stored in the function subroutine name RSFC, and a return to the calling program is made.

```
302       DOUBLE PRECISION FUNCTION POLYNM(X,K)
303       POLYNM = X**K
304       RETURN
305       END
306C
307C
308C
309C
```

POLYMN is the function subroutine mentioned before. Here the definition is simply a function of powers of X.

```
310       FUNCTION TRFC(R)
311       TRFC = 0.
312       IF(R.LE.2.55)RETURN
313       TRFC = (78.05/57.0) * SQRT((R/2.55)**2 -1)   ;*COMM TRIM OPTION
314       RETURN
315       END
```

Lines 310-315 represent a trim function for the southern boundary of the collector field that is available within the code for a commercial system. It was not used for the Barstow plant. R is the radius of a particular circle in tower heights. The value returned in TRFC is the azimuthal angle, measured from due south, at which a circle of heliostats terminates. Note that if R is less than 2.55, the circle is allowed to close around to the south road.

```
316C
317C
318C
319       FUNCTION HSTEP(R1,R3,HALFAZ,HTD)
```

The radial spacing function, RSFC, computes the distance between the representative heliostat and the neighbor directly between itself and the tower. This means the radius of circle #3 is established given the starting location of circle #1. It remains for the radius of circle #2 to be calculated. This is the circle which contains the heliostats which the representative heliostat "peeks between" to see the tower and receiver in the radial stagger configuration. The spacing of this circle is determined by the routine HSTEP. The radii R1 and R3 of the circles immediately behind and before the circle in question are input along with one half the angular azimuthal heliostat separation and the tower height in unit of DMIR. The resultant value of HSTEP will locate the intermediate circle in the proper location using the RSFC function and an iterative method.

```
320   100 FORMAT(1X,I6,4F12.4)
321       NCNT = 0
322       HLFWAY = (R1+R3)/2.
323       DELA = R1-R3
```

The format statement of line 320 is for an optional write statement during the iterative process to reveal the process of obtaining a solution. NCNT is a counter for the iterations. HLFWAY is the radius halfway between R1 and R3, and DELTA is the distance between circles of radius R1 and R3.

```
324    10 AZMI = 2.*HALFAZ*HLFWAY
325       ELEV = ATAN(HTD/HLFWAY)
326       DELB = RSFC(ELEV,AZMI)
```

Line 324 starts the iterative process. The azimuth and elevation at the halfway mark are defined in lines 324-325. Then in line 326, the radial spacing function RSFC is used to define DELB, a step from the halfway mark towards the tower.

```
327       BETA = DELA*DELB/(DELA+DELB)
328       HSTEP = R3 + BETA
```

With DELA and DELB defined, a value of BETA is obtained, which, when added to the radius of circle R3, results in HSTEP, the radius of the intermediate circle. Line 327 merely equates the reciprocal of BETA to the sum of the reciprocals of DELA and DELB, and provides a good estimate for HSTEP in line 328.

```
329       NCNT = NCNT + 1
330C       WRITE(6,100) NCNT,R1,R3,HLFWAY,HSTEP
```

NCNT is incremented by one and if desired, the comment can be removed from line 330 to write the current trial, the radii of circles R1 and R3, the halfway mark, and the guess for the intermediate circle, HSTEP.

```
331       IF(ABS(HSTEP-HLFWAY).LT. .0005  .OR.  NCNT.GT.9 )
332      & GO TO 20
333       HLFWAY = HSTEP
334       GO TO 10
335    20 RETURN
336       END
```

If HSTEP and HLFWAY are within 0.0005 DMIR units of each other, or if we have done more than 9 trials, control is transferred to statement 20 and a return is made to the calling routine. If not, HSTEP is loaded into HLFWAY and control is transferred to statement 10 which is line 324. A new value is then obtained for HSTEP and tested on the second iteration. In this process, the spacing coefficients of CELAYC (I,J) are used to define the intermediate circles just as they define all others. This iterative process usually converges to a value of HSTEP in two or three trials.

Line 336 marks the end of the package of routines called INPUTS. The second package of routines called LAY uses the inputs and function subroutines in INPUTS to generate heliostat location coordinates.

Appendix C
THE INDIVIDUAL HELIOSTAT PERFORMANCE CODE

C.1 THE HELIOSTAT FIELD VARIABLES

The individual heliostat performance code is similar to the cellwise performance code with the sum over cells being replaced by a sum over heliostat. Each heliostat has a coordinate vector and a number of special properties. Table C-1 gives a complete list of heliostat field variables.

Table C-1. List of Heliostat Field Variables

#	Variable	Dimension*	Purpose
1	XC	MAXH	X component of heliostat
2	YC	MAXH	Y component of heliostat
3	ZC	MAXH	Z component of heliostat
4	AZ	MAXH	Azimuth component of heliostat
5	FINT	MAXF	Receiver interception fraction
6	FCOSI	MAXF	Cosine of incidence
7	FMIRR	MAXF	Fraction of useful area
8	FAREA	MAXF	Effective fraction of area
9	FSAB	MAXF	Fraction of afternoon insolation weighted FMIRR
10	ASAB	MAXF	Annual average of FSAB
11	ERGM1	MAX2	KW/m^2 of daily redirected power
12	ERGM2	MAX2	MW/m^2 of annual redirected power
13	RTPOW	MAX2	Fraction of relative heliostat performance

*MAXH, MAXF, and MAX2 are input parameters which control the core requirements of the program.

MAXH must be given a value which is larger than the total number of heliostats in the coordinate layout.

$$MAXF \leq MAXH$$

$$MAX2 = \begin{cases} MAXF/2 \text{ for symmetric fields,} \\ 1 \text{ for asymmetric fields.} \end{cases}$$

MAX2 gives the dimension of vectors which require an east-west symmetry assumption. If no such symmetry exists MAX2 is set to 1 and the SUMIT and RELPOW subroutines are bypassed. MAXF can be reduced in accordance with controls to the SUBFLD subroutine which limits the set of heliostats to be processed. Any circle-sector region can be selected for processing.

If MAXF = 2000, then the field vectors require 23K core. The IH code requires an additional 45K core, making it possible to operate with CORE = 70K, which is a convenient level for time sharing. Life would not be so simple for a commercial system with MAXF = 20,000 so that

$$CORE = 45K + 230K = 285K.$$

For internal purposes, the IH code numbers heliostat circles from the outside to inside. The outer circle is number 1. The first heliostat in the layout is in the outer circle and is the first heliostat which is west of south. Consecutive heliostats move around the circles in clockwise fashion until a circle is filled and then the next heliostat goes to the first position in the next inner circle.

At present the layout process is symmetric. This means that heliostat locations come in east-west pairs, regardless of deletes, roads, field boundaries, and trim controls. The pairs are written to the output heliostat file consecutively, but they are not consecutive in the core storage vectors. Field asymmetry can be introduced by removing heliostats from the performance model in several ways. The ISKIP function provides for a list of removed heliostats. The SUBFLD subroutine limits the effective field to an arbitrary circle-sector region.

In the future, modifications will be needed to layout fields with an east-west incline, or non-symmetric field boundaries, and/or non-flat fields.

C.2 THE LAYOUT PROCESSOR

The layout processor achieves three main results.

1) Input data from the RCELL optimization program determines a set of radii for a circular heliostat layout which is consistent with the heliostat mechanical limits and a selected zonal layout scheme.

2) Heliostat locations are determined and the heliostat coordinate file is written. The locations provide radial stagger neighborhoods with the peak through feature. Proceeding toward the tower, the neighborhoods become azimuthally compressed until it is necessary to create a new zone with expanded azimuthal separations. The outer circle of an inner zone has deleted heliostats in order to avoid direct blocking. There is also an extended pattern of azimuthal slippage to minimize losses in the vicinity of the delete. The available heliostat locations are limited by the field boundaries and roads.

3) The actual set of heliostats is transmitted to the performance model. The set of heliostats equals the set of locations minus a list of removed heliostats which is used to achieve a specified power level or to study particular regions of the field.

Figure C-1 shows the overall structure of the IH code. Notice that the LAYOUT subroutine comes prior to the performance model which is contained in YEAR and can be executed independently. Figure C-2 shows the overall structure of the layout processor revealing most of its subroutines. For further details see Appendix B.

C.3 THE PERFORMANCE MODEL

The individual heliostat performance code is similar to the cellwise performance code except that:

1) The representative heliostats of the cellwise model are replaced by a complete set of heliostats. Cell structure is restored for certain output purposes, and

2) The receiver model is not available in the individual heliostat code and receiver information is input via the node file and the aims file.

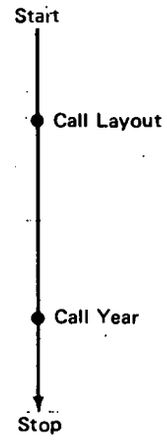

Figure C-1. Overall Structure of IH Code as Seen by the INPUT Module

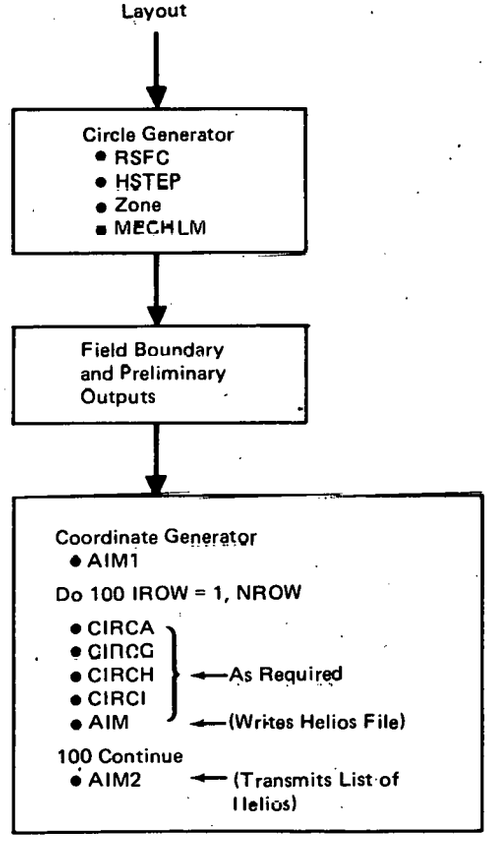

Figure C-2. Structure of the Layout Processor
See Appendix B for Definitions and Details

Table C-2 lists all Input/Output files. The AIMS file inputs the aiming strategy data which is output by the receiver subroutine in the cellwise system. This array of data is interpolated to the individual heliostats and written to the Helios file. The AIMS data cannot be used in any other way. The other I/O files will be explained under the appropriate subroutines in Section C.6.

The IH performance code is contained in the subroutine YEAR. Figure C-3 shows that YEAR divides into three phases. Time dependence occurs only in the second phase which is called the diurnal phase. Details of each phase are shown in Figure C-4.

Table C-2. List of I/O File Codes

Code	File	Subroutine
05	System STD Read	
06	System STD Write	
09	AIMS - Aim points from cellwise program	AIM
10	HELIOS - Coordinate Data	AIM
11	PLOTD - Circle/sector data for plotter	CIRSEC
14	NODE1 - Receiver Interception Data	FINTP1
24	NODE2 - Receiver Interception Data	FINTP2
30	CARD.F - Data to be card punched	PANPOW
38	Temporary Random File for Helios Panel Sums	FINTP1
39	Temporary Seq. File for PANPOW versus TIME	FINTP1
40	Temporary Seq. File for Cellwise Panel Sums	FINTP1

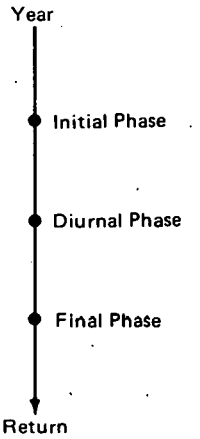

Figure C-3. The Overall Structure of YEAR

```
INITIAL PHASE
      LOADS AND OUTPUTS FINT
      INITIALIZES SUBLD IF DESIRED

DIURNAL PHASE
      (DAILY HEADING)
      700 LOOP FOR DAYS
      600 LOOPS FOR HOURS
      (INSOLATION MODEL)
      500 LOOP FOR CIRCLES IN COLLECTOR FIELD
      501 LOOP FOR HELIOSTATS IN CIRCLE
      (HELIOSTAT ORIENTATION)
      CALL SAB3 FOR SHADING AND BLOCKING
      501 CONTINUE
      500 CONTINUE
      (HOURLY OUTPUTS)
      600 CONTINUE
      (DAILY OUTPUTS)
      700 CONTINUE

FINAL PHASE
      ANNUAL OUTPUTS
```

Figure C-4. The Main Loops in YEAR

Figure C-4 shows the major loops occurring in YEAR including the call to the shading and blocking subroutine SAB3 and indicating the occurrence of outputs.

The only output from the initial phase is for FINT. A variety of output options are available. SECTOR can provide a FINT output for each heliostat although this is usually not desired. CELTUR can provide an array of N-S cellwise averages for FINT with or without a contour map. CIRSEC can provide an array of circle-sector averages for FINT with averages and with or without an additional write to a disk file for plotter applications.

The first output in the diurnal phase is the daily heading and the last output of the diurnal phase is an hourly summary. Figure C-5 is an example of the daily heading and hourly summary outputs.

```
ON THE 92ND DAY AFTER VERNAL EQUINOX
EARTH = 0.10163220E 01 ASU
SOLAR ELEVATION AT NOON = 78.4407 DEGREES
DAY = 14.3565 HOURS
SUNRISE AZIMUTH = 117.1763 DEGREES


AT 5.000 HOURS THE SUN GIVES
860.224 WATTS/M2. THE TOWERTOP COLLECTOR HAS
3356.014 M2 OF EFFECTIVE AREA AND PROVIDES
2.887 MEGAWATTS OF DIRECTED POWER


HOURS      USUNX      USUNY      USUNZ      ESUN      ZSUN
5.000  -  0.144261  -  0.906217   0.397441  23.4183  -99.0450
```

Figure C-5. Daily Heading and Hourly Summary Outputs. The length of day and azimuth of sunrise refer to the input elevation of startup.

The diurnal phase outputs are given below. Except for items (4) and (5) all of these outputs are available in the full range of output styles as described for the FINT vector.

1) Fraction of Mirror Reflecting = FMIRR
2) Cosine of Incidence Angle = FCOSI
3) Effective Fraction of Mirror = FAREA

4) The Hourly Summary Output
5) The CPU Time
6) Afternoon Insolation Weighted Average of FMIRR = FSAB
7) Daily Total KWH/m^2 Reflected = ERGM1
8) Daily Relative Total Power = RTPOW
9) Annual Afternoon Insolation Weighted Average of FMIRR = ASAB
10) Annual Total MWH/m^2 Reflected = ERGM2
11) Annual Relative Total Power = RTPOW

The final phase outputs are as follows:

1) Annual Summary of Insolation,
2) Annual Summary of Cosines,
3) Annual Summary of FMIRR,
4) Annual Summary of FAREA,
5) Annual Summary of Receiver Power,
6) Annual Summary of System Efficiencies,
7) Annual Summary of System Efficiencies/COSI,

and, finally

8) PANPOW and PANEFF Outputs.

The last executable statement in YEAR calls PANPOW which in turn calls PANEFF. The PANPOW subroutine and the PANEFF subroutine make the following outputs

1) Annual Summary of Incident PANEL Power in MW
2) Annual Summary of Absorbed PANEL Power in MW
3) Annual Summary of System Efficiencies
4) Annual Summary of System Efficiencies/COSI
5) Annual Summary of Dimensionless Panel Gradients
6) Annual Summary of Receiver Asymmetry Ratios
7) Annual Summary of Panel MAXIMA in MW printed above Panel Number of the MAXIMA
8) Annual Summary of Panel MINIMA in MW printed above Panel Number of the MINIMA
9) Annual Summary of Incident Panel Power for a constant direct beam intensity at all times of 950 W/m^2
10) (Same for Absorbed Panel Power)
11) Annual Summary of system Efficiencies for a direct beam intensity of 950 W/m^2 at all times - Losses Included
12) Annual Summary of System Efficiencies/COSI

If PANPOW is called, the previous system efficiency outputs do not occur since they would be redundant. The annual summary outputs normal include seven days with seven output times/day. The times begin at noon and end at an input elevation angle which represents a reasonable shutoff condition. The times are equispaced from noon to shutoff. The days are equispaced from summer solstice to winter solstice. However, any selection of time can be studied. Outputs for the seasonally symmetric days can easily be generated by applying a small correction to the insolation.

C.4 MODES OF OPERATION

This section describes the applications which are anticipated for the IH code system. At the risk of repetition it should be mentioned that RCELL provides coefficients for an optimized layout. The IH code does not contain the economic model and does not optimize. Furthermore, the cellwise code writes the Node file and the Aims file which are read by the IH code when receiver interception, receiver panel power, receiver flux density and/or the aiming strategy are required. Typically, a cellwise receiver run and an RCELL optimizer run would be required before starting an individual heliostat study.

Generally, one expects to make a series of layout runs prior to a detailed performance study. The layout process is very fast and adjustments can be made in the zonal structure, and/or the approach to various boundaries. As soon as a reasonable preliminary layout is obtained one should get the total receiver power at the design time. This will require a node file and the use of the shading and blocking subroutine. If the total thermal power is higher than specified, the requirement can be achieved by removing an appropriate number of heliostats from the existing layout, or by generating a new less dense layout. If the receiver power is too low a denser layout may be required. Having achieved the specified total thermal power, the next problem concerns the flux density distribution and time dependence of the panel powers. The appropriate subroutine outputs are available and again modifications in layout may be required. If all design requirements are satisfied, the various outputs can be used to predict performance and to analyze the quality of the design.

C.5 THE SUBROUTINE STRUCTURE AND COMMON GROUPS

Table C-3 gives a list of all subroutines and functions which occur in the individual heliostat performance code. Figure C-1 shows the two major calls which occur in the MAIN program after the relevant input data. Figure C-6 shows every call which occurs directly in YEAR. The LAYOUT subroutine calls the subroutines and functions which are listed under files INPUT and LAY of Table C-3. The subroutine YEAR involves all of the other subroutines which are listed under files FIELD, RSABS, and ANNUAL in Table C-3. Table C-4 gives a list of all common groups and shows the subroutines in which they occur.

C.6 DESCRIPTION OF SUBROUTINES CALLED BY YEAR

FINTP1 reads the receiver interception data from the cellwise performance model. This data is contained in the so called node file and is ready by file code 14. Panel interception fractions are formed and written to file code 40. Subroutine HINT is called to interpolate receiver interception fractions to the individual heliostats. HINT also has an option to interpolate panel fractions. Panel fractions are converted to panel powers and written to file code 39. COMBO is called if a blend of aiming strategies is required.

TOOPAN and COMBO are used to blend node files representing different aiming strategies. There may be two node files: one file for a two point aiming strategy and a second file for a one point aiming strategy. It may happen that, neither the one point, nor the two point aiming strategy can produce a satisfactory flux density profile, but a blend of the two strategies may be satisfactory. TOOPAN reads the headers from both files and COMBO combines the receiver nodal interception matrices in some selected ratio.

HINT interpolates receiver interception data to the individual heliostat locations. A vector of receiver interception fractions is kept in core with a component for each heliostat. Similarly an array of panel interception fractions is kept in random file 38. The linear interpolation is supported by data relating to the representative heliostats in the cellwise performance model. It is easy to locate the individual heliostats with respect to the representatives of the cell model.

Table C-3. List of Files, Subroutines, and Functions for Individual Heliostat Performance Code

Files	Subroutines	Functions
INPUT	MAIN	
	LSQF*	ISKIP
	VALF*	RSFC, POLYNM, TRFC, HSTEP
LAY	LAYOUT	
	ZONE	
	MECHLM	
	COORDS	
	CIRCA	
	CIRCG	
	CIRCH	
	CIRCI	
	AIM (A1M1)†	
	DATIM††	
	AIM2	
	WREAD	
	TRIM	
	ROADS	
YEAR	YEAR	
RSABS	SAB3	
	EVENT	
	FINTP1 (FINTP3)	
	TOOPAN (COMBO)	
	HINT (CSPANL)	
FIELD	CELTUR	
	CIRSEC	
	SECTOR	
	SECPRT	
	ASKPRT	
	SUBFLD	
	ACONTR (VCONTR)	
ANNUAL	SUMIT	
	RELPOW	
	PANPOW	
	PANEFF	

*IMSL subroutines.
†Items in parenthesis are entry points.
††System subroutine for date and time.

```
                    Year
                      ● FINTP1(FINT)
                      ● CELTUR(FINT)
                      ● SECTOR(FINT)
                      ● SUBFLD

DO 700 NDAY  =  1, JMAX
DO 600 IHOR  =  1, IMAX
DO 500 IMIR  =  IROW1, IROW2
DO 501 JMIR  =  1; NR

501 CONTINUE  ● SAV3(FMIRR)
              ● CELTUR(FMIRR)
500 CONTINUE  ● SECTOR(FMIRR)
              ● CELTUR(FCOSI)
              ● CELTUR(FAREA)
              ● FINTP3
              ● SUMIT

600 CONTINUE
              ● CELTUR (FSAB)
              ● SECTOR(FSAB)
              ● SUMIT(ERGM1)
              ● RELPOW

700 CONTINUE
              ● CELTUR(ASAB)
              ● SECTOR(ASAB)
              ● SUMIT(ERGM2)
              ● RELPOW
              ● ANNUAL SUMMARY OUTPUT
              ● PANPOW

                    RETURN
```

Figure C-6. Subroutine Calls in YEAR. SUMIT and RELPOW also call CELTUR and SECTOR for output purposes. CELTUR calls CIRSEC and VCONTR for additional outputs.

Table C-4. List of Common Groups and the Subroutines in Which They Occur

Common Group	Subroutines
ATMOS	INPUT, YEAR
BOUND	INPUT, LAYOUT, AIM, ROADS
CALCX	INPUT, LAYOUT, YEAR, FINTP3, TOOPAN, CELTUR, SUMIT, RELPOW, PANPOW
CELL	INPUT, LAYOUT, AIM, YEAR, FINTP3, HINT, CELTUR
CSOUT	INPUT, YEAR, SUMIT, RELPOW
CTROUT	INPUT, YEAR, SUMIT, RELPOW
DIMSS	SAB3, EVENT
DSKIP	INPUT, AIM2
FINT	INPUT, YEAR
GRLAY	INPUT, LAYOUT, ZONE, YEAR
GROPT	INPUT, LAYOUT, COORDS, AIM, AIM2, YEAR, CIRSEC
GRPB	INPUT, LAYOUT, CIRCH, YEAR, SAB3, CELTUR, SECTOR, ASKPRT, SUBFLD, SUMIT, RELPOW
GRPC	LAYOUT, ZONE, COORDS, CIRCA, CIRCG, CIRCH, CIRCI, AIM, AIM2, YEAR, FINTP3, HINT, CELTUR, CIRSEC, SECTOR, SECPRT, SUMIT, RELPOW
GRPLS	INPUT, YEAR
GRPSB	LAYOUT, AIM, YEAR, SAB3, SUMIT, PANPOW, PANEFF
GRP3	YEAR, SAB3
GRP4	YEAR, SAB3
GRP5	YEAR, SAB3
GRP6	YEAR, SAB3, FINTP3
GRP7	INPUT, YEAR, SAB3
GRP11	LAYOUT, YEAR, FINTP3, HINT, SUMIT, RELPOW, PANPOW, PANEFF
GRP12	YEAR, RELPOW
GRP13	YEAR, PANPOW, PANEFF
GRPO1	INPUT, YEAR, PANPOW, PANEFF
HELI2	INPUT, SAB3
RECVR	INPUT, YEAR, FINTP3
SECOUT	INPUT, YEAR, SUMIT, RELPOW
SITE	INPUT, LAYOUT, AIM, YEAR, HINT

Table C-4. List of Common Groups and the Subroutines in Which They Occur (Continued)

Common Group	Subroutines
TIME	INPUT, YEAR, SUMIT, RELPOW, PANPOW, PANEFF
TIMES	INPUT, YEAR
TOWER	INPUT, FINTP3, PANPOW, PANEFF
XLOSS	INPUT, PANPOW, PANEFF
XYOUT	INPUT, YEAR, SUMIT, RELPOW
ZONEO	LAYOUT, ZONE, COORDS, CIRCA, CIRCG, CIRCH, CIRCI, AIM, AIM2, YEAR
ZONE1	LAYOUT, ZONE, COORDS
ZONE2	LAYOUT, ZONE, COORDS, CIRCA, CIRCG, CIRCH, CIRCI
ZONE3	INPUT, RSFC, LAYOUT, MECHLM, COORDS, YEAR
ZONE4	CIRCA, CIRCG, CIRCH, CIRCI, AIM

CSPANL is an entry point of HINT which reads the file of individual heliostat panel fractions and converts them into circle-sector panel powers which are written to print and card output.

SUMIT integrates ERGM1 over the hours in a day, and ERGM2 over the days in a given year. ERGM1 is a vector of redirected energy in MWH/m^2 for the individual heliostats. Redirected power or energy includes the effect of the insolation model, the diurnal motion, the heliostat mounting and layout, and the shading and blocking effects. However, the receiver interception is not included. This subroutine assumes east-west symmetry in the collector field, and morning-afternoon symmetry in insolation. If these symmetries are lacking similar outputs can be obtained from FSAB and ASAB in YEAR.

RELPOW outputs a dimensionless measure of relative heliostat performance called RTPOW. This output is a renormalized version of ERGM1 or ERGM2 (according to whether daily or annual performance is used) such that the average of RTPOW over all heliostats equals 1. CELTUR and SECTOR output is available. There are two additional outputs which provide the "Distributions of Glass Area and Redirected Power with Respect to RTPOW."

PANPOW is the last call made by YEAR. It provides annual summary output for the receiver panel powers, their statistics and several measures of system efficiency. Any receiver having tubes can be broken into sets of tubes called panels. The current external cylindrical receiver has 24 panels as shown in Figure 5-1. PANPOW provides the following list of outputs:

1) Annual Summary of Incident Panel Power
2) Annual Summary of Absorbed Panel Power
3) Annual Summary of System Efficiency
4) Annual Summary of System Efficiency/COSI
5) Annual Summary of Dimensionless Panel Gradients
6) Annual Summary of Receiver Asymmetry Ratios
7) Annual Summary of Receiver Panel Maxima over Panel Number of Maxima
8) Annual Summary of Receiver Panel Minima over Panel Number of Minima.

All of these outputs list the same set of day and hours. Items (3), (4), (6), and (7) appear as tables of day and hours, whereas items (1), (2), and (5) are lists of (day, hour) combinations in order to provide space for the panel output.

The absorbed panel power P_A is obtained from the incident power P_I by the linear transformation

$$P_A = aP_I - 6$$

where a and b are constants representing the multiplicative and subtractive losses of the receiver.

a = Coefficient of absorption, and
b = Convective and Radiative loss for specific operating conditions.

The system efficiency is defined by the total redirected power absorbed by the receiver divided by the total redirected power produced by the collector field. A second measure of system efficiency is provided by dividing the total efficiency by COSI. (This removes the unavoidable cosine of incidence effect.)

The dimensionless panel gradients G_i are defined as

$$G(i) = (P_A(i) - P_A(I-1))/(P_A(i) + P_A(i-1))$$

where i = 1...24. The panel maxima, panel minima and locations are determined by quadratic fitting. The panel asymmetry ratios are panel maxima divided by panel minima. These statistics are useful for receiver control studies.

PANEFF is called by PANPOW in order to output under conditions of altered insolation. We are currently assuming that the insolation is 950W/m^2 at all times, however, other insolation conditions could be provided. Site specific insolation is output via PANPOW, if desired, but it could be sent to PANEFF. The following outputs are available:

1) Annual Summary of Incident Panel Power
2) Annual Summary of Absorbed Panel Power
3) Annual Summary of System Efficiencies
4) Annual Summary of System Efficiencies/COSI

SAB3 is the individual heliostat version of RSABS which is the improved shading and blocking processor for the split rectangular heliostat model.

SUBFLD redefines the collector field arrays, which are the coordinate arrays for heliostats and the interception fraction array FINT (and others), to contain data for the heliostats within specified subfield boundaries.

SECTOR generates the sector by sector printout of field variables for individual heliostats. SECTOR calls SECPRT to format the output print line. SECPRT in turn calls ASKPRT to insert an asterisk indication of where deletes occurred in the collector field layout process.

CELTUR may generate several possible outputs. If no print outputs are called for, CELTUR simply returns the field variable average to the calling program. CELTUR calls CIRSEC if the CIRSEC output option is set. CIRSEC finds field variable averages over circle sector elements and outputs and results in tabular form. In addition, CELTUR sets up the xy grid structure and calls VCONTR, which may, depending on output switch settings, print cell averages of the field variable in a table format, or it may also output a contour map.